

For Reference

NOT TO BE TAKEN FROM THIS ROOM

Ex LIBRIS
UNIVERSITATIS
ALBERTAEISIS



THE UNIVERSITY OF ALBERTA

MOMENTUM ACCOMMODATION OF GAS MOLECULES
ON ROUGH AND SMOOTH SOLID SURFACES

by



TIMOTHY DAVID ELLIS

A THESIS

SUBMITTED TO THE FACULTY OF GRADUATE STUDIES AND RESEARCH
IN PARTIAL FULFILMENT OF THE REQUIREMENTS FOR THE DEGREE
OF DOCTOR OF PHILOSOPHY

DEPARTMENT MECHANICAL ENGINEERING

EDMONTON, ALBERTA

SPRING, 1975

ABSTRACT

Tangential momentum transfer occurs between a moving solid surface and a stationary free molecular gas, and can be characterized by a tangential momentum accommodation coefficient σ . This thesis is an evaluation of these coefficients for helium, argon and nitrogen on gold and silver surfaces. The moving surface was a magnetically suspended rotating sphere and momentum transfer was monitored as an angular deceleration due to drag. Fresh gold and silver surfaces were obtained by sublimation onto the sphere substrate surfaces under ultra-high vacuum conditions. Results for rough and smooth substrate surfaces were obtained, as well as results for thin and thick coatings.

Values of σ were found to be insensitive to differences in interaction energy of surface atoms and gas molecules for thin silver layers. Values of σ for this situation were 0.92 to 0.98. For thicker films σ values were less consistent; varying from 0.85 to 1.02 for silver, and 0.79 to rapidly changing values of the order of 1.2 for gold. The lower values obtained were probably due to a smoothing effect introduced by the thicker films. The rapid change in the large σ value for gold may have been due to spontaneous sintering of the film.

Rough surfaces formed by sandblasting the substrate resulted in σ values greater than unity, which indicates

that some back reflection of molecules occurred. Roughness measurements of these surfaces were performed using stereographic scanning electron microscopy. A simple roughness model derived from stereo-micrographic measurements gave qualitative understanding of this situation. Essentially, this model showed that the "windward" slope of a roughness hill receives more momentum than the "leeward" and therefore can reflect more momentum. Values of σ on rough surfaces varied from above 1.14 for helium on silver to 1.02 for nitrogen on silver.

ACKNOWLEDGEMENTS

The author would like to express his sincere appreciation to the following:

Dr. D.J. Marsden for guidance and help in all stages of the thesis work.

Mr. Donald McFarlane who acting as a consultant, designed and constructed the electronic circuits.

Miss Verna Hoffman and Mrs. Susan Flynn of the Ontario Hydro Research Laboratory who patiently and cheerfully typed the thesis.

The Department of Mechanical Engineering and the National Research Council for financial support.

The Staffs of the Mechanical Engineering Machine Shop and the U of A Glass Shop for construction of the experimental apparatus.

Many staff members and graduate students in Mechanical Engineering and other departments for helpful discussion on various aspects of the thesis work.

TABLE OF CONTENTS

CHAPTER		PAGE
I	INTRODUCTION	1
	1-1 Definitions and General	
	Statement of Problem	1
	1-2 Vacuum Technology	2
	1-3 Gas-Surface Interactions	3
II	THEORY	10
	2-1 Free Molecular Maxwellian Gas, Definition and Transport	
	Properties	10
	2-2 Tangential Momentum Accommodation Coefficient	12
	2-3 Energy Accommodation Coefficient	16
	2-4 The Free Molecular Nature of the Gas	22
	2-5 Surface Roughness Model	25
III	APPARATUS	36
	3-1 The Suspension, Turning and Counting Systems	36
	3-2 Residual Drag	40
	3-3 Energy Accommodation Apparatus	40
	3-4 Vacuum System	43

CHAPTER		PAGE
IV	CALIBRATIONS AND ERROR ANALYSIS	47
	4-1 Pressure Gauge Calibration	47
	4-2 Background Impurity	52
	4-3 Error Analysis for Tangential Momentum Accommodation Coefficient	56
V	RESULTS OF ROUGHNESS MEASUREMENTS	60
	5-1 Examination of Surface Roughness	60
	5-2 Thickness of Deposited Films	67
VI	TANGENTIAL MOMENTUM AND ENERGY	
	ACCOMMODATION RESULTS	70
	6-1 Experimental Procedure	70
	6-2 Introduction to Tangential Momentum Accommodation Results	73
	6-3 Smooth Ball Results for Silver	74
	6-4 Rough Ball Results for Silver	94
	6-5 Smooth Ball Results for Gold	111
	6-6 Energy Accommodation Coefficients	120
VII	DISCUSSION	128
	7-1 Pressure Gauge Drift	128
	7-2 Smooth Ball Results	128
	7-3 Sandblasted Ball Results	130
	7-4 Comparison with Other Work	131
VIII	CONCLUSIONS	134

	BIBLIOGRAPHY	137
APPENDIX I	APPROXIMATE SOLUTION FOR ENERGY ACCOMMODATION COEFFICIENT	140

CHAPTER		PAGE
APPENDIX II	ELECTRONIC CIRCUITS	145
	II-1 Magnetic Suspension System	145
	II-2 Counting Circuit	146
	II-3 Rotational Drive System	148
	II-4 Energy Accommodation Measurement Circuits	148
APPENDIX III	CALCULATION OF TEMPERATURE	
	COEFFICIENT OF TUNGSTEN FILAMENT	152
APPENDIX IV	FORMULATION FOR STEREOGRAPHIC HEIGHT DETERMINATION	156

LIST OF SYMBOLS

a	wire radius
a_0	size characterization of normal incidence micrograph
a_5	size characterization of micrograph 5° from normal
c_m	most probable molecular speed
c_p	ball specific heat
c_1, c_2, c_3	velocity coordinate system
d	height on micrograph
E_r	reflected energy per unit time
E_s	reflected energy per unit time at surface temperature
f	Maxwellian velocity distribution function
f_1	initial ball speed at time t_1
f_2	final ball speed at time t_2
f_R	residual drag correction
g	molecular degrees of freedom
I	mass moment of inertia, electrical current
I_{HEAT}	filament heating current
K_o	thermal conductivity
K_n	Knudsen number
k	Boltzmann's constant
L	wire length
m	mass of one molecule
n	molecule number density
P_i	incident normal momentum per unit time

P_r	reflected normal momentum per unit time
P	gas pressure
P_B	Baratron gauge pressure
P_M	McLeod gauge pressure
P_{MV}	mercury vapour pressure
Q	heat flux
R_{FIL}	filament resistance
R_s	ball radius
r, ϕ, θ	spherical polar coordinates
S	speed ratio
S_o	Stephan-Boltzmann constant
T	temperature
T_f	filament temperature
T_i	incident gas temperature
T_r	reflected gas temperature
T_s	surface temperature
T_w	wall temperature
t	time
u	surface velocity
W	torque
x	length variable on filament
\bar{x}	non-dimensional length variable
α	energy accommodation coefficient
β	temperature coefficient of resistivity
ΔV_{FIL}	voltage drop across filament
ΔV_R	voltage drop across precision resistor
ϵ	emissivity, relative error

η	free molecularity parameter
θ	temperature difference, $T_f - T_w$
$\bar{\theta}$	normalized temperature difference
θ_{AV}	average θ
λ	mean free path
ρ	ball mass density
ρ_f	wire resistivity
σ	tangential momentum accommodation coefficient
τ_i	incident tangential momentum per unit time
τ_r	reflected tangential momentum per unit time
ϕ	roughness angle from horizontal
ψ	incident stream to surface angle, roughness angle from vertical
ω	angular velocity of ball

LIST OF TABLES

<u>NUMBER</u>		<u>PAGE</u>
2-1	Free Molecular Parameter	24
2-2	σ Values for Diffuse and Specular Reflection from Furrow	33
4-1	Preliminary Baratron Gauge Calibration	49
4-2	Baratron Gauge Calibration with Room Temperature Trap	51
5-1	Stereographic Roughness Measurements on Sandblasted Ball	65
6a	Average Tangential Momentum Accommo- dation Coefficients for Silver on Smooth Balls	75
6-1	Values of σ for Nitrogen on Smooth Silver	76
6-2	Values of σ for Helium on Smooth Silver	82
6-3	Values of σ for Argon on Smooth Silver	90
6b	Average Tangential Momentum Accommo- dation Coefficients for Silver on Rough Balls	95
6-4	Values of σ for Nitrogen, Argon and Helium on Sandblasted Bare Steel	96
6-5	Values of σ for Nitrogen on Rough Silver	99
6-6	Values of σ for Helium on Rough Silver	104
6-7	Values of σ for Argon on Rough Silver	108

<u>NUMBER</u>		<u>PAGE</u>
6c	Average Tangential Momentum Accommodation Coefficients for Gold on Smooth Balls	112
6-8	Values of σ for Nitrogen on Smooth Gold	113
6-9	Values of σ for Helium on Smooth Gold	117
6-10	Values of σ for Nitrogen, Argon and Helium on Silver on Tungsten	121

LIST OF FIGURES

<u>NUMBER</u>		<u>PAGE</u>
2-1	Gas Velocity Coordinate System	11
2-2	Ball Coordinate System	13
2-3	Reflection of Molecules for Three Cases of σ	15
2-4	Hot Wire Element of Length	18
2-5	Elemental Thermal Conductivity	20
2-6	Model for Free Molecular Analysis	23
2-7	Furrow Cross-Section	25
2-8	Coordinate System for Translating Gas	26
2-9	Incident Momentum on Moving Furrow	27
2-10	Specular Reflection from Furrow	28
2-11	Diffuse Reflection from Furrow	31
2-12	σ Values for Diffuse and Specular Reflection from Furrow	34
3-1	Suspension System Schematic	37
3-2	Energy Accommodation Apparatus	41
3-3	Schematic of Vacuum System	44
4-1	Schematic of Pressure Calibration Apparatus	48
4-2	Calibration of Baratron versus McLeod Gauge for Room Temperature Cold Trap	53
5-1	Schematic of Scanning Electron Microscope Beam and Target	60

<u>NUMBER</u>		<u>PAGE</u>
5-2	Scanning Electron Micrograph at Normal Incidence of Sandblasted Ball	62
5-3	Scanning Electron Micrograph at 5° from Normal Incidence of Sandblasted Ball	63
5-4	Tallysurf Trace for Sandblasted Flat AISI 440 Stainless Steel Surface	66
5-5	Scanning Electron Micrograph at High Magnification of Smooth Ball	68
6-1	Tangential Momentum Accommodation Co- efficients for Nitrogen on Smooth Silver	81
6-2	Tangential Momentum Accommodation Co- efficients for Helium on Smooth Silver	89
6-3	Tangential Momentum Accommodation Co- efficients for Argon on Smooth Silver	92
6-4	Tangential Momentum Accommodation Co- efficients for Nitrogen on Rough Silver	103
6-5	Tangential Momentum Accommodation Co- efficients for Helium on Rough Silver	107
6-6	Tangential Momentum Accommodation Co- efficient for Argon on Rough Silver	110
6-7	Tangential Momentum Accommodation Co- efficient for Nitrogen on Smooth Gold	116
6-8	Tangential Momentum Accommodation Co- efficient for Helium on Smooth Gold	119
6-9	Zero Pressure Heat Transfer on Heated Filament versus Filament Resistance	126

NUMBER		PAGE
I-1	Temperature Distribution	
	Filament $\theta(x)$ versus x/L , Helium	
	Test d	144
II-1	Suspension Circuit Schematic	145
II-2	Counting Circuit Schematic	146
II-3	Counting Oscilloscope Trace	147
II-4	Rotating Drive Apparatus Schematic	149
II-5	Filament Temperature Control and Heater Circuit	151
III-1	Calibration Filament Resistance versus Temperature	154
III-2	Energy Accommodation Filament Resistance versus Temperature	155
IV-1	Diagram for Stereographic Height Determinations	156

LIST OF PHOTOGRAPHIC PLATES

NUMBER		PAGE
5-2	Scanning Electron Micrograph at Normal Incidence of Sandblasted Ball	62
5-3	Scanning Electron Micrograph at 5° from Normal Incidence of Sandblasted Ball	63
5-5	Scanning Electron Micrograph at High Magnification of Smooth Ball	68

CHAPTER I
INTRODUCTION

1-1 Definitions and General Statement of Problem.

This thesis deals with the measurement of transfer of momentum between a rarefied gas and a moving solid surface. The behavior of a rarefied or low density gas can be analyzed by considering the motion of gas molecules individually interacting with the surface, unlike higher density flows which are normally analyzed by continuum formulations. The rarefied gas in these measurements is free molecular, which means that individual molecules reflected after interacting with the solid have few enough collisions with incident molecules that incident properties are not affected.

Specifically, the transfer of tangential momentum between a rotating sphere and a free molecular gas is measured as a decelerating drag on the sphere. The tangential momentum accommodation coefficient, σ , is a measure of the efficiency of this exchange, and is defined as

$$\sigma = \frac{\tau_i - \tau_r}{\tau_i} \quad (1-1)$$

where τ_i is the tangential momentum incident on the surface due to gas molecules colliding with that surface and τ_r is the tangential momentum reflected from the surface as carried by the reflected molecules.

Equation 1-1 is valid only for a coordinate system fixed on the sphere.

1-2 Vacuum Technology.

Research in low density gas dynamics and vacuum technology has been necessary because of the many physical processes which occur only when much of the normal atmospheric air is removed. Processes requiring long uninterrupted beams of particles such as are found in cathode ray and other electronic tubes, mass spectrometers, electron microscopes, and particle accelerators are examples. Many industrial processes requiring vacuum are in regular usage. Thus, the production of vacuum has become important, as has the study of the effects of the remaining gas molecules.

A necessary part of vacuum technology is an examination of molecules adsorbed on, and diffused into the walls of the vacuum system. These molecules are continuously evaporated and re-adsorbed, and therefore have a vapour pressure which becomes significant when it is of the same order of magnitude as the vacuum system pressure. Most machined and fabricated surfaces are covered with layers of oil which inhibit the production of low pressure; therefore scrupulous cleaning is required. After cleaning, layers of oxide and other adsorbed gases are still present, and are normally removed by heating the vacuum surfaces. The high temperature raises the vapour pressure of the layers, allowing desorption

and removal much more quickly than is possible at normal temperatures. This procedure, termed baking, removes all but the most stable layers which will have a low vapour pressure.

Pumping at vacuum pressures can be done in a number of ways; one common method, gettering, used in this work is discussed briefly. Gettering makes use of the property of atomically clean surfaces of active metal that they combine chemically with gases that adsorb on them and effectively remove them from the system. Getter pumps continuously or intermittently produce new clean surfaces by subliming bulk metal onto a pumping surface. The bulk metal, often titanium, is subliming by heating to a temperature where its vapour pressure is high. Weakly adsorbing molecules are permanently pumped only after burial by a successive subliming layer. Getter-ion pumps also known as sputter-ion pumps produce fresh adsorbing layers by accelerating high energy ions toward the bulk which throws off material onto a nearby surface. This type of pumping becomes effective below 10^{-2} torr and therefore requires an initial rough pumping from atmospheric pressure. Roughing pumps are normally positive displacement mechanical pumps.

1-3 Gas-Surface Interactions.

The exchange of momentum and energy for a gas-surface collision depends on various physical parameters. Some of

these parameters are as follows:

- 1) Ratio of molecular weights of the test gas and the metal surface.

A classical elastic collision model can be used to visualize the effect of relative masses on the exchange.

- 2) Interaction potential of gas and surface.

The relative size of adsorption energy and the thermal energy of motion of the surface is important. Reference (1) gives much elaboration of parameters 1 and 2.

- 3) Adsorbed gas layers.

Adsorption of gas layers on the surface affects exchanges partly through parameters 1 and 2.

- 4) Surface roughness.

Roughness is particularly important for tangential momentum accommodation which is the main concern of this thesis.

The energy and momentum interactions of gases and solids are of interest for calculation of forces and energy transfers of components within vacuum systems and high altitude vehicles such as orbiting and re-entering satellites. Much theoretical and experimental work has been done on these interactions. Experiments have included direct measurements of forces resulting from momentum exchange and direct measurement of heat loss due to molecular energy transfer, as well as more fundamental measurements of molecular interactions using molecular beams directed at a solid target surface. The reflection or scatter of these incident molecules is measured

in terms of reflected beam intensity as a function of reflection angle. The more direct measurements of drag or energy transfer are concerned with finding accommodation coefficients without directly measuring any reflected angular distribution, while molecular beam measurements are concerned with more detailed information on reflection.

The present work deals with tangential momentum exchange between a rotating sphere and a stationary free molecular gas. This sphere is suspended freely in a magnetic field and accelerated as the rotor of an induction motor to a speed of up to 1000 revolutions per second. Tangential momentum drag is determined by measuring deceleration due to momentum exchange with the stationary test gas when current to the field coils is turned off and the ball allowed to coast.

Some previous work of the type performed in this thesis has been done, and might be broadly classified as drag measurements on bodies in motion relative to a free molecular or near free molecular gas. Lord and Harbour (2) measured drag on a magnetically suspended sphere similar to that of the work reported here. Test gases were air, Krypton and di-iodo-methane at pressures from 10^{-2} to 10 torr; and values of σ found were about 1.0. Much of the work of Lord and Harbour dealt with drag at pressures high enough to be in the transition regime of gas flow, so most of their results are not directly comparable to those of this thesis.

Other previous measurements of tangential momentum accommodation were made by Millikan and co-workers Blankenstein and Stacy (3), (4) (5), and later by Hurlbut (6). In each case, the apparatus used a rotating cylinder which exerted a drag torque on another concentric cylinder. The second cylinder was suspended on a torsional fibre measuring torsion due to drag as a function of angular deflection.

Experiments by Blankenstein produced values of σ from 0.96 to 1.00 for hydrogen, helium, air and oxygen on polished silver oxide. The work by Hurlbut showed σ to be 0.90 to 1.00 for oxygen, air and nitrogen on aluminum. Hurlbut found also that aging or soaking the aluminum surfaces at vacuum pressures reduced σ to about 0.60. This soaking was thought to have allowed a film of oil to settle on the surface, effectively smoothing the surface.

Work by Thomas and Lord (7) using magnetically suspended ball produced σ values from 0.824 for helium on smooth steel to 1.075 for xenon on roughened steel. Some molecular beam experiments have included determinations of tangential and normal forces caused by impingement of the beam on the target. However, many of these beams were at high velocities not comparable to those of this thesis.

The magnetic suspension and turning systems of this thesis are based on the work of Beams (8) and are modifica-

tions of a system built by McFarlane and Benson (9).

The use of magnetic suspension eliminates problems of bearing friction, mechanical feedthrough of rotary motion into the vacuum system, bearing lubrication in vacuum environment and rotor balancing. After disassembly of the suspension system, the vacuum system is bakeable to 300°C.

Much of the work of this thesis has been to control and assess the role of adsorbed gas layers and surface roughness on the momentum exchange. In order to relate measurements to a known type of surface, new metallic surfaces were prepared on top of the ball surface substrate. These chemically more reliable surfaces were produced by deposition of thin metal films on the ball by sublimation from heated filaments. This is a similar procedure to supplying titanium for getter pumping surfaces, except that in this case, gold and silver were used in order to have surfaces that do not react chemically with the test gas. Sublimation was carried out at low pressures in the 10^{-9} torr range, in order to avoid contamination as much as possible. The test gases used were helium, nitrogen and argon which do not adsorb readily on either metal at room temperature.

Molecular beam studies such as those of Weinberg and Merrill (10) show roughness to be an important factor in surface exchanges. They found that specular reflections were not achieved until silver target surfaces were electro-polished. Experiments were performed for this thesis with

sphere surfaces which were either mechanically smooth or artificially roughened. The spheres were actually balls designed for use in ball bearings and were quite smooth for machined surfaces. Electropolishing was attempted and did not decrease roughness. The rough surface tests were done with the ball artificially roughened by sandblasting. Roughness was measured at least qualitatively for both types of surface using scanning electron microscope techniques.

A subsidiary apparatus to determine energy transfer was built and run concurrently with drag experiments. This apparatus consisted of a thin heated wire, also covered with fresh metal, from which the energy loss to the surrounding gas was measured. This apparatus is similar in design to those of Thomas and co-workers (11, 12). The wire was heated by passing a current through it and its temperature determined from its temperature coefficient of resistivity. The power loss from the wire was used to calculate energy accommodation coefficients. These energy accommodation coefficients provide a useful comparison to momentum coefficients since the energy coefficient also provides a measure of the gas-surface interaction.

The use of a magnetic suspension system together with modern vacuum equipment allowed for system baking and consequent ultra high vacuum conditions. Such conditions made it possible to study freshly deposited surfaces which, although

probably contaminated by background gases, did not have the gross contamination associated with everyday surfaces. Surface roughness of specimens used was investigated using a scanning electron microscope, allowing qualitative conclusions to be drawn regarding the effect of surface roughness on tangential momentum exchange. The work presented here differs from that of references 2 to 6 largely because of the fresh surface production and roughness measurement.

CHAPTER II

THEORY

2-1 Free Molecular Maxwellian Gas, Definition and Transport Properties.

The gas surrounding the ball is assumed to be free molecular, Maxwellian and stationary. The free molecular assumption can be made at low pressure where the mean free path of gas molecules is large, which means that molecules reflected from the ball have few enough collisions with other molecules that no net circulating motion of molecules results. This situation is discussed more fully in section 2-4.

The distribution function for a Maxwellian gas is given by

$$f(v_x, v_y, v_z) dv_x dv_y dv_z = \frac{n m^{3/2}}{(2\pi k T)^{3/2}} \exp\left\{-\frac{(v_x^2 + v_y^2 + v_z^2)}{2kT}\right\} dv_x dv_y dv_z \quad (2-1)$$

where v_x , v_y , and v_z are the velocities related to a cartesian coordinate system x , y and z ,

n is the total number of molecules per unit volume,

k is Boltzmann's constant,

m is the mass of one molecule,

T is the macroscopic gas temperature,

and $f(v_x, v_y, v_z)$, the distribution function, is the number

of molecules per unit volume with velocities v_x to $v_x + dv_x$, v_y to $v_y + dv_y$ and v_z to $v_z + dv_z$.

Equation 2-1 is derived for particles such as neutral gas molecules which obey Maxwell-Boltzmann statistics. It is assumed that intermolecular potential energy is negligible compared to kinetic energy, and that particles are numerous enough to obey statistical analysis. The subject of Maxwell-Boltzmann statistics is dealt with in several books on statistical thermodynamics such as Sontag and Van Wylen (13) and Lee, Sears and Turcott (14).

To evaluate momentum transfer from the gas molecules to the ball, transport properties of the gas with an element of surface must be discussed. Consider an element of surface dA on the ball moving with velocity u corresponding to the peripheral velocity of the ball; x , y and z coordinates are chosen as shown in figure 2-1 with the y axis parallel to velocity u , and the z axis normal to the paper.

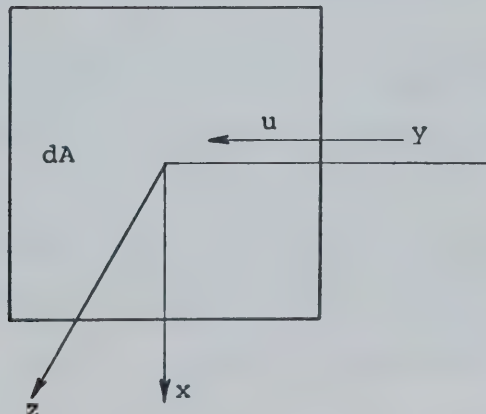


FIGURE 2-1 GAS VELOCITY COORDINATE SYSTEM

For the purpose of analysis, the gas will be assumed to move with velocity $+u$, while the surface is considered stationary. The net incident tangential momentum per unit time, $d\tau_i$, which is incident on dA will be

$$d\tau_i = \int_{v_x = -\infty}^{\infty} \int_{v_y = -\infty}^{\infty} \int_{v_z = -\infty}^{0} mv_z(v_y + u) f dv_x dv_y dv_z dA.$$

Integration leads to $d\tau_i = \frac{nmc_m u}{2\sqrt{\pi}} dA$ (2-2)

where $c_m = \sqrt{\frac{2kT}{m}}$ is the most probable speed of gas molecules.

For stationary Maxwellian gas molecules incident on dA , all angles of incidence are equally probable, resulting in no net tangential momentum being transferred to a stationary surface. Only when the gas and surface move with respect to one another does any net transfer occur.

2-2 Tangential Momentum Accommodation Coefficient

Total incident momentum on the ball surface can be obtained by integrating over elements of areas as shown in figure 2-2.

Elements dA are chosen as annular rings $2\pi r R_s d\phi$, where ϕ is an angle from the vertical axis of rotation, R_s is the ball radius, and $r = R_s \sin\phi$ is the radius of an element from the axis of rotation.

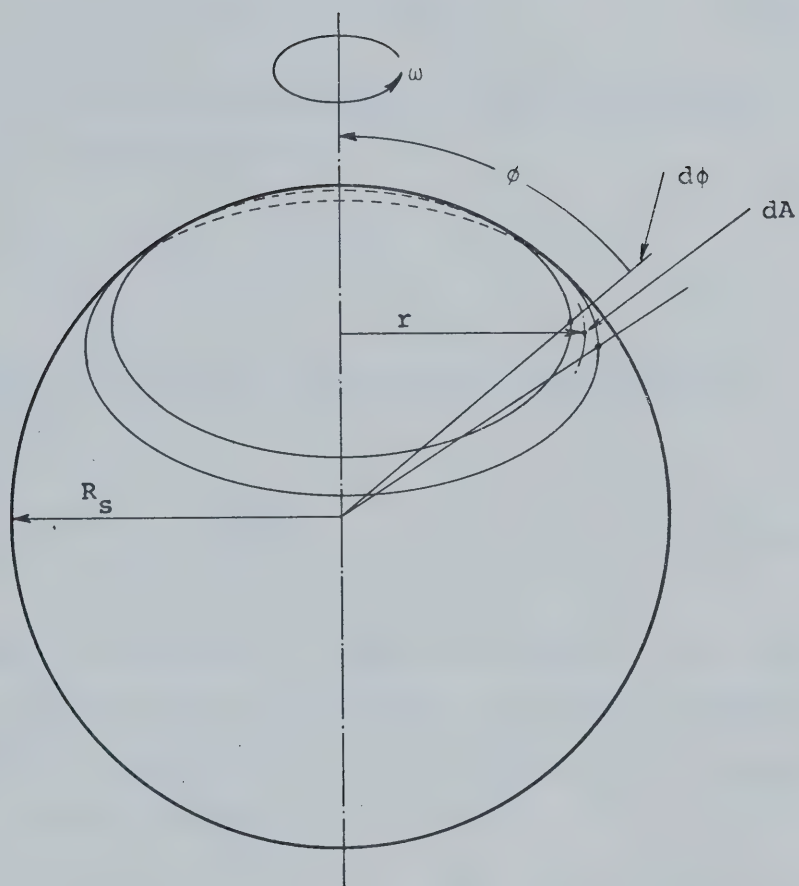


FIGURE 2-2 BALL COORDINATE SYSTEM

For a speed of rotation ω , each element has a peripheral velocity $\omega r = \omega R_s \sin\phi$. Substituting in equation 2-2, again assuming that the gas moves with respect to the stationary surface,

$$d\tau_i = nmc_m \sqrt{\pi} \omega R_s^3 \sin^2\phi d\phi. \quad (2-3)$$

The incident tangential momentum per unit time on the sphere, τ_i , is then given by

$$\tau_i = \int_A d\tau_i.$$

Tangential momentum accommodation coefficient is defined as

$$\sigma = \frac{\tau_i - \tau_r}{\tau_i}. \quad (1-1)$$

Examination of equation 1-1 shows that when $\tau_r = \tau_i$, then $\sigma = 0$. This situation is described as specular reflection and indicates that molecules are reflected with no change in the tangential component of velocity. If $\tau_r = 0$, $\sigma = 1$, and this is termed diffuse reflection. Molecule reflection is equally probable in any direction, thus net tangential momentum reflected is zero relative to the surface. In our case this means that no memory remains of the incident bulk velocity u .

Practical values of σ usually show neither specular nor diffuse reflection but something in between. Figure 2-3 shows the reflected distribution for specular and diffuse reflection for many molecules at one angle of incidence as well as a possible distribution for $0 < \sigma < 1$.

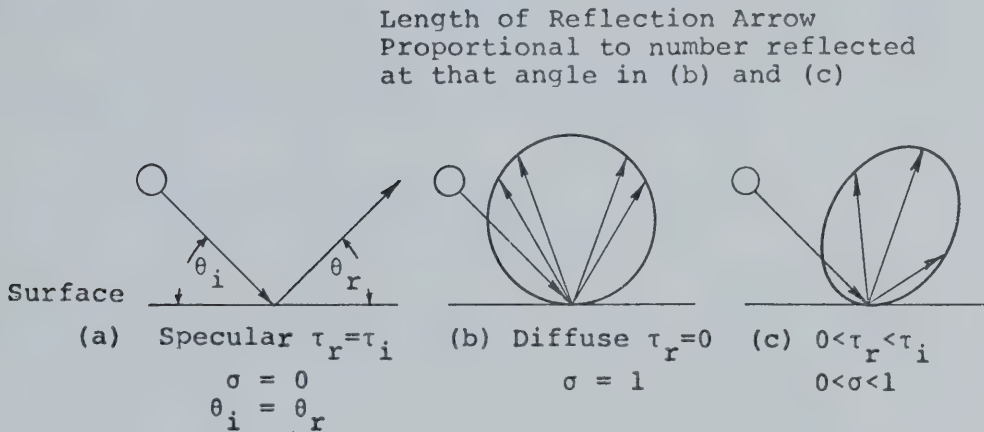


FIGURE 2-3 REFLECTION OF MOLECULES FOR
THREE CASES OF σ .

The net tangential momentum per unit time transferred to the surface is given by $\tau_i - \tau_r = \sigma \tau_i$. The drag torque W on the rotating ball can now be found to be

$$W = \sigma \int_A r d\tau_i \quad (2-4)$$

if σ is not a function of ω . Later results show $\sigma \neq \sigma(\omega)$ within the limits of ω used in experiments. Substituting equation 2-3 into equation 2-4 and integrating ϕ from 0

to π we find that

$$W = 4/3 \omega \sigma R_s^4 \sqrt{2\pi mkT} \quad (2-5)$$

using the substitution that gas pressure $p = nkT$.

Angular acceleration $\frac{d\omega}{dt} = -\frac{W}{I}$, where I is the moment of inertia and equals $8/15 \rho \pi (R_s)^5$ for a sphere of density ρ .

$$\text{Therefore } \frac{d\omega}{dt} = -5\omega\sigma \frac{p}{\sigma R_s} \sqrt{\frac{m}{2\pi kT}}. \quad (2-6)$$

Separating variables and integrating yields

$$-\int_{\omega_1}^{\omega_2} \frac{d\omega}{\omega} = \int_{t_1}^{t_2} \frac{5\sigma p}{\rho R_s} \sqrt{\frac{m}{2\pi kT}} dt,$$

where ω_1 is the angular velocity at some time t_1 and ω_2 is a lower angular velocity at some later time t_2 .

Integration gives

$$\sigma = \frac{\rho R_s \sqrt{\frac{2\pi kT}{m}} \ln \frac{\omega_1}{\omega_2}}{5p (t_2 - t_1)}. \quad (2-7)$$

Equation 2-7 shows that σ can be obtained without measuring directly any reflected distribution of molecules.

2-3 Energy Accommodation Coefficient.

Energy accommodation coefficient, α , is defined as

$$\alpha = \frac{E_r - E_i}{E_s - E_i} \quad (2-8)$$

where E_i is incident energy of gas molecules,
 E_r is reflected energy of gas molecules,
and E_s is the reflected energy that gas molecules would
have for a macroscopic temperature which is the
surface temperature.

Incident energy can be calculated just as incident tangential momentum was in section 2-1. Again, an element of area dA is assumed with the same coordinates as figure 2-1, except that both gas and surface are stationary in this case. The energy, dE_i , incident on the surface per unit time from the gas at macroscopic temperature T_i will be

$$dE_i = \int_{-\infty}^0 \int_{-\infty}^{\infty} \int_{-\infty}^{\infty} f v_z \left(\frac{m}{2} (v_x^2 + v_y^2 + v_z^2) + \left(\frac{g-3}{2} \right) k T_i \right) dv_x dv_y dv_z.$$

The term $\left(\frac{g-3}{2} \right) k T_i$ arises from energy transferred as a result of internal energy modes where g is the total number of degrees of freedom of the molecules. Integration and re-organization yields

$$dE_i = \left(\frac{g+1}{2} \right) \sqrt{\frac{k}{2\pi m}} n k T_i^{3/2} dA. \quad (2-9)$$

Equation (2-9) shows that incident energy is dependent only on temperature for a given number of molecules of a particular gas. An alternative form of the equation is

$$dE_i = \left(\frac{g+1}{2} \right) \sqrt{\frac{k}{2\pi m T_i}} p T_i dA. \quad (2-10)$$

Examination of equation 2-8, indicates that if $E_r = E_s$, then $\alpha = 1$, which also means that $T_r = T_s$. Thus, if the incident molecular temperature is changed to the surface

temperature before reflection, energy is completely accommodated. If no energy is exchanged, $T_r = T_i$ and $\alpha = 0$. Practical values of α are between 0 and 1, indicating that reflected temperature is between incident gas and wall temperature.

If T_s is greater than T_i , incident molecules carry away energy upon reflection from the surface if $\alpha > 0$. The amount of energy removed from a surface area A per unit time will be

$$E_r - E_i = \alpha (E_s - E_i) = \left(\frac{g+1}{2}\right) \sqrt{\frac{k}{2\pi m T_i}} P (T_s - T_i) A. \quad (2-11)$$

Equation 2-11 does not follow directly from equation 2-10 but is obtained after equating incident and reflected numbers of molecules.

As explained briefly in Chapter I, α is evaluated from energy transfer from a heated wire, the theory of which follows. Figure 2-4 shows an elemental length dx of a thin wire in a free molecular gas heated by a current I . The temperature $T(x)$ of the element varies along the length.

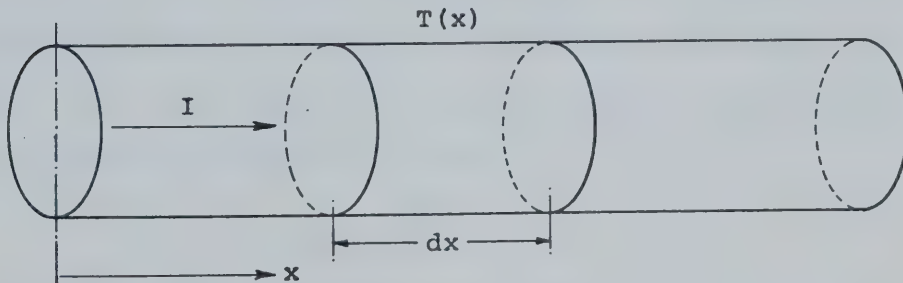


FIGURE 2-4 HOT WIRE ELEMENT OF LENGTH

Energy is transferred by conduction along the wire by radiation to the cooler surroundings, and by gas molecule conduction. Each mode of transfer is examined in detail, as is energy generation.

(a) Generation

Power generated by electrical current in the element is

$$I^2 \rho_f dx / \pi a^2$$

where ρ_f is resistivity and a is wire radius. Resistivity is actually a function of temperature, this function being linear to a close approximation, for the tungsten filaments used in the experiments. Thus, the generated power becomes

$$I^2 \rho_{f0} (1 + \beta (T_f - T_{f0})) dx / \pi a^2$$

where ρ_{f0} is resistivity at a reference temperature T_{f0} , and β is the temperature coefficient of resistivity. The temperature of the surface T_s becomes T_f the filament temperature.

(b) Conduction along the wire

Fourier's law is given as $Q = -K_o \nabla T A$ where Q is energy flux rate, K_o is thermal conductivity, T is the temperature gradient, and A is the area through which the energy flux acts. For a one-dimensional system assuming $K_o \neq K_o(T_f)$, the conduction energy flux rate is

$$- \pi a^2 K_o \frac{dT_f}{dx}$$

Figure 2-5 shows an element of filament of length dx at temperature T_f . Temperature gradients at faces 1 and 2 of the element are $\frac{dT_f}{dx}$ and $\frac{dT_f}{dx} + \frac{d^2 T_f}{dx^2} dx$. From Fourier's law,

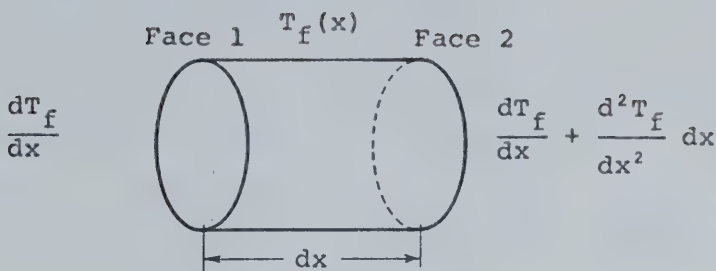


FIGURE 2-5 ELEMENTAL THERMAL CONDUCTIVITY

the net energy flux rate from the element is

$$-\pi a^2 K_o \frac{d^2 T_f}{dx^2} dx$$

(c) Radiation

If the walls of the vacuum system surrounding the filament are at temperature T_w , radiation energy transfer rate is given by $2\pi a \epsilon S_o (T_f^4 - T_w^4) dx$. This expression is valid only when a is small compared to the dimensions of the vacuum system, as was the case in the experiments performed. S_o is the Stephan-Boltzmann constant and ϵ is emissivity.

(d) Molecular Conduction

To evaluate molecular conduction, the assumption is made that incident molecules have a temperature T_w . This assumption is similar to the assumption that no circulating motion of molecules occurs around the rotating ball. Using this assumption, and changing notation, equation 2-11 gives the result that molecular conduction energy transfer rate is

$$2\pi a\alpha \left(\frac{g+1}{2}\right) \sqrt{\frac{k}{2\pi m T_w}} p(T_f - T_w) dx.$$

Consideration of all these energy transfer modes gives the resulting differential equation

$$\pi a^2 k \frac{d^2 T_f}{dx^2} = - I^2 \rho_{fo} \left(\frac{1+\beta(T_f - T_o)}{\pi a^2} \right) + 2\pi a\alpha \left(\frac{g+1}{2}\right) \sqrt{\frac{k}{2\pi m T_w}} p(T_f - T_w) + 2\pi a S_o \epsilon (T_f^4 - T_w^4). \quad (2-12)$$

Since the total resistance of the wire R is measured, the quantity $\frac{\rho_{fo}}{\pi a^2}$ can be written as $\frac{R_o}{L}$ when R_o is a reference temperature resistance and L is total wire length.

The solution to equation 2-12 is difficult due to the non-linearity of the radiation term. An initial approximation for values of α can be generated by assuming that the entire filament is at the average temperature as deduced from the resistance of the filament. Two experiments are performed to determine one value of α ; one at very low pressure to determine energy transfer due to end conduction and radiation, and another at the same average temperature but at a higher pressure where molecular conduction is also present. The difference in power input for these two cases gives an approximation to the actual molecular conduction loss and α is determined within the limits of that approximation.

Appendix I presents a better approximation to the solution of equation 2-12 but requires an order of magnitude

analysis of various terms in the equation. The analysis can be done only after discussion of the apparatus and the dimensions involved, and after presentation of numerical values for current and temperatures from experiments in section 5-5.

2-4 The Free Molecular Nature of the Gas

The transport equations derived in the previous section are valid only for free molecular gases. These gas molecules are ones for which incident molecules are unaffected by reflected ones. For non-free molecular flow in the case of the heated wire, higher temperature molecules leaving the wire will tend to cause bulk heating of the gas, thus changing the incident gas temperature. For the case of the ball, reflected molecules will collide with surrounding molecules and impart some of the bulk momentum gained from the ball. This causes the molecules adjacent to the ball to be dragged along as in a boundary layer changing the assumed incident momentum.

This phenomenon can be analyzed by a model shown in Figure 2-6, which shows the ball of Radius R_s surrounded by the gas. A point A is chosen one mean free path, λ , away from the closest point on the ball. The conditions at A determine the extent to which the gas is free molecular. Two types of molecules will arrive at A, those which had their last collision with the ball and those which had their last collision with the wall (or some other

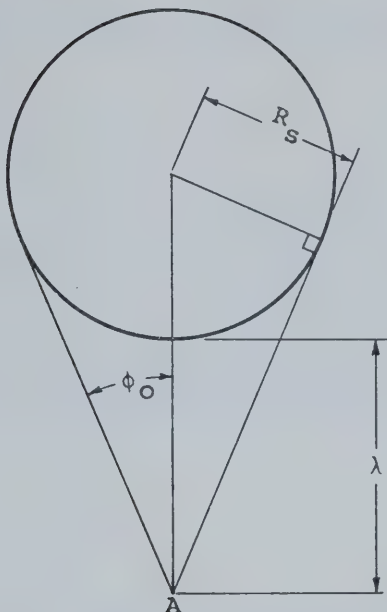


FIGURE 2-6 MODEL FOR FREE MOLECULAR ANALYSIS

molecule which had stationary characteristics). Since practical values of σ are nearly 1.0, the first group will have much the peripheral velocity, and the second group will be on the average stationary. The group with the peripheral velocity will approach A through a solid angle related to the linear angle ϕ_o , while the second group will arrive from all other solid angles. By integration of the surface area of a sphere, it can be shown that the solid angle related to ϕ_o will be $2\pi(1 - \cos\phi_o)$. Therefore, the fraction, η , scattered into A from the ball will be given by

$$\eta = \frac{2\pi(1 - \cos\phi_o)}{4\pi - 2\pi(1 - \cos\phi_o)} = \frac{1 - \cos\phi_o}{1 + \cos\phi_o}$$

$$\text{where } \phi_o = \sin^{-1} \frac{R_s}{\lambda + R_s}$$

For the test gases, helium, nitrogen and argon, the pressure at which experiments are run is 10^{-3} to 10^{-2} torr. Table 2-1

gives values of η for the 3/8-inch diameter balls used for all experiments.

TABLE 2-1 FREE MOLECULAR PARAMETER

Gas	Helium			Nitrogen				Argon		
	10^{-3}	5×10^{-3}	10^{-2}	10^{-3}	5×10^{-3}	10^{-2}	2×10^{-2}	10^{-3}	5×10^{-3}	10^{-2}
Pressure in Torr	10^{-3}	5×10^{-3}	10^{-2}	10^{-3}	5×10^{-3}	10^{-2}	2×10^{-2}	10^{-3}	5×10^{-3}	10^{-2}
λ CM	14.72	2.94	1.47	4.80	.96	.48	.24	6.67	1.33	.67
η	2.5×10^{-4}	4.9×10^{-3}	1.5×10^{-2}	2.0×10^{-3}	2.9×10^{-2}	7.1×10^{-2}	1.45×10^{-1}	1.1×10^{-3}	1.8×10^{-2}	4.8×10^{-2}

Experiments performed by Benson (9) for essentially the same geometry presented here showed that noticeable transition occurred starting at 2×10^{-2} torr for nitrogen. The usual criterion used to study the free molecular nature of a gas is the Knudsen number K_n defined as the mean free path / a characteristic system dimension. Knudsen number is defined to indicate the number of molecules unaffected by collision with other molecules and is roughly equivalent to $\frac{1}{\eta}$. Studies by Thomas documented by Wachmann (15) showed that at $K_n = 12$ conditions were quite free molecular for hot wire heat transfer studies. $K_n > 10$ is generally assumed to be free molecular.

2-5 Surface Roughness Model

Values of σ greater than 1.0 are possible if some of the reflected molecules are scattered back opposite to the incident tangential direction. A simple model is presented here to show how roughness could produce such a condition.

As a first approximation, a rough surface might be considered to consist of furrows with flat bottoms and sides that slope at an angle ψ to the surface normal. Figure 2-7 shows one furrow in cross section. When related to ball geometry, the surface normal is a ball radius and the furrow runs along a longitudinal line.

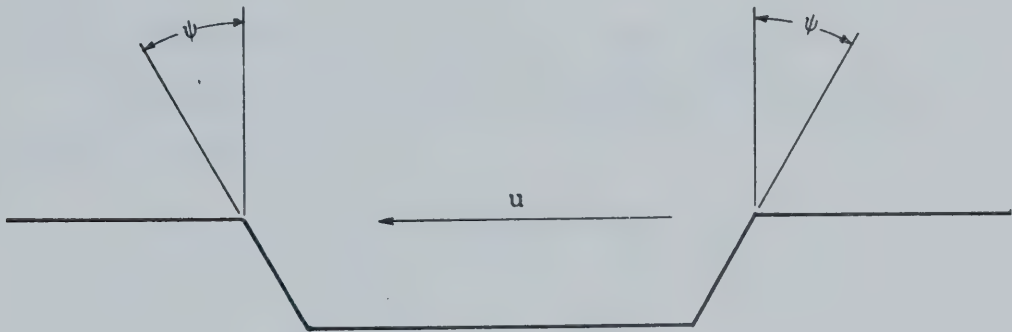


FIGURE 2-7 FURROW CROSS-SECTION

The first step in the solution is to determine incident momentum on each sloping face, which can be done approximately using equations given by Patterson (16).

Considering first a small area dA inclined to a Maxwellian stream of gas with a macroscopic drift velocity u , the surface normal \hat{n} being inclined at an angle ψ to

this velocity. Velocity coordinates are fixed as shown in figure 2-8.

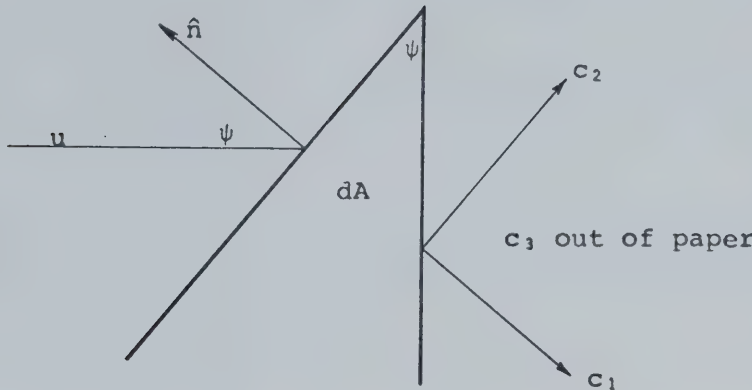


FIGURE 2-8 COORDINATE SYSTEM FOR TRANSLATING GAS

$$\text{The non-dimensional quantities } C = \frac{c}{c_m} = \frac{c}{\sqrt{2kT/m}},$$

$$\text{and } S = \frac{u}{c_m}$$

are defined, where S is termed the speed ratio.

The number of particles N_i , incident on area dA in time dt is given by

$$N_i = \frac{nc_m}{\pi^{3/2}} \int_{c_1=-\infty}^{c_1=\infty} \int_{c_2=-\infty}^{c_2=\infty} \int_{c_2=-\infty}^{c_3=\infty} (c_1 + S \cos \psi) e^{-(c_1^2 + c_2^2 + c_3^2)} dc_3 dc_2 dc_1 dA dt. \quad (2-13)$$

Evaluating 2-13

$$N_i = \frac{nc_m}{2\sqrt{\pi}} [\exp(-S^2 \cos^2 \psi) + \sqrt{\pi} \{1 + \text{erf}(S \cos \psi)\} S \cos \psi] dA dt. \quad (2-14)$$

Similarly the incident momentum normal to area dA is given by

$$P_i = \frac{1}{2} n m c_m^2 \left[\frac{1}{2} (1+2S^2 \cos^2 \psi) \{1+S \cos \psi\} + \frac{S}{\sqrt{\pi}} \cos \exp(-S^2 \cos^2 \psi) \right] dA dt. \quad (2-15)$$

Also the incident momentum tangent to area dA is given by

$$T_i = \frac{1}{2} n m c_m^2 S \sin \psi \left[\frac{1}{\sqrt{\pi}} \exp(-S^2 \cos^2 \psi) + \{1 + \text{erf}(S \cos \psi)\} S \cos \psi \right] dA dt. \quad (2-16)$$

This information can be applied to solve the momentum transfer problem for the geometry of figure 2-7, redefined more completely in figure 2-9.

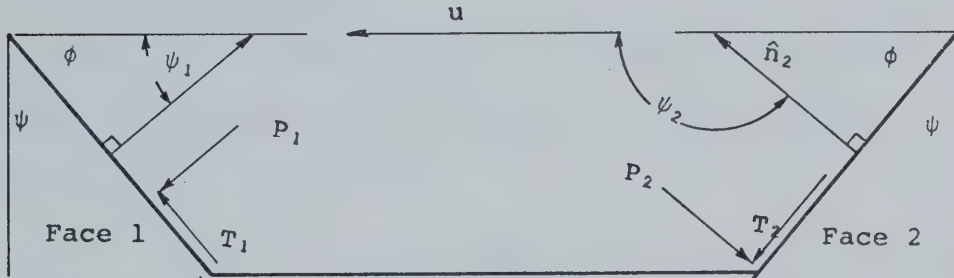


FIGURE 2-9 INCIDENT MOMENTUM ON MOVING FURROW

ϕ is defined as $\pi - \psi$ to facilitate later comparison with experimental results. By geometry $\psi_2 = \pi - \psi_1$, and $\psi_1 = \psi$. τ_i the momentum incident on face 1 parallel to u is given by

$$\tau_{i1} = P_1 \cos \psi + T_1 \sin \psi. \quad (2-17)$$

Similarly

$$\tau_{i2} = -P_2 \cos \psi + T_2 \sin \psi. \quad (2-18)$$

These relationships are approximate since the derivations of equations 2-14 to 2-16 assumed c_2 to be integrated

between limits $-\infty$ to $+\infty$, which implies that molecules can strike the face from any angle in the hemisphere above that face. For $\phi > 0$, this is not true because then no molecules penetrate upwards through the furrow floor.

Using this approximate incidence model it is now possible to predict a macroscopic σ for that portion of area of the rough ball which is inclined at angle ψ . The assumption that a face 2 occurs as often as a face 1 will be made for both diffuse and specular reflection.

(a) Specular Reflection.

Figure 2-10 shows the reflection expected from the incident situation shown in figure 2-10. T_1' is the reflection of T_1 and so on.

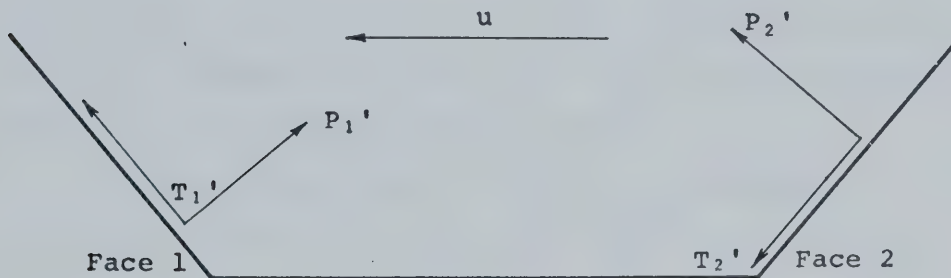


FIGURE 2-10 SPECULAR REFLECTION FROM FURROW

For specular reflection, $T_1' = T_1$ and $T_2' = T_2$ while $P_1' = -P_1$ and $P_2' = -P_2$.

The net reflected momentum τ_r tangent to the ball surface summed over faces 1 and 2 will be

$$\tau_r = T_1' \sin\psi + T_2' \sin\psi - P_1' \cos\psi + P_2' \cos\psi, \quad (2-19)$$

where τ_r is positive in the direction u.

Using equations 2-15 and 2-16 with the appropriate angles and noting the relationship between the primed and unprimed momentum variables, equation 2-19 becomes

$$\begin{aligned} \tau_r = \frac{1}{2} nmc_m^2 & \left[\sin^2\psi \frac{2S}{\sqrt{\pi}} e^{-S^2 \cos^2\psi} + 2 \sin^2\psi \operatorname{erf}(Scos\psi) Scos\psi \right. \\ & \left. - \cos\psi (1+2S^2) \operatorname{erf}(Scos\psi) - \cos^2\psi \frac{2S}{\sqrt{\pi}} e^{-S^2 \cos^2\psi} \right] \end{aligned} \quad (2-20)$$

for unit area and time.

Examination of equation 2-20 shows that $\tau_r (\psi = \frac{\pi}{2}) = \frac{nmc_m^2 S}{\sqrt{\pi}}$ which is twice the answer obtained in equation 2-2

for the incident tangential momentum on the smooth ball.

Since for the smooth case $\tau_r = \tau_i$ for specular reflection, and in the present case face 1 plus face 2 gives two unit areas, the answers agree as they should.

From the definition $\sigma = \frac{\tau_i - \tau_r}{\tau_i}$ we can evaluate σ . τ_i will be defined as $\tau_i (\psi = \frac{\pi}{2}) = \frac{nmc_m^2 S}{\sqrt{\pi}}$ since that is

the definition used for the evaluation of σ from experimental results on both sand blasted and smooth balls.

Substituting for τ_i and τ_r gives

$$\begin{aligned} \sigma = & \left\{ \frac{2S}{\sqrt{\pi}} + \frac{2S}{\sqrt{\pi}} \exp(-S^2 \cos^2\psi) (\cos^2\psi - \sin^2\psi) + \operatorname{erf}(Scos\psi) 2S^2 \cos^3\psi \right. \\ & \left. + \cos\psi \operatorname{erf}(Scos\psi) \right\} \left/ \frac{2S}{\sqrt{\pi}} \right. . \end{aligned} \quad (2-21)$$

Experiments presented in chapter V show that σ is

independent of angular speed of the ball, and therefore the speed ratio. Equation 2-21 does not indicate this to be true. For small S however, it can be shown that $\sigma \neq \sigma(S)$ by the analysis following. In the experimental results, the largest speed ratio occurs for argon with the ball rotating at 1000 revolutions per second. This yields a value $S = .075$.

The expansions

$$\text{erf}(S \cos \psi) = \frac{2}{\sqrt{\pi}} \left(S \cos \psi - \frac{S^3 \cos^3 \psi}{3} + \frac{S^5 \cos^5 \psi}{5} - \dots \right) \quad (2-22)$$

and

$$\exp(-S^2 \cos^2 \psi) = 1 - S^2 \cos^2 \psi + \frac{S^4 \cos^4 \psi}{2} - \dots \quad (2-23)$$

can be used to modify equation 2-21. Since $S^2 < 5.6 \times 10^{-3}$, any term of order S^2 times a previous term can be neglected, since the experimental scatter in measuring σ is at least 2%. This reduces equations 2-22 and 2-23 to only one term each, which if substituted in equation 2-21 yields

$$\sigma = 3 \cos^2 \psi. \quad (2-24)$$

Equation 2-24 is the tangential momentum accommodation coefficient for the sloped part of a pitted surface for specular reflection at low speed ratio. To evaluate the true σ , the ratio of sloping to flat area would have to be established.

(b) Diffuse Reflection.

Figure 2-11 shows the reflection for a diffuse interaction.



FIGURE 2-11 DIFFUSE REFLECTION FROM FURROW

As in the specular case, P_1' and P_2' are the reflected normal momentum and T_1' and T_2' are 0 since the diffuse reflection is symmetric. To assess P_1' and P_2' a fictitious gas is assumed to be beneath each of face 1 and face 2. The effusion of these imaginary stationary Maxwellian gases at surface temperature gives the same velocity distribution as an ideal diffuse reflection.

The incident number of molecules on faces 1 and 2, N_1 and N_2 , can be calculated from equation 2-14 where $\psi = \psi$ and $\pi - \psi$.

This gives

$$N_1 = \frac{nc_m}{2\sqrt{\pi}} \left[e^{-S^2 \cos^2 \psi} + \sqrt{\pi} \{1 + \text{erf}(S \cos \psi)\} S \cos \psi \right] \quad (2-25)$$

$$N_2 = \frac{nc_m}{2\sqrt{\pi}} \left[e^{-S^2 \cos^2 \psi} - \sqrt{\pi} \{1 - \text{erf}(S \cos \psi)\} S \cos \psi \right]. \quad (2-26)$$

The fictitious gases must have number densities n_1' and n_2' such that the flux back and forth across the faces are equal, so

$$\frac{n_1' c_m}{2\sqrt{\pi}} = N_1 \quad (2-27)$$

and $n_2' c_m$

$$\frac{n_2' c_m}{2\sqrt{\pi}} = N_2. \quad (2-28)$$

Since $S = 0$ for the fictitious gas,

$$P_1' = \frac{1}{4} n_1' m c_m^2 \quad (2-29)$$

$$P_2' = \frac{1}{4} n_2' m c_m^2. \quad (2-30)$$

From figure 2-12 it can be seen that

$$\tau_r = P_2' \cos\psi - P_1' \cos\psi. \quad (2-31)$$

Using the definition $\sigma = \frac{\tau_i - \tau_r}{\tau_i}$ and $\tau_i = \frac{n m c_m^2 S}{\sqrt{\pi}}$ as in the specular case, and using equation 2-25 to 2-31 we find that $\sigma = 1 + \frac{\pi}{4} \cos^2\psi$.

In this case, no approximation is required to make σ independent of S .

(c) Comparison of Specular and Diffuse Reflection.

Table 2-2 and figure 2-12 present a comparison of σ for each type of reflection on that part of the surface which is inclined.

It can be seen that when the surface is inclined at more than about 40° to a tangent to the ball, specular reflection produces a greater σ than diffuse.

TABLE 2-2

σ VALUES FOR DIFFUSE AND
SPECULAR REFLECTION FROM FURROW

ϕ DEGREES	σ DIFFUSE	σ SPECULAR
0	1.000	0
10	1.024	.090
20	1.092	.351
30	1.196	.750
40	1.325	1.240
50	1.461	1.760
60	1.589	2.250
70	1.693	2.649
80	1.762	2.909
90	1.785	3

For the specular case σ can be greater than for the diffuse case because molecules will be reflected back against the stream from face 1 with more tangential velocity. It must be noted that for any surface other than an ideal

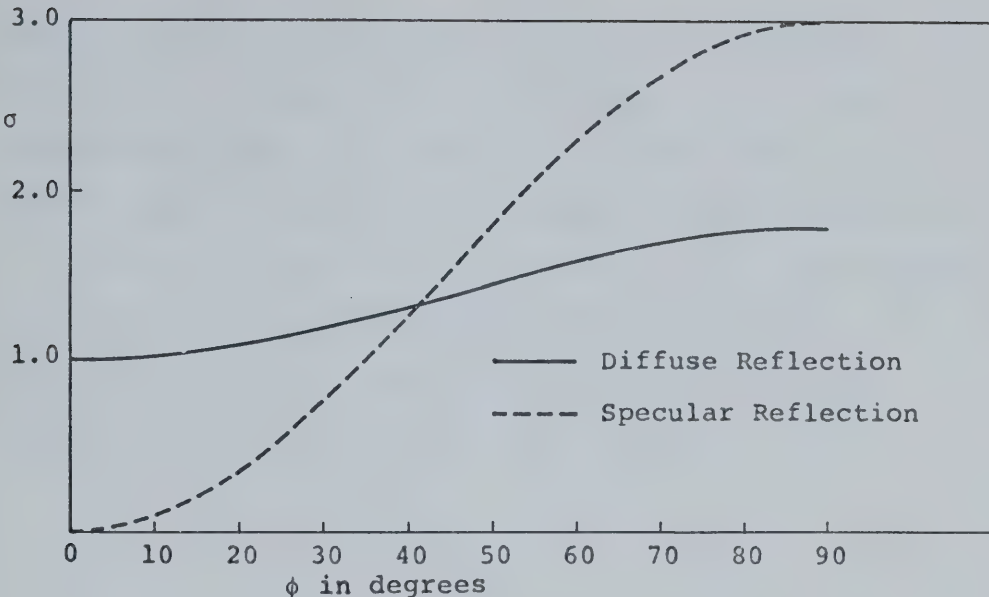


FIGURE 2-12 σ VALUES FOR DIFFUSE AND
SPECULAR REFLECTION FROM FURROW

smooth one, σ actually includes a component of normal momentum transfer. The difficulties of precise measurement of topography down to atomic dimensions makes it a problem to separate the tangential and normal momentum effects. Thus, the empirical coefficient, σ , is a convenient and useful way to characterize a rough or smooth surface.

Further information on the qualitative validity of the rough surface analysis is provided in a paper by A.J. Jerofeev (17) who obtained information about reflection from a rough surface by computer visualizations of large number of incident molecules. The rough surface was made up of planks whose horizontal and vertical lengths were chosen from random numbers. Reflections were done for diffuse and specular cases for two situations; average vertical length equal to average horizontal length, and

average vertical length equal to one half horizontal length. The equal length situation produced greater σ for the specular case with both cases being greater than 1.0. At vertical length one half of horizontal, σ was greater than 1.0 for the diffuse case and less than 1.0 for the specular case. This agrees qualitatively with our model at ψ of 45° and 27° using the fact that $\phi_{AV} = \tan^{-1}$ (average vertical length/average horizontal length).

CHAPTER III

APPARATUS

3-1 The Suspension, Turning and Counting Systems.

A schematic of the suspension system is shown in figure 3-1. Suspension was achieved by an electromagnet placed above the ball, and fed with the precise current required such that the magnetic force equalled the gravitation force. Such a suspension is basically unstable in that a small upward displacement of the ball results in increased magnetic coupling.

Stability was achieved by means of an electronic circuit with feedback from a photodiode sensor to control the current to the suspension magnet. A light source and photodiode were positioned so that the suspended ball cut off part of the light to the photodiode. Vertical movement of the ball would then either increase or decrease the light reaching the photodiode and a correction to the suspension current would be made. The electronic circuits used are presented in Appendix II.

After removing the vertical instability, one is still faced with a horizontal instability. A small horizontal displacement of the ball reduces the magnetic coupling, which gives rise to a downward displacement and then a corresponding increase in electromagnet current. This pulls the ball back up and into line with the electromagnet

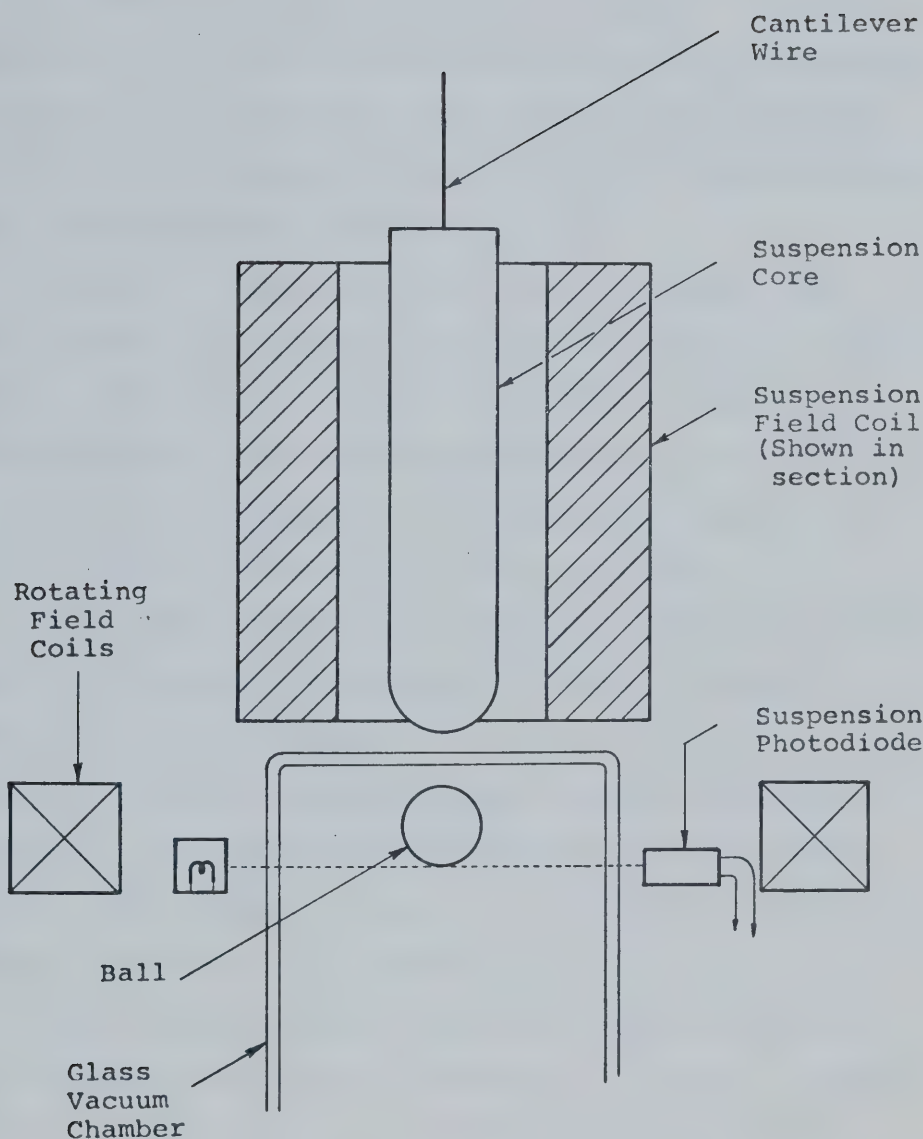


FIGURE 3-1 SUSPENSION SYSTEM SCHEMATIC

and in the absence of damping an oscillatory motion results. This problem was overcome by mounting the electromagnet core on a vertical cantilever wire spring, which allows the core to follow the horizontal motion of the ball. The spring then returns the core and therefore the ball to the stable position. Oil surrounding the magnet core damps the vibration of the core as well as acting as a coolant for the entire electromagnet assembly.

Figure 3-1 also shows two of the four field poles which serve to turn the ball as the rotor of an AC induction motor. The poles are mounted on a ferrite ring with opposite poles having reverse polarity, the two sets being driven 90° apart in phase. The poles are excited by an 8250 Hz signal produced by an audio oscillator.

To determine the angular velocity of the ball, a small semicircumferential longitudinal scratch is engraved on the ball, and a photodiode is placed so as to accept light reflected from the suspension light source. Once each revolution, the scratch passes through this reflection position and produces a pulse due to the lower light intensity reflected by the scratch.

After suitable amplification, the photodiode signal is fed through conditioning circuits to a digital counter which counts the number of revolutions in 10 seconds. This count is then recorded by a digital printer. The circuits involved are discussed in Appendix II.

To avoid any possibility of double counting, the scratch is always maintained in a vertical position by permanently magnetizing one end on the ball.

The balls used in experiments were of the type used for bearings and were chosen for their excellent tolerances on size and roundness and smooth ground finish. The balls were 3/8 inch in diameter and made of AISI 440 stainless steel. The diameter of the glass vacuum envelope was 1-1/2 inches.

The subliming filament was located adjacent to the ball inside the vacuum envelope and consisted of a length of .005 inch tungsten wire wound around a piece of high purity .015 inch silver wire. The tungsten was spot welded to thick leads of a Varian nickel wire feedthrough. By passing about 2 amps through the tungsten, the silver was made to sublime. Baffles were appropriately placed to prevent subliming silver from covering the glass vacuum envelope where the suspension photodiode and light bulb acted. After careful outgassing, silver could be sublimed with little system pressure rise. Gold used for sublimation was obtained by cutting strips from pure foil which were then wound with tungsten wire in the same manner as the silver.

3-2 Residual Drag.

Eddy currents induced in the rotating ball produced some magnetic drag which had to be accounted for to determine the deceleration caused by the gas alone. The drag, termed residual magnetic drag, was equivalent to the drag produced by a gas at a pressure of up to 5×10^{-4} torr. Residual drag was determined at low pressure and a corresponding correction was applied to high pressure measurement.

Causes of magnetic drag are:

- 1) Lateral oscillations of the ball which cause fluctuating magnetic fields on the ball and therefore eddy currents.
- 2) Electric noise in the suspension electromagnet current.
- 3) Magnetic inhomogeneity of the balls.

Equation 2-7 can be rewritten as

$$\sigma = \frac{\rho R_s \sqrt{\frac{2\pi kT}{m}} \ln \frac{f_1}{f_2 + f_R}}{5p t_2 - t_1} \quad (3-1)$$

where f_1 and f_2 are the measured revolutions per second, and f_R is a correction for the residual drag.

3-3 Energy Accommodation Apparatus.

The hot filament apparatus for measuring α is shown schematically in figure 3-2. This figure shows the filaments

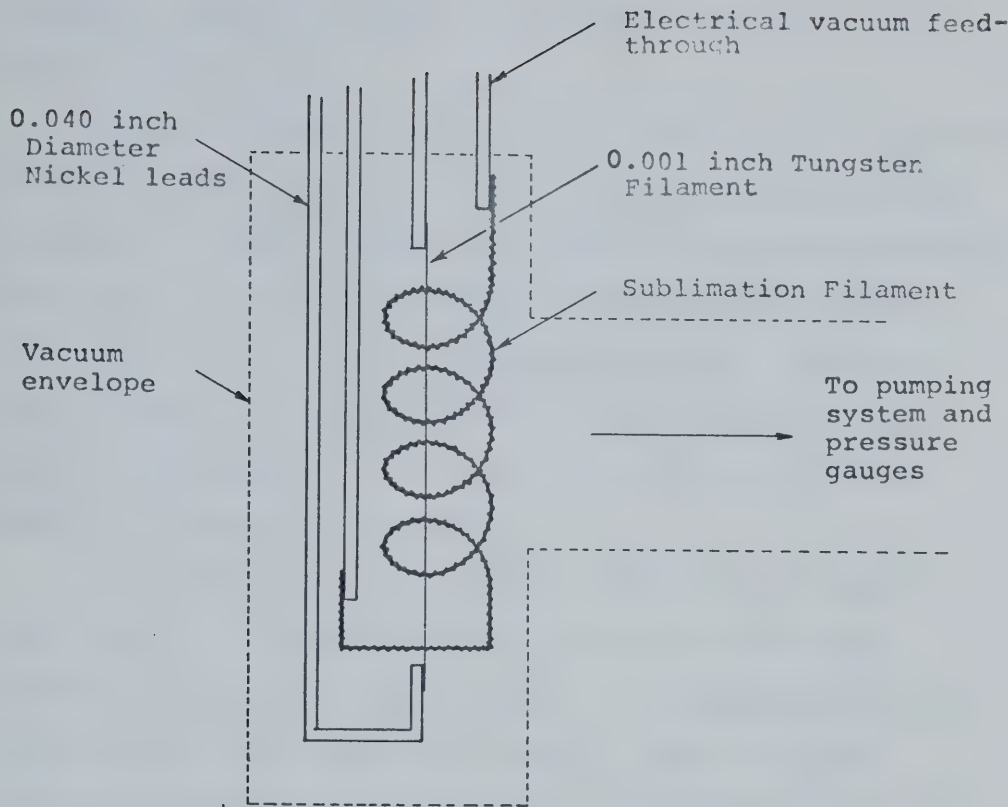


FIGURE 3-2 ENERGY ACCOMMODATION APPARATUS

and a representation of the electrical feedthrough and vacuum system walls. The tungsten filament from which a was determined was of 0.001 inch diameter and 10.98 centimeters long, and was cut from a spool of wire obtained from Sylvania Precision Materials. This was chosen because of its electropolished finish and 3% tolerance on diameter. The subliming filament consisted of a 0.005 inch tungsten wire wound around high purity 0.015 inch silver wire, which was looped in a spiral about the fine filament. Both

filaments were spot welded to the 0.040 inch nickel of a Varian feedthrough.

Average filament temperature is sensed by its resistance using the temperature coefficient of resistivity property. Appendix III gives results of a temperature versus resistance calibration of the tungsten filament as determined from measurements in a constant temperature bath. A stainless steel filament corresponding to the ball material could not be used because of the low sensitivity of stainless steels to changes in temperature.

Two measurements were made to determine the power loss from the filament, the DC voltage drop across the filament, and the DC voltage across a precision 20.05 ohm resistor in series with the filament. These voltages were measured with accurate digital voltmeters which were able to read to about 0.5% of a typical voltage drop. The ratio of filament and precision resistor voltage drops ΔV_{FIL} and ΔV_R were used to calculate filament resistance R_{FIL} , and DC heating current $I_{DC} = \Delta V_R / 20.05$. Power input to the filament was then determined.

An electronic system was developed which kept the filament resistance and therefore average temperature constant for various power loss conditions. This system, which used a small AC sensing current to determine resistance, is described in Appendix II. The author wishes to express special thanks to Mr. Don McFarlane who, acting as a consultant, designed and built the circuits for this

system and the suspension system for the ball.

The temperature of the ends of the wire must be measured to allow for the approximate solution of the differential equation of the filament temperature (equation 2-11). A chromel-alumel thermocouple was spot welded to the short upper nickel lead on to which the filament is attached. This temperature was determined to be within $1-1/2^{\circ}\text{C}$ of room temperature for any normal heating current to the filament.

3-4 Vacuum System.

Figure 3-3 is a schematic of the vacuum system and figure 3-4 is a photograph of it which also shows the suspension system. The symbols in the schematic are based on those given in the Leybold Vacuum Handbook (18) with some additions as required. The ultra-high vacuum system was made of stainless steel and glass and was bakeable to 300°C in the area shown enclosed by the broken line envelope in figure 3-3. A Varian LD100 Leak Detector which contained a mobile pumping stand was used for rough and bakeout pumping. The unit contained an Edwards ED250 double stage roughing pump, a 40 litre per minute diffusion pump using Octoil, and a small single stage backing pump.

Ultra-high vacuum (UHV) was achieved with two sputter-ion pumps, a Varian 15 litre per second diode pump, and a G.E. 25 litre per second triode pump. Other pumping was

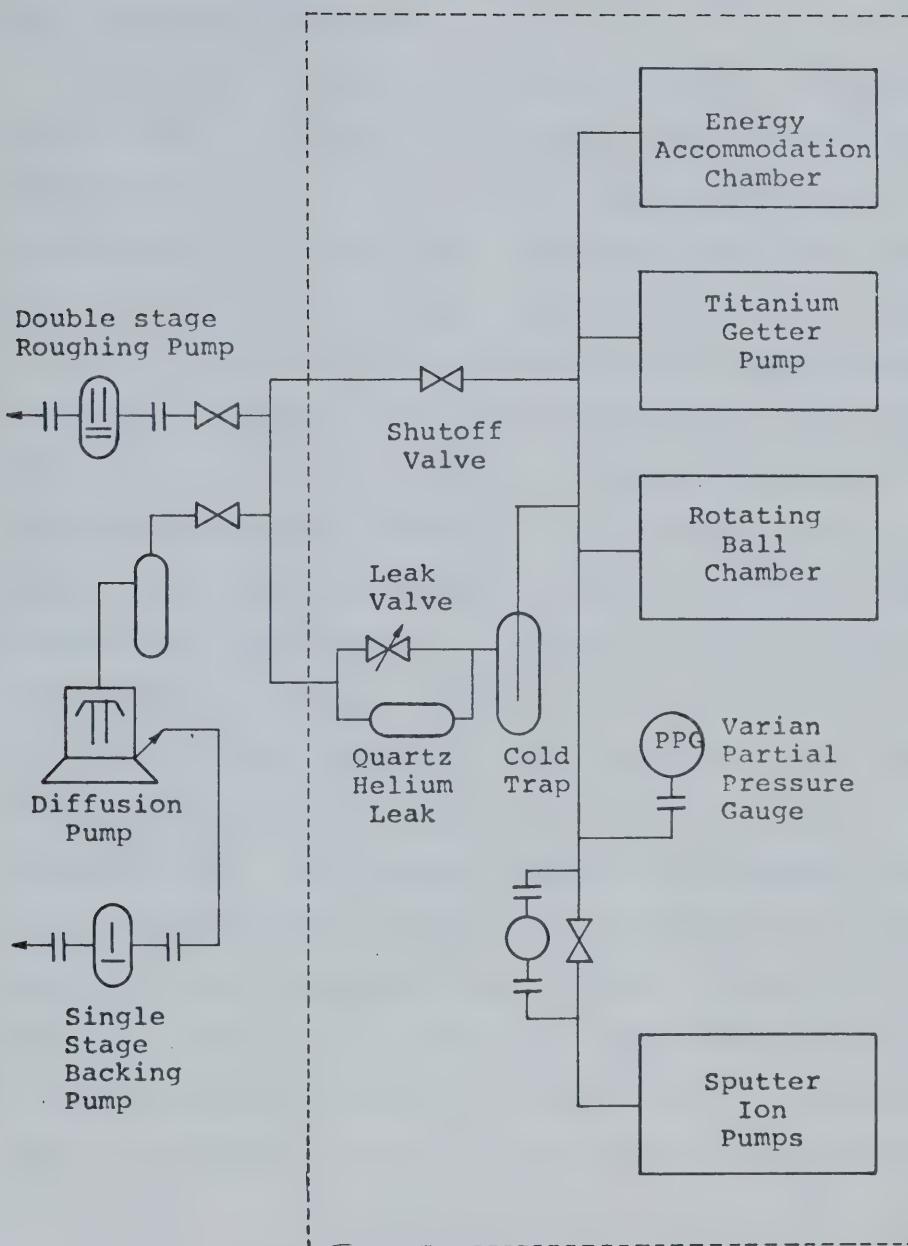


FIGURE 3-3 SCHEMATIC OF VACUUM SYSTEM

provided by a titanium sublimation getter pump cooled by water or liquid nitrogen.

A bakeable Varian shutoff valve was used to connect the UHV system to the diffusion pump. This type of valve closes leak tight by compressing a copper gasket against a stainless steel knife edge. All tube connections were made using OFHC copper gaskets pinched between knife edges.

Test gas pressures were measured with an MKS Baratron capacitance manometer with a type 90H-3 head. This gauge consists of a metal membrane which deflects due to a pressure differential across it, the deflection being measured as a capacitance change between the membrane and two adjacent electrodes. An AC bridge circuit is used to monitor this capacitance change which is amplified and fed to a meter on the control unit. A remote output was fed to a time base chart recorder to give an automatic pressure signal. To correctly assess the meaning of the diaphragm deflection, one side (the reference side) was pumped down to a negligibly low pressure of about 10^{-9} torr by the sputter ion pumps, while the other side was at test pressures of about 10^{-3} to 10^{-2} torr. A shutoff valve was positioned so as to isolate the two arms of the head leading to the two sides of the diaphragm; this valve served also to remove the UHV pumps from the rest of the system so that tests could be done at static pressure. Normal UHV pumping and zeroing of the Baratron gauge was done with this valve open at pressures around 10^{-9} torr.

Admission of gas was achieved using a very fine Varian leak valve or, in the case of helium, by heated quartz tube. Gas impurities were removed as much as possible by the titanium getter pump and a liquid nitrogen trap. A more thorough discussion of this, and a description of the inlet piping is presented in section 4-2 on residual gas background.

A Varian partial pressure gauge was used to quantitatively identify impurities in the vacuum system at pressures below 5×10^{-5} torr. This gauge is a mass spectrometer which accelerates ions through a magnetic field in a radial path, the radius of which depends upon the charge to mass ratio of the ions. Gases of masses from 1 to 70 AMU can be resolved.

The partial pressure gauge was also operated as a total pressure gauge for pressure conditions below 5×10^{-4} torr where the Baratron no longer gave reliable readings.

CHAPTER IV
CALIBRATIONS AND ERROR ANALYSIS

4-1 Pressure Gauge Calibration.

The MKS Baratron Pressure Gauge was calibrated using a Consolidated Vacuum Corporation mercury McLeod Gauge readable from 10^{-4} torr to 10 torr, but with appreciable sensitivity only above 10^{-3} torr. The gauge is read in either the linear or the square law manner depending on pressure. A schematic of the calibration apparatus is shown in figure 4-1. All tubing to the left of the stopcock D was 1/4-inch diameter stainless steel tubing and to the right was 12 millimeter glass tubing. The length of this tubing from D to the unknown side of the Baratron was about 2 inches, and from D to the McLeod gauge was about 60 inches. All metal tube connections were made with Swagelock fittings, and these along with the ground glass connections and joints made by a glassblower were tested with a helium leak detector to be leak free. All steel and glass tubing was cleaned before assembly and flamed out prior to calibration. The calibration was a static one performed with valve C closed to isolate the diffusion pump, valve D open to join the McLeod and Baratron gauges and valve A closed so the reference side of the Baratron could be pumped by the ion pump. This reference pressure was below 10^{-6} torr and therefore negligible compared to test pressures. For a static system pressure

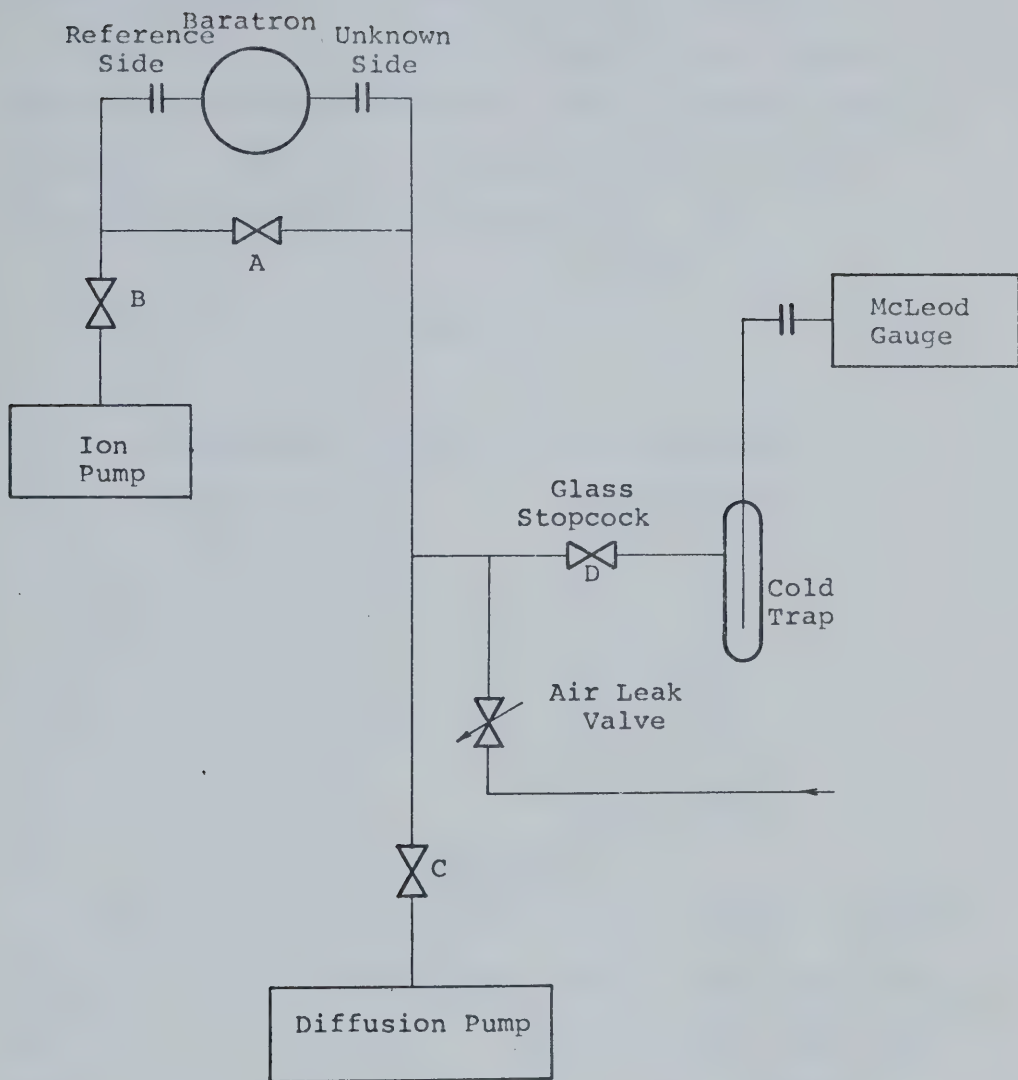


FIGURE 4-1 SCHEMATIC OF PRESSURE CALIBRATION APPARATUS

rises as the mercury rises due to changing system volume, therefore the Baratron reading was taken just as the mercury rose slowly to the McLeod gauge cutoff. At a constant mercury level, the Baratron reading remained

essentially constant, indicating little outgassing.

Results of a preliminary calibration test carried out with the cold trap filled with a dry ice-ethanol mixture are shown in table 4-1. This mixture was at -72°C as measured by an alcohol thermometer.

TABLE 4-1

PRELIMINARY BARATRON GAUGE CALIBRATION

Baratron Gauge reading in torr	McLeod Gauge reading in torr
1.1×10^{-3}	0.4×10^{-3}
1.18×10^{-2}	1.00×10^{-2}
4.60×10^{-2}	4.25×10^{-2}
4.940×10^{-1}	4.75×10^{-1}
4.592×10^{-1}	$4.48 \times 10^{-1}*$

*Trap at room temperature.

These results show major differences in the readings of the two gauges even at high pressure where the McLeod gauge has good readability. Two major errors exist in trapped McLeod gauge measurements at these pressures, thermal transpiration and mercury pumping. Thermal transpiration was probably not the major error, since the cold trap was particularly designed to be symmetric. A more likely cause of error is the pumping or migration of mercury vapour from the McLeod gauge and condensation in the cold trap. The flow of mercury vapour has been shown

to set up appreciable pressure gradients in a direction compatible with the differences noted here. Ishii and Nakayama (19) and Meinke and Reich (20) discuss this problem theoretically and experimentally.

To eliminate this error, it was decided to run the calibration with the cold trap at room temperature, the final reading of the preliminary set being taken in this manner. The room temperature trap gave a 2.4% difference in reading for the two gauges, while the cooled trap gave a 3.9% difference at roughly the same pressure in the 10^{-1} torr range.

The warm trap type of reading gives rise to an inherent error that mercury vapour can reach the Baratron gauge, and its vapour pressure will be measured as part of the Baratron reading. The McLeod gauge however, will ignore the partial pressure of mercury, since most of the mercury vapour will precipitate out when the gas is compressed in the glass capillaries. Since at 24°C, the test temperature, the equilibrium vapour pressure of mercury $p_{MV} = 1.70 \times 10^{-3}$ torr (21), this is a significant error for the pressure measurements of interest in these momentum accommodation studies. Calibrations carried out with a warm trap are given in table 4-2 and figure 4-2.

Table 4-2 gives Baratron and McLeod gauge pressures p_B and p_M and the difference between these two readings. The final column % Difference gives the relative error between McLeod and Baratron gauges when mercury vapour

TABLE 4-2

 BARATRON GAUGE CALIBRATION
 WITH ROOM TEMPERATURE TRAP

P_B Baratron Torr $\times 10^{-3}$	P_M McLeod Torr $\times 10^{-3}$	$P_B - P_M$ Torr $\times 10^{-3}$	% Difference $\frac{P_B - (P_M + P_{MV})}{P_B}$
4.2	2.2	2.0	4.8
4.8	3.0	1.8	2.1
7.6	5.8	1.8	1.3
9.6	7.6	2.0	3.1
15.4	13.2	1.8	0.6
19.0	16.9	2.1	2.1
36.3	33.8	2.5	2.2
51.3	47.8	3.3	3.1
72.2	67.5	4.7	4.2

pressure, p_{MV} , is added to the McLeod gauge reading. The % Difference column indicates a small error of about 1 to 5% in agreement between the two gauges. The intercept in figure 4-2 at zero McLeod gauge pressure is 1.8×10^{-3} torr which agrees well with published values of mercury vapour pressure. Accommodation calculations were done directly from p_B without recourse to this calibration and error was assumed to be 5%. Maximum observed Baratron drift over a test period was 2×10^{-4} torr, so p_B values less than

4×10^{-3} torr were assumed to have an error of $2 \times 10^{-4}/p_B$. Both error assumptions appear to be quite pessimistic.

4-2 Background Impurity.

Impurity of the gas will arise from two sources, the low pressure background before gas admission, and the impurity brought in with the gas. The low pressure background as determined by closing the valve to the sputter-ion pumps, gave a total pressure of 5×10^{-9} to 10^{-8} torr, and consisted mainly of hydrogen and some water vapour.

The gas admission system was described briefly in section 3-4. Copper tubing, leak free and thoroughly cleaned inside with steel wool and acetone was used for lines between commercial cylinders of gas and the leak apparatus. These lines were evacuated by a liquid nitrogen trapped oil diffusion pump to a pressure below 10^{-3} torr as measured by a thermocouple gauge. Upon valving off the diffusion pump, pressure rose slowly to less than 10^{-2} torr. Gas was let into these lines from gas bottles through a regulator to a pressure of one atmosphere. Gas was then leaked into the UHV system where a liquid nitrogen cold trap and a titanium getter pump removed further impurities. The titanium getter was not used when the test gas was nitrogen because nitrogen pumping would occur.

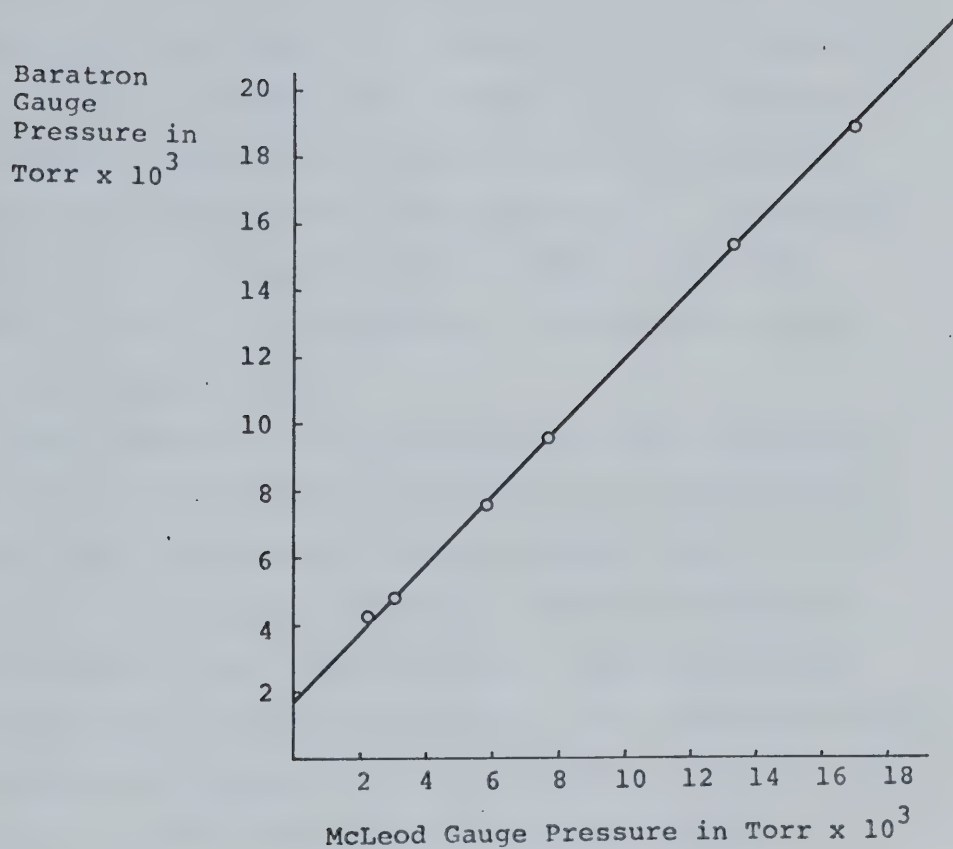


FIGURE 4-2 CALIBRATION OF BARATRON VERSUS
MCLEOD GAUGE PRESSURE FOR ROOM
TEMPERATURE COLD TRAP

4-2.1 Helium Admission.

The quartz tube for leaking helium, was a General Electric Model 22HL020 consisting of a thin quartz tube heated by a nichrome wire to temperatures up to 850°C. Young and Whetten of the General Electric Research Laboratory, Schenectady (22), reported very low impurities for gas admitted through one of these tubes. For tank helium which contained 120 parts per million of hydrogen and other impurities, they found hydrogen at 10 parts per million to be the only impurity gas above 1 part per million. They estimated hydrogen to have about 20% of the leak rate of helium.

The tank helium used in these experiments was quoted as being pure to 50 parts per million, and the addition of 10^{-2} torr of background in the entrance tubing would add about 15 parts per million to atmospheric pressure gas in tubing. Based on the work of Young and Whetten, it is expected that the impurities in admitted helium would be 10 parts per million. The cold trap and titanium getter would be expected to reduce this impurity somewhat.

The tank argon had impurities of about 100 parts per million which would be expected to reduce this impurity somewhat.

4-2.2 Argon Admission.

The tank argon had impurities of about 100 parts per million which would be admitted through the leak valve with the test gas. Since titanium does not pump argon, the getter pump was operated with argon tests and would reduce this contamination somewhat as would the cold trap.

4-2.3 Nitrogen Admission.

Tank nitrogen impurity was about the same as argon, however the nitrogen purity inside the UHV system would be lower since the getter pump could not be operated with nitrogen tests. Titanium adsorbs nitrogen readily with high pumping speed. In fact the getter pump was used to remove the nitrogen gas after testing. It is expected therefore that background impurity for nitrogen tests was above 10^{-7} torr.

4-2.4 Gettering Effectiveness

Tests showed the titanium getter to be effective in reducing background above 10^{-7} torr down to 10^{-8} torr for a period of more than 30 minutes, sufficient time for a test. Getter pumping was found to be most effective when the pump was cooled with liquid nitrogen, partly because the pump assembly eventually produced outgassing when uncooled. Unfortunately it was found to be impractical to cool with liquid nitrogen during tests because severe Baratron drift resulted from the changes in temperature produced. The getter pump could be operated without cooling for the low titanium deposition rate required at 10^{-7} torr. Hydrogen was found to be especially well pumped by the getter pump and water vapour and carbon monoxide are also well pumped.

Background contamination with helium as test gas is expected to be about 10^{-8} to 5×10^{-8} torr, background for argon 5×10^{-8} to 10^{-7} torr, and nitrogen 10^{-7} to

10^{-6} torr. The composition of contamination expected in these cases is uncertain due to imprecise knowledge of background constituents. Both gold and silver are relatively inert and rapid adsorption is not expected at room temperature. Wells and Fort (23) in work function studies of water vapour adsorption on gold, found detectable adsorption only at pressures above 10^{-6} torr. Information given in tables by Hayward and Trapnell (24), and by Lewin (25), indicate room temperature chemisorption of oxygen and possibly carbon monoxide on silver, and only possibly carbon monoxide on gold. Bagg and Bruce (26) measured adsorption of oxygen on silver at 473°K.

4-3 Error Analysis for Tangential Momentum Accommodation Coefficient.

Equation 3-1 shows the formulation for finding σ ,

$$\sigma = \frac{\rho R_s \sqrt{\frac{2\pi kT}{m}} \ln \frac{f_1}{f_2 + f_R}}{5pt} \quad (3-1)$$

where f_R is the residual drag correction added to the final frequency. The error in σ , expressed as $d\sigma$ is found by the chain rule of differentiation, to be

$$\begin{aligned} d\sigma = & \frac{d\sigma}{dp} dp + \frac{d\sigma}{dR_s} dR_s + \frac{d\sigma}{dT} dT + \frac{d\sigma}{dm} dm + \frac{d\sigma}{df_1} df_1 \\ & \frac{d\sigma}{dp} dp + \frac{d\sigma}{df_2} df_2 + \frac{d\sigma}{df_R} df_R + \frac{d\sigma}{dt} dt \end{aligned} \quad (4-1)$$

Dividing by σ , we get

$$\frac{d\sigma}{\sigma} = \frac{dp}{p} + \frac{dR_s}{R_s} + \frac{dT}{2T} - \frac{dm}{2m} + \frac{dp}{p} + \frac{dt}{t} \\ + \left(\frac{df_1}{f_1} - \frac{df_2}{f_2 + f_R} - \frac{df_R}{f_2 + f_R} \right) \Bigg/ \ln \left(\frac{f_1}{f_2 + f_R} \right). \quad (4-2)$$

Defining $\Delta f = f_1 - (f_2 + f_R)$,

$$\ln \frac{f_1}{f_2 + f_R} = \ln \frac{f_2 + f_R + \Delta f}{f_2 + f_R} = \ln \left(1 + \frac{\Delta f}{f_2 + f_R} \right);$$

which can be expanded in a series

$$\ln \frac{f_1}{f_2 + f_R} = \frac{\Delta f}{f_2 + f_R} + \frac{1}{2} \left(\frac{\Delta f}{f_2 + f_R} \right)^2 + \frac{1}{3} \left(\frac{\Delta f}{f_2 + f_R} \right)^3 + \dots \quad (4-3)$$

For practical measurements $\frac{\Delta f}{f_2 + f_R} < 0.1$; therefore the series will be truncated to one term, since the error analysis is quite approximate. This also means that

$$f_2 + f_R \approx f_1. \quad (4-4)$$

Substituting 4-3 and 4-4 into 4-2, we find that

$$\epsilon_\sigma \approx \epsilon_p + \epsilon_{R_s} + \frac{\epsilon_T}{2} - \frac{\epsilon_m}{2} + \epsilon_p + \epsilon_t + \epsilon_{f_1} + \epsilon_{f_1} + \epsilon_{f_2}; \quad (4-5)$$

where $\epsilon_\sigma = \frac{d\sigma}{\sigma}$, the relative error in the measurement of σ ,

with similar notation being adopted for the other variables, except that $\epsilon_{f_1} = \frac{df_1}{\Delta f}$, $\epsilon_{f_2} = \frac{df_2}{\Delta f}$ and $\epsilon_{f_R} = \frac{df_R}{\Delta f}$.

Assuming independent errors

$$\epsilon_\sigma \approx \left(\epsilon_p^2 + \epsilon_{R_s}^2 + \frac{\epsilon_T^2}{2} + \frac{\epsilon_m^2}{2} + \epsilon_p^2 + \epsilon_t^2 + \epsilon_{f_1}^2 + \epsilon_{f_2}^2 + \epsilon_{f_R}^2 \right)^{\frac{1}{2}} \quad (4-6)$$

Pressure error has been discussed in detail in section 4-1 and $\epsilon_p = .05$ will be assumed for test gas pressure

greater than 4×10^{-3} torr, but will be somewhat greater at lower pressure.

ϵ_{R_s} will be considered negligible since ball bearings are made to very exact tolerance of size. Ball mass was determined by weighing on a microbalance and agreed well with the manufacturer's specifications. Therefore ϵ_p is considered negligible. ϵ_t is also negligible since time was measured by an accurate electrical stopwatch.

Error $\epsilon_{f_1} = \frac{df}{\Delta f}$ is calculated below for a usual Δf of 10.0 revolutions per second. The uncertainty of count is 0.1 revolution per second when triggering is done properly. Correct trigger operation is indicated by the oscilloscope trace and by steadiness of frequency printout. Therefore, $\epsilon_{f_1} = \epsilon_{f_2} = .01$ or greater if Δf is smaller than 10.0 revolutions per second. From measurements $df_R = .05$ revolution per second except in a few cases, which will be noted individually. Therefore $f_R = .005$.

Temperature error might result from three sources; heating of the ball due to loss of kinetic energy, variation of room temperature and heating of the system walls near the ball by the suspension coil. Suspension coil heating will be small, since water was continuously circulated through the oil in which the coil was immersed.

Heating produced by loss of kinetic energy during deceleration can be estimated by finding the kinetic energy of the ball at its highest speed. The temperature rise of the ball resulting from all this energy being reduced to

thermal energy can be estimated. If ΔT is the theoretical temperature change, we find that

$$I\omega^2/2 = 4/3\pi\rho R_s^3 c_p \Delta T,$$

where c_p is the heat capacity of the ball material. For a speed of 1000 revolutions per second the temperature change is less than 2°C . Since such changes in kinetic energy occur over a period of about $1/2$ hour, ample time is available for radiation and molecular conduction heat transfer. Kinetic energy heating will be considered negligible. Extending this argument, heating from magnetic eddying effects which produce residual drag, will also be neglected.

Perhaps the most important temperature effect is the variation of room temperature, particularly for helium experiments with the heated quartz tube leak. Variation is estimated to be no more than 3°K which for a room temperature about 300°K gives $\epsilon_T = 0.01$.

An error in the value of σ measured could arise, if the mass of the incident gas molecules is not the same as that of the test gas due to impurities, particularly if the molecular weight of the impurities is very different from that of the test gas. In view of the discussion of impurities in section 4-2, this type of error will be assumed negligible.

Solving equation 4-6 with the values quoted for ϵ 's, we find that $\epsilon_\sigma = 0.053$. It can be seen that pressure error is by far the most important source of error.

CHAPTER V
RESULTS OF ROUGHNESS MEASUREMENTS

5-1 Examination of Surface Roughness.

Smooth and rough ball topography was examined using a scanning electron microscope, a brief description of which follows.

The scanning electron microscope, abbreviated SEM, operates much like a television system in that a specimen area is scanned by a thin beam of electrons incident on the surface as in figure 5-1. Some electrons incident on the target surface will be elastically scattered and are termed

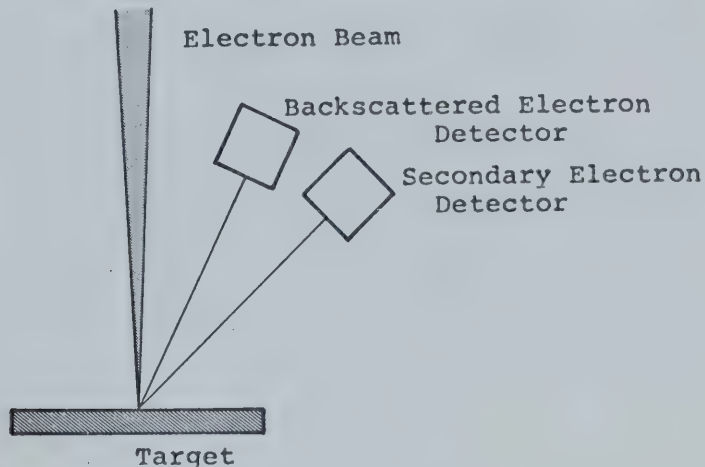


FIGURE 5-1 SCHEMATIC OF SCANNING ELECTRON MICROSCOPE BEAM AND TARGET

backscattered, while some will enter the specimen to produce secondary electrons, some of which will be re-emitted from the surface. Detectors measure quantities of each type of electron, producing a signal for a given position of the

scanning beam. A cathode ray tube with a similar scan produces a micrograph in which the amount of light at a particular position is determined by the detector signal. The more useful mode uses the re-emitted secondary electrons. Artifacts are determined by differences in contrast (ie numbers of collected electrons) as follows:

- a) High peaks on sharp edges where charge collects, produce many electrons and appear brighter on the micrograph.
- b) Faces of artifacts oriented toward the detector result in more collected electrons and therefore are brighter than those oriented away.
- c) Planes whose normals are along the axis of the beam receive the maximum incident electron density and will appear brighter than more sloping faces, subject to the condition of b).

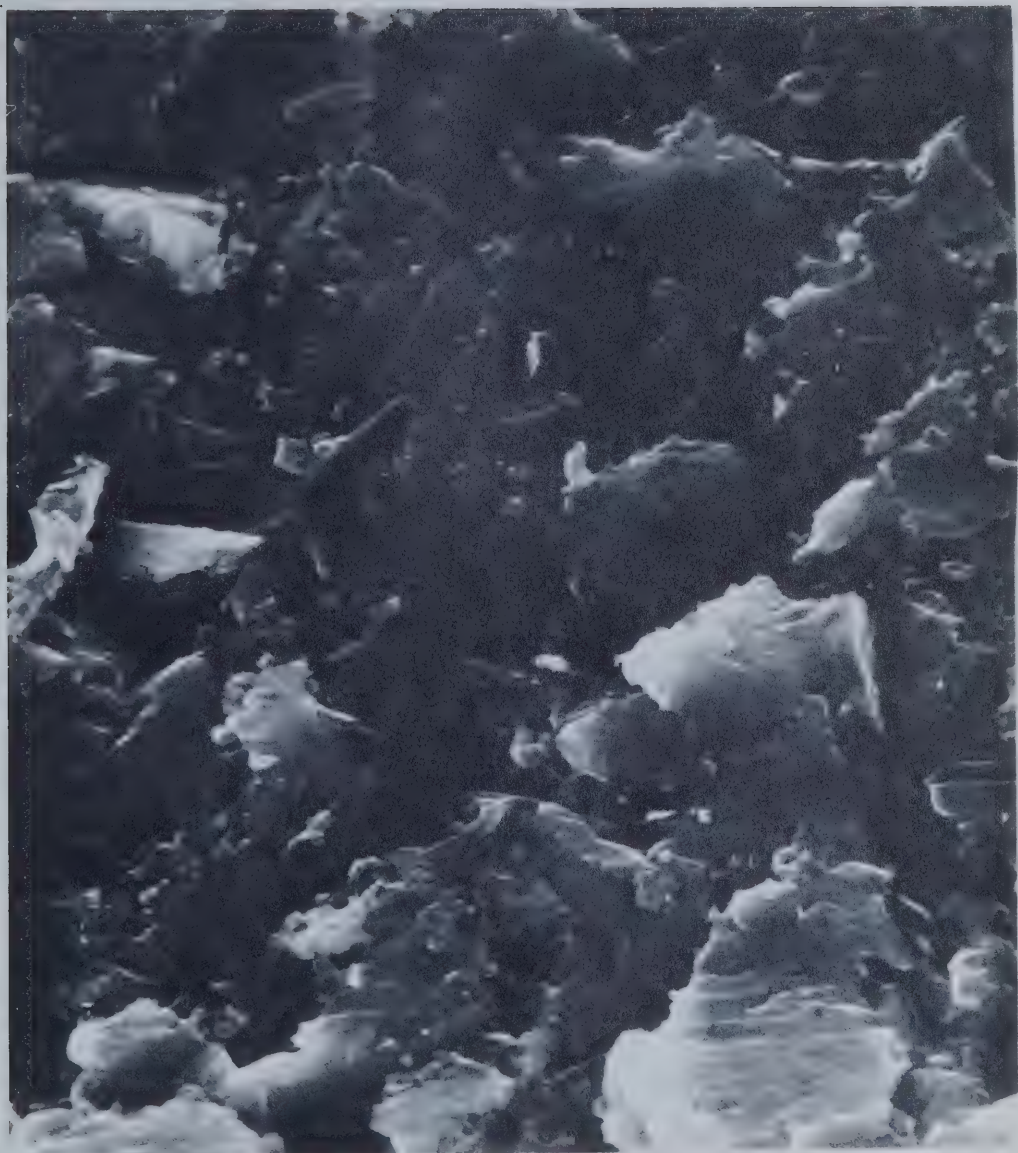
The ultimate resolution of the SEM in a horizontal plane is governed by the surface area of secondary electrons produced by the incident electron beam. In the instrument used in these investigations, a Cambridge Scientific Instrument Stereoscan S4, the beam width is 80A° , which produces a width of about 100A° of secondary electrons.

Figures 5-2 and 5-3 show prints of stereo micrographs of an area of the ball prepared by sandblasting. Figure 5-2 is taken with the electron beam normal to the surface (ie along a ball radius), while 5-3 was taken after rotating the specimen through 5° about a line which is horizontal on the micrograph. Table 5-1 gives results of measurements of



Magnification on micrograph 8000

FIGURE 5-2 SCANNING ELECTRON MICROGRAPH AT
NORMAL INCIDENCE OF SANDBLASTED
BALL



Magnification on micrograph 8000

FIGURE 5-3 SCANNING ELECTRON MICROGRAPH AT
5° FROM NORMAL INCIDENCE OF
SANDBLASTED BALL.

distance between the numbered points on the micrographs, a_0 being the distance at normal incidence and a_5 at 5° from the normal, measured in inches. Points were chosen as having the most spectacular height or depth as determined from viewing in a stereo viewer. Measurements of a_0 and a_5 were obtained by taping the micrographs to a wall and measuring heights with a cathetometer, an optical microscope, fitted with a vernier height gauge. Height d in table 5-1 is the difference in elevation of points in the same units as horizontal distance and θ is the angle of inclination between points, $\theta = \tan^{-1} \frac{d}{a_5}$. θ is positive clockwise about the tilt axis looking from left to right. The formula

$$d = \frac{-a_0 + a_5 / \cos 5^\circ}{\tan 5^\circ}$$

used to determine d is derived in Appendix IV.

a_0 _{TRUE} and d _{TRUE} are the actual sizes on the surface in microns as determined from the magnification of about 8000 on figure 5-1 and 5-2.

Supplementary information of the rough balls is obtained using a mechanical roughness meter, a Rank Taylor Hobson Tallysurf 4, which operates by moving a stylus across the specimen area. Unfortunately this apparatus could not be used on a specimen with a curvature as great as the 3/8-inch diameter balls. To obtain information, a piece of AISI 440 stainless steel bar was machined and ground smooth and flat and then sandblasted with the same grit used on the balls.

TABLE 5-1

 STEREOGRAPHIC ROUGHNESS MEASUREMENTS
 ON SANDBLASTED BALL

Location	a_0 Inches	a_s Inches	d Inches	θ Degrees	a_0 _{TRUE} Microns	d _{TRUE} Microns
1-1	.2480	.2453	-.021	- 5°	.5	.04
2-2	.1498	.1659	-.177	-47°	.3	.4
3-3	.2399	.2495	+.121	+27°	.5	.2
4-4	.2535	.2705	-.211	-40°	1.5	.4
5-5	.8609	.7799	-.925	-47°	1.7	1.8
6-6	.6372	.6171	-.205	-18°	1.3	.4
7-7	.1150	.1852	+.813	+82°	.2	1.6
8-8	.2251	.2929	+.791	+74°	.5	1.6
9-9	.3742	.2792	-1.082	-72°	.7	2.2

This flat piece was then inspected in the Tallysurf to obtain some approximation of a sandblasted ball surface. This procedure can be considered as only an approximation since it is unlikely that grain structure and hardness are identical.

Figure 5-4 is the output of the Tallysurf for flat steel surface. A horizontal dimension of one inch (the distance between broad vertical lines) represents .01 inch on the specimen, and one vertical division represents 20 μ inches. The centre line average roughness of this measurement is 12 μ inches as determined by a separate meter reading on the instrument.

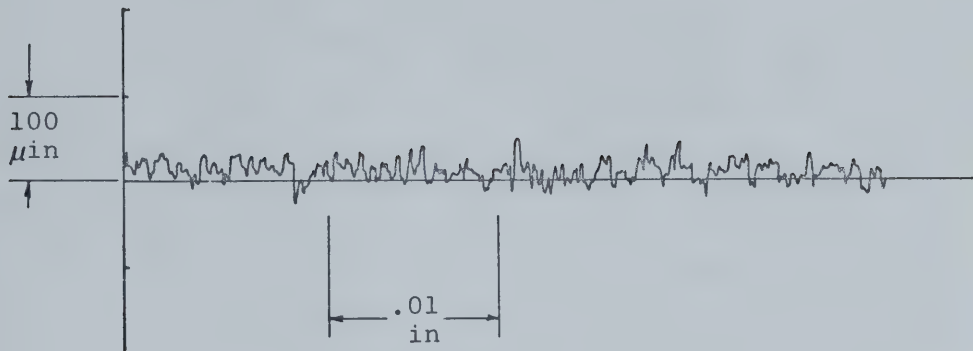


FIGURE 5-4 TALLYSURF TRACE FOR SANDBLASTED FLAT
AlS1 440 STAINLESS STEEL SURFACE

By counting the number of peaks per horizontal division, one can estimate an average distance between peaks of $10 \mu\text{m}$ which is larger by an order of magnitude than those artifacts chosen in the stereo micrographs. In fact, the stylus of the Tallysurf has a $2.5 \mu\text{m}$ tip dimension which makes measurement of that order uncertain and anything smaller impossible. Lower magnification micrographs of the balls show larger artifacts of 5 to $10 \mu\text{m}$ which agrees with the Tallysurf findings. The average roughness angle for the Tallysurf trace can be assumed to be

$$\theta_{AV} = \tan^{-1} \left(\frac{12 \mu\text{inch}}{10 \mu\text{m}} \right)$$

or $\theta_{AV} = 2^\circ$.

One can say that the sandblasted surface appears to be quite rough on a scale of $1 \mu\text{m}$ with very steep slope in some

areas. Superimposed on this is a larger size roughness of about 10 μm which has a much gentler slope.

Topographical measurements on the smooth ball proved to be more difficult due to the extreme smoothness of the surface. Figure 5-5 is a scanning electron micrograph of magnification 70,000 times on the print, with 1.2 inches on the print representing 2000A°. This micrograph shows little contrast except on a very small scale, where a coarse texture appears. Unfortunately, this coarse texture is smaller than 100A° which is the ultimate resolving power of the SEM, and therefore must be considered meaningless for topographical studies.

5-2 Thickness of Deposited Films.

Considerable difficulty was found in assessing or controlling the thickness of the silver or gold films. Sublimation was assumed to have taken place when the glass surrounding the sublimating filament darkened, the only quantitative information used being that a 700A° thick layer of silver is 95% reflecting (27). Thus when the glass surrounding the filament became opaque, it was assumed to be covered with silver of that order of thickness. An opaque layer was formed on the glass after 2 to 5 sublimations. Geometric considerations would give a thickness of about 5 to 10A° for 200A° on the glass. Thus a layer of that order is assumed for each deposited film termed "thin silver".



Magnification on micrograph 70,000

FIGURE 5-5 SCANNING ELECTRON MICROGRAPH AT HIGH MAGNIFICATION OF SMOOTH BALL

Thicker films had a greater but undetermined thickness, the criterion for deposition of these films being that a visible layer appeared on the ball. Since no colour change was noticed for thick silver deposition on the ball, a visible gold film was first placed on the ball and tests were run. Subsequent silver tests were then done over the gold films.

All results for gold films were for relatively thick surfaces, since it was quite difficult to control deposition rate. The gold was found to soften before sublimation and wet the surface of the tungsten filament, producing a new configuration. This new configuration produced much more rapid evaporation within a period of a few seconds.

CHAPTER VI
TANGENTIAL MOMENTUM AND
ENERGY ACCOMMODATION RESULTS

6-1 Experimental Procedure.

The procedure followed in experiments on a fresh thin unsintered layer of silver is outlined below:

- 1) Suspend ball and accelerate to test speed at ultra high vacuum condition.
- 2) Degas quartz leak (for helium tests) and subliming filament.
- 3) Measure initial residual drag and stabilize energy accommodation apparatus.
- 4) Fill liquid nitrogen in gas entrance system and deposit titanium gettering film to ensure maximum gas purity. Sublime silver onto ball.
- 5) Seal off sputter-ion pumps and the reference side of the Baratron by closing the appropriate valve.
- 6) Admit test gas to test pressure and evaluate σ and α .
- 7) For successive test pressures admit further gas and evaluate σ and α .
- 8) Open valve to sputter-ion pumps and evacuate system to low pressure.
- 9) Measure final residual drag.
- 10) Decelerate ball to rest.

This procedure varied somewhat for other types of metal surface layer as noted below. When the film was to be sintered, the following procedure was followed:

- 1) Suspend ball and turn extremely slowly.
- 2) Deposit silver.
- 3) De-suspend ball and sinter using electron bombardment or small oven.
- 4) Allow system to cool (2 to 4 hours).
- 5) Re-suspend ball, accelerate and measure initial residual drag.
- 6) Proceed as in steps 5) to 10) for the unsintered case.

When a gold or thick film of silver was to be sublimed it was found to be impossible to do so with the ball suspended because of the large amount of light produced. This light reflected off the ball into the photodiode circuit which sensed that the ball was in a position which was too high. Consequently suspension current was reduced and the ball dropped onto its support. It was therefore found necessary to remove the suspension magnets and lift the ball with a small permanent magnet. Manipulation of this magnet turned the ball so total coverage could be achieved. This procedure took considerably longer than deposition in the suspended position and allowed greater contamination, also possible damage to the deposited layer could occur due to crushing against the glass. The permanent magnet induced permanent magnetism into parts of the ball which increased the residual drag and therefore that error.

The electron bombardment sintering method was abandoned because heating was probably not very even (ie the side of the ball away from the filament would not receive the same energy as the near side). The oven sintering method provided much more control of ball temperature.

In total, 6 balls were used numbered chronologically, balls 2 and 4 being sandblasted. Tests on ball 1 and 2, termed "older tests", were done with only the diode sputter-ion pump and no titanium getter pump. In several of these tests with noble gases, no final residual drag measurement was obtained due to difficulties in starting the diode pump. This problem was eliminated by the addition of the easier starting triode pump. Thick layer tests were done on balls 5 and 6.

Residual drag for a given speed was estimated by a linear interpolation between the initial and final values. As noted in the error analysis, the two values did not normally differ greatly.

In cases where pressure varied rapidly equation 2-7 is not valid except for a linear variation of pressure with time. Using the equation

$$\int_{\omega_1}^{\omega_2} \frac{d\omega}{\omega} = - \int_{t_1}^{t_2} \frac{5\sigma p}{\sigma R_s} \sqrt{\frac{m}{2\pi kT}} dt_1$$

$\int_{t_1}^{t_2} pdt$ can be evaluated numerically using Simpson's

rule and σ can be found. This procedure was found necessary occasionally for a first admission of nitrogen.

6-2 Introduction to Tangential Momentum Accommodation Results.

Tangential momentum accommodation coefficient measurements and calculations are presented in sections 6-3 to 6-5.

For all results, a plot and table accompanies the written presentation. Identification of a particular test (ie one set of determinations of deceleration) is made by giving it the number of its notation in the appropriate table. A run is defined as one particular determination of deceleration at a particular pressure, several runs making up a test.

Each test is complete with information in the table of ball number, initial and final residual drag, surface preparation, values of individual accommodation coefficients, and an average accommodation coefficient for a test. In cases where two or more runs are at approximately the same pressure, only one admission of gas has been made. Small pressures changes occur for nitrogen due to adsorption on the system walls and in the getter pump, and for all gases occurs due to some leakage through the valve which isolates the pumps and the reference side of the Baratron from the rest of the UHV system.

Two values of σ are presented for each run, σ and

σ corrected. σ is that value calculated from equation 2-8 using the counter time assuming a print of count every 10 seconds. This value includes a small error because, although the count is done over 10 seconds, the printing is over a slightly longer period because of a small setup time. An electric stopwatch was used to determine this error and σ corrected was then calculated.

Most tests were done at pressures from 4×10^{-3} to 7×10^{-3} torr, the lower limit set to maximize pressure measurement accuracy, and the upper limit set to avoid possible problem of non-free molecular gas effects. Helium results were extended to pressures of 9×10^{-3} since transition effects are less severe for this gas than for argon or nitrogen.

6-3 Smooth Ball Results for Silver.

The results of silver deposited on unsandblasted silver balls are given in table 6-1 and figure 6-1 for nitrogen, table 6-2 and figure 6-2 for helium, and table 6-3 and figure 6-3 for argon. The average values of σ , termed σ_{AV} are presented for these tests in table 6a. Unless otherwise stated, the films are thin.

Table 6a indicates repeatability of values of σ_{AV} for each gas to about 2% for the thin films on ball 1 and 3 with slight variation in σ_{AV} found for different gases on

TABLE 6a

 AVERAGE TANGENTIAL MOMENTUM ACCOMMODATION
 COEFFICIENTS FOR SILVER ON SMOOTH BALLS

	Ball 1 Older Tests		Ball 3	Ball 5 Thick Films	Ball 6 Thick Films
σ_{AV} for Nitrogen	1c	0.94	1a 0.92		
	1d	0.95**	1b 0.91		
σ_{AV} for Helium	2e	0.98	2a 0.92	2c 0.86	
	2f	0.96	2b 0.93	2d 0.95 to 1.02	
σ_{AV} for Argon	3a	0.94			
	3b	0.92**			

** Electron bombarded to about 300°C.

these two balls. Electron bombardment sintering seems to have little if any effect on σ_{AV} .

TABLE 6-1

 VALUES OF σ FOR NITROGEN
 ON SMOOTH SILVER

(a) Ball 3, Unsintered.

Counter Time min	Pressure Torr $\times 10^3$	f_1 Rev per sec	f_2 Rev per sec	f_R Rev per sec	σ	σ Corrected
4	7.55	680.8	652.8	1.4	0.929	0.916
4	7.50	652.3	625.0	1.4	0.933	0.920
4	7.50	625.0	599.0	1.3	0.929	0.916
4	7.45	599.0	574.1	1.3	0.932	0.919
4	7.45	574.1	550.5	1.2	0.929	0.916

$$\sigma_{AV} = 0.92$$

Initial residue 0.37 Rev per sec per min
 at 700.0 Rev per sec

Final residue 0.29 Rev per sec per min
 at 520.0 Rev per sec.

TABLE 6-1 (CONT'D)

 VALUES OF σ FOR NITROGEN
 ON SMOOTH SILVER

(b) Ball 3, Unsintered.

Counter Time min	Pressure Torr $\times 10^3$	f_1 Rev per sec	f_2 Rev per sec	f_R Rev per sec	σ	σ Corrected
4	6.60	572.0	551.2	1.2	0.913	0.900
4	6.45	551.2	531.3	1.2	0.924	0.911
4	6.40	531.3	512.4	1.1	0.920	0.906
4	6.35	512.4	494.2	1.1	0.923	0.910
4	6.30	494.2	476.8	1.1	0.920	0.906
4	6.30	476.8	460.1	1.1	0.912	0.899

$$\sigma_{AV} = 0.91$$

Initial residue 0.32 Rev per sec per min

at 600.0 Rev per min

Final residue 0.26 Rev per sec per min

at 460.1 Rev per min.

TABLE 6-1 (CONT'D)

 VALUES OF σ FOR NITROGEN
 ON SMOOTH SILVER

(c) Ball 1, Older Test, Unsintered.

Counter Time min	Pressure Torr $\times 10^3$	f_1 Rev per sec	f_2 Rev per sec	f_R Rev per sec	σ	σ Corrected
3	4.50	882.0	864.8	0.8	0.961	0.946
3	5.40	848.9	829.5	0.8	0.945	0.931
3	6.20	811.7	790.3	0.8	0.955	0.941
3	7.70	769.1	744.4	0.8	0.944	0.930
3	7.70	719.4	696.4	0.8	0.938	0.924*

$$\sigma_{AV} = 0.94$$

* Resublimation with gas in system

 Initial residue 0.27 Rev per sec per min
 at 922.5 Rev per sec

 Final residue 0.25 Rev per sec per min
 at 685.0 Rev per sec.

TABLE 6-1 (CONT'D)

 VALUES OF σ FOR NITROGEN
 ON SMOOTH SILVER

(d) Ball 1, Older Test, Electron Bombarded.

Counter Time min	Pressure Torr $\times 10^3$	f_1 Rev per sec	f_2 Rev per sec	f_R Rev per sec	σ	σ Corrected
3	4.50	838.6	821.8	0.7	0.992	0.978
3	5.50	812.9	793.8	0.6	0.964	0.950
3	6.30	777.5	756.8	0.6	0.958	0.943
3	7.60	740.3	716.8	0.6	0.952	0.938

$$\sigma_{AV} = 0.95$$

Initial residue 0.23 Rev per sec per min
 at 870.0 Rev per sec

Final residue 0.18 Rev per sec per min
 at 707.5 Rev per sec.

TABLE 6-1 (CONT'D)
 VALUES OF σ FOR NITROGEN
 ON SMOOTH SILVER

(e) Ball 6, Unsintered, Thick Film.

Counter Time min	Pressure Torr $\times 10^3$	f_1 Rev per sec	f_2 Rev per sec	f_R Rev per sec	σ	σ Corrected
4	4.60	337.6	328.0	0.4	1.083	1.067
4	5.85	318.1	307.0	0.3	1.020	1.005
8	6.60	295.6	273.2	0.5	1.000	0.986
7	6.60	273.8	255.9	0.3	0.994	0.979
4	7.38	246.4	235.6	0.1	1.039	1.017

$$\sigma_{AV} = 1.01$$

Initial residue 0.12 Rev per sec per min
 at 341.5 Rev per sec

Final residue 0.01 Rev per sec per min
 at 231.8 Rev per sec.

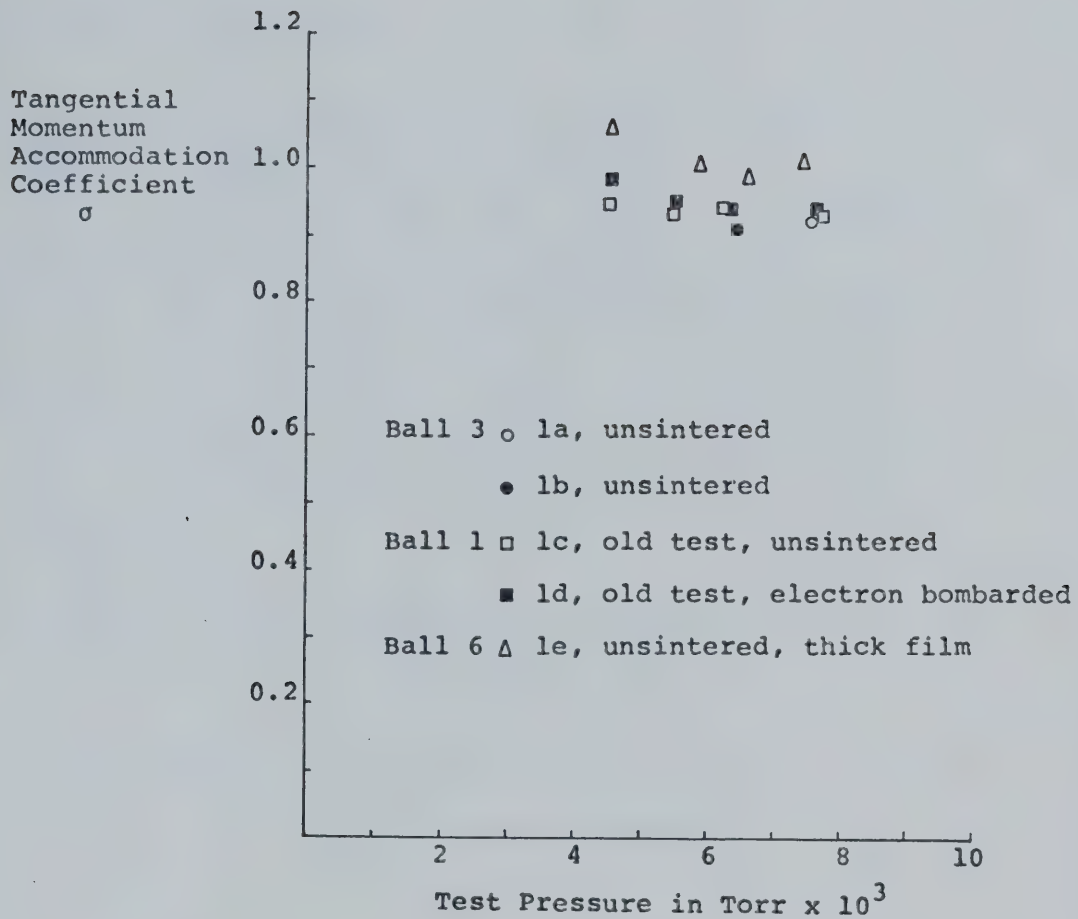


FIGURE 6-1 TANGENTIAL MOMENTUM ACCOMMODATION COEFFICIENT FOR NITROGEN ON SMOOTH SILVER

TABLE 6-2

 VALUES OF σ FOR HELIUM
 ON SMOOTH SILVER

(a) Ball 3, Unsintered.

Counter Time min	Pressure Torr $\times 10^3$	f_1 Rev per sec	f_2 Rev per sec	f_R Rev per sec	σ	σ Corrected
4	7.10	708.0	697.0	0.6	0.935	0.921
4	7.10	697.0	686.3	0.5	0.931	0.918
4	7.05	686.3	675.8	0.5	0.934	0.920
4	7.05	675.8	668.0	0.4	0.934	0.920

$$\sigma_{AV} = 0.92$$

Initial residue 0.15 Rev per sec per min
 at 710.0 Rev per sec

Final residue 0.10 Rev per sec per min
 at 655.0 Rev per sec.

TABLE 6-2 (CONT'D)

 VALUES OF σ FOR HELIUM
 ON SMOOTH SILVER

(b) Ball 3, Unsintered.

Counter Time min	Pressure Torr $\times 10^3$	f_1 Rev per sec	f_2 Rev per sec	f_R Rev per sec	σ	σ Corrected
4	7.05	930.7	916.4	0.6	0.944	0.935

Initial residue 0.14 Rev per sec per min
 at 967.0 Rev per sec

Final residue 0.15 Rev per sec per min
 at 888.0 Rev per sec.

TABLE 6-2 (CONT'D)

 VALUES OF σ FOR HELIUM
 ON SMOOTH SILVER

(c) Ball 5, Thick Film.

Counter Time min	Pressure Torr $\times 10^3$	f_1 Rev per sec	f_2 Rev per sec	f_R Rev per sec	σ	σ Corrected
5	5.00	363.4	358.2	0.8	0.874	0.861
4	6.80	347.9	342.8	0.6	0.859	0.848
4	8.15	330.0	322.1	0.6	0.883	0.870

$$\sigma_{AV} = 0.86$$

No initial residue

Final residue 0.15 Rev per sec per min

at 321.0 Rev per sec.

TABLE 6-2 (CONT'D)

 VALUES OF σ FOR HELIUM
 ON SMOOTH SILVER

(d) Ball 5, Thick Film.

Counter Time min	Pressure Torr $\times 10^3$	f_1 Rev per sec	f_2 Rev per sec	f_R Rev per sec	σ	σ Corrected
7	5.00	355.7	348.1	0.8	0.989	0.976
3	4.98	346.7	343.6	0.4	0.940	0.927
7	6.75	332.6	323.0	0.6	1.042	1.027
8	8.00	310.8	298.9	0.6	1.038	1.024
8	7.95	298.9	287.5	0.6	1.038	1.024
8	7.88	287.5	276.6	0.6	1.039	1.024

Initial residue 0.13 Rev per sec per min

at 369.0 Rev per min

Final residue 0.06 Rev per sec per min

at 267.5 Rev per min.

TABLE 6-2 (CONT'D)

VALUES OF σ FOR HELIUM
ON SMOOTH SILVER

(e) Ball 1, Old Test.

Counter Time min	Pressure Torr $\times 10^3$	f_1 Rev per sec	f_2 Rev per sec	f_R Rev per sec	σ	σ Corrected
3	4.20	778.0	772.0	0.5	1.010	0.995
3	5.20	763.1	756.1	0.5	0.999	0.984
3	6.40	743.5	735.3	0.5	0.973	0.958
3	7.20	721.5	712.4	0.5	0.996	0.981
3	7.70	702.7	693.4	0.5	0.979	0.964

$$\sigma_{AV} = 0.98$$

Initial residue 0.18 Rev per sec per min

at 790.0 Rev per sec

No final residue.

TABLE 6-2 (CONT'D)

 VALUES OF σ FOR HELIUM
 ON SMOOTH SILVER

(f) Ball 1, Old Test.

Counter Time min	Pressure Torr $\times 10^3$	f_1 Rev per sec	f_2 Rev per sec	f_R Rev per sec	σ	σ Corrected
3	4.20	704.4	699.5	0.1	0.994	0.979
3	5.70	691.3	684.9	0.1	0.961	0.946
3	6.60	677.3	670.0	0.1	0.968	0.954
2	7.50	661.1	655.6	0.1	0.981	0.966
2	8.50	644.0	638.0	0.1	0.971	0.957

$$\sigma_{AV} = 0.96$$

Initial residue 0.038 Rev per sec per min

at 712.5 Rev per sec

No final residue.

TABLE 6-2 (CONT'D)

 VALUES OF σ FOR HELIUM
 ON SMOOTH SILVER

(g) Ball 1, Older Test.

Counter Time min	Pressure Torr $\times 10^3$	f_1 Rev per sec	f_2 Rev per sec	f_R Rev per sec	σ	σ Corrected
5	4.20	949.5	937.4	1.3	0.977	0.963
2.5	5.00	911.7	904.9	0.6	0.979	0.965
2	7.00	874.6	867.5	0.5	0.971	0.956

$$\sigma_{AV} = 0.96$$

Initial residue 0.25 Rev per sec per min
 at 995.0 Rev per sec

Final residue 0.26 Rev per sec per min
 at 860.0 Rev per sec.

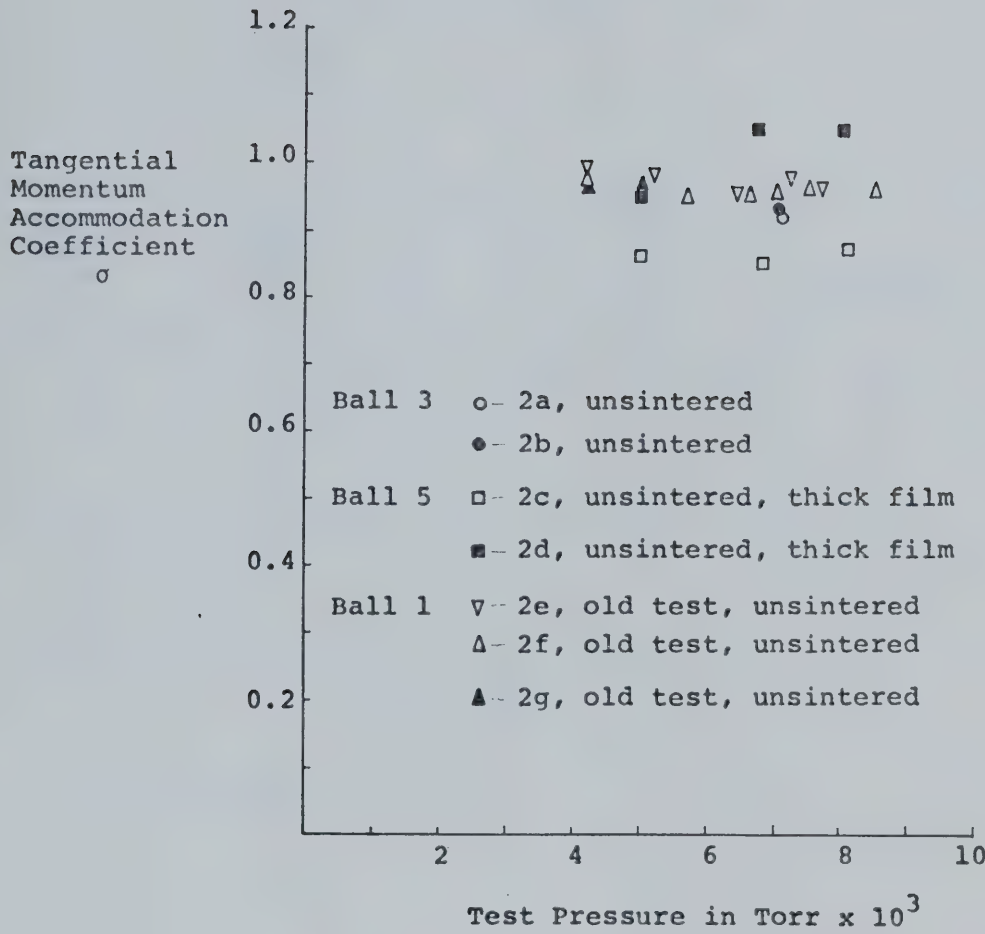


FIGURE 6-2 TANGENTIAL MOMENTUM ACCOMMODATION COEFFICIENTS FOR HELIUM ON SMOOTH SILVER

TABLE 6-3

 VALUES OF σ FOR ARGON
 ON SMOOTH SILVER

(a) Ball 1, Old Test.

Counter Time min	Pressure Torr $\times 10^3$	f_1 Rev per sec	f_2 Rev per sec	f_R Rev per sec	σ	σ Corrected
3	2.30	748.6	739.5	0.4	0.962	0.948
3	3.30	734.5	722.1	0.4	0.945	0.931
2	4.20	714.7	704.4	0.3	0.953	0.939

$$\sigma_{AV} = 0.94$$

Initial residue 0.13 Rev per sec per min
 at 754.0 Rev per sec

No final residue.

TABLE 6-3 (CONT'D)

VALUES OF σ FOR ARGON
ON SMOOTH SILVER

(b) Ball 1, Older Test, Electron Bombarded.

Counter Time min	Pressure Torr $\times 10^3$	f_1 Rev per sec	f_2 Rev per sec	f_R Rev per sec	σ	σ Corrected
3	2.45	821.0	810.7	0.2	0.957	0.942
3	3.60	803.5	789.1	0.2	0.938	0.924
3	4.60	782.1	764.4	0.2	0.931	0.918
2	5.60	744.3	730.7	0.1	0.928	0.914
3*	5.60	702.3	683.3	0.2	0.917	0.904

* Resublimation at test pressure

$\sigma_{AV} = 0.92$

Initial residue 0.06 Rev per sec per min
at 826.0 Rev per sec

No final residue.

Tangential
Momentum
Accommodation
Coefficient

σ

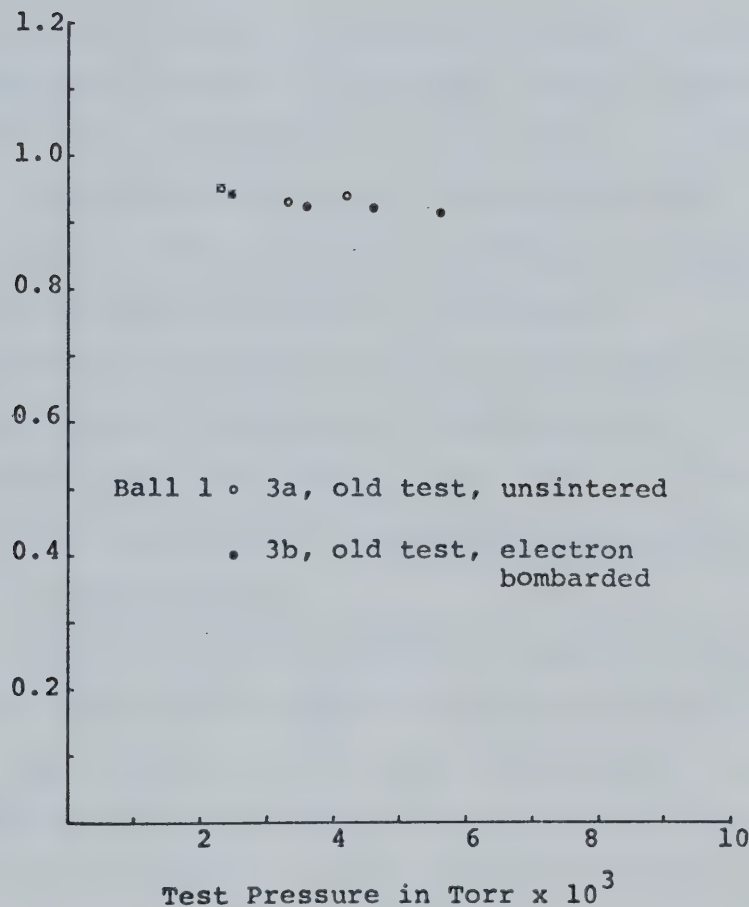


FIGURE 6-3 TANGENTIAL MOMENTUM
ACCOMMODATION COEFFICIENTS
FOR ARGON ON SMOOTH SILVER

For thick silver films, results were somewhat different from thin films and rather less consistent. Test 2c for helium gave $\sigma_{AV} = 0.86$ which was the lowest value found for any silver test. Test 2d for helium which preceded test 2c, and 1e for nitrogen gave σ 's which were higher than those for thin films, with much scatter in σ values from run to run.

In tests 1c and 3b, the final run of each was performed after an additional sublimation performed without removing the test gas. This resublimation did not affect σ values appreciably. This demonstrates that the heating of the sublimation filament does not seriously affect the average temperature of molecules incident on the surface.

Resublimation is expected to produce clean surfaces for some time; however sublimation at high pressure is known to produce particularly porous films (26) which will tend to give high values of σ . Resublimation runs are not included in σ_{AV} calculations.

Tests 2a and 2b for helium afford a comparison of the effect of test gas purity in that 2a was performed after admission of gas through the leak valve, and 2b after admission through the quartz tube. Since values of σ were essentially the same for both tests it can be concluded, in view of the excellent purity of quartz tube helium, that contamination did not affect σ for thin silver.

The comparison between 2a and 2b is also useful because it indicates that little pressure reading error resulted

from the heating of the quartz leak. The Baratron pressure gauge is temperature sensitive as discussed in section 4-1, and as stated in the instrument manual. Initially, considerable thermal zero drift was noted upon heating of the quartz tube near the Baratron, but this effect disappeared when thermal insulation was provided between the quartz tube and the Baratron.

6-4 Rough Ball Results for Silver.

Tests 4a, 4b and 4c were done on a roughened ball with the contaminated stainless surface. Table 6-5 and figure 6-4 are tests of nitrogen on silver on the roughened surface. Table 6-6 and figure 6-5 are for helium, and table 6-7 and figure 6-6 are for argon, both on the silvered rough surface. All deposits of silver are thin deposits for these tests. Table 6b presents a summary of the results in the form of σ_{AV} for these tests on the rough ball.

Rough ball tests can be seen to give considerably higher values of σ than those for smooth balls. Values of σ for rough balls are found to be greater than 1.0 indicating that the back reflection mechanism may be an important process here. Helium accommodation on silver is higher than nitrogen or argon accommodation. Several tests on the rough surface indicate little or no effect on σ from variation of angular velocity of the ball.

TABLE 6b

 AVERAGE TANGENTIAL MOMENTUM ACCOMMODATION
 COEFFICIENTS FOR SILVER ON ROUGH BALLS

	Ball 1 Older Tests	Ball 4
σ_{AV} for Nitrogen		5a 1.05 5b 1.04** 5c 1.06** 5d 1.03 4a 1.09+
σ_{AV} for Helium	6c 1.14	6a 1.15 6b 1.10* 4c 1.10+
σ_{AV} for Argon		7a 1.06 7b 1.05* 4b 1.03+

* Oven sintered to 260°C

** Electron bombarded to about 300°C

+ Bare stainless steel.

TABLE 6-4

 VALUES OF σ FOR NITROGEN, ARGON AND
 HELIUM ON SANDBLASTED BARE STEEL

(a) Nitrogen, ball 4.

Counter Time min	Pressure Torr $\times 10^3$	f_1 Rev per sec	f_2 Rev per sec	f_R Rev per sec	σ	σ Corrected
3	3.50	316.7	310.9	0.5	1.111	1.094
4	5.85	303.5	291.7	0.6	1.110	1.094
2	6.95	280.4	273.9	0.3	1.115	1.095

$$\sigma_{AV} = 1.09$$

Initial residue 0.16 Rev per sec per min
 at 327.5 Rev per sec

Final residue 0.16 Rev per sec per min
 at 268.6 Rev per sec.

TABLE 6-4 (CONT'D)

 VALUES OF σ FOR NITROGEN, ARGON AND
 HELIUM ON SANDBLASTED BARE STEEL

(b) Argon, ball 4.

Counter Time min	Pressure Torr $\times 10^3$	f_1 Rev per sec	f_2 Rev per sec	f_R Rev per sec	σ	σ Corrected
3	3.70	404.4	395.2	0.7	1.059	1.043
2	5.00	383.6	376.1	0.5	1.046	1.030
2	5.80	365.1	356.9	0.5	1.043	1.028
2	6.40	343.2	334.7	0.5	1.047	1.031
2	7.30	321.8	313.0	0.5	1.017	1.001

$$\sigma_{AV} = 1.03$$

Initial residue 0.23 Rev per sec per min

at 413.0 Rev per sec

No final residue.

TABLE 6-4 (CONT'D)

VALUES OF σ FOR NITROGEN, ARGON AND
HELIUM ON SANDBLASTED BARE STEEL

(c) Helium, ball 4.

Counter Time min	Pressure Torr $\times 10^3$	f_1 Rev per sec	f_2 Rev per sec	f_R Rev per sec	σ	σ Corrected
3	4.00	403.6	399.8	0.6	1.190	1.173
3	5.60	394.5	389.8	0.6	1.116	1.100
3	7.20	383.6	378.0	0.6	1.090	1.074
3	8.20	370.2	363.9	0.6	1.132	1.115

 $\sigma_{AV} = 1.10$ (excluding run 1)Initial residue 0.22 Rev per sec per min
at 407.5 Rev per sec.Final residue 0.18 Rev per sec per min
at 346.5 Rev per sec.

TABLE 6-5

 VALUES OF σ FOR NITROGEN
 ON ROUGH SILVER

(a) Ball 4.

Counter Time min	Pressure Torr $\times 10^3$	f_1 Rev per sec	f_2 Rev per sec	f_R Rev per sec	σ	σ Corrected
2	6.43	304.8	298.6	0.2	1.069	1.054
2	6.30	298.6	292.7	0.2	1.057	1.042
4	5.98	260.3	250.6	0.3	1.063	1.048
4	5.93	250.6	241.3	0.3	1.068	1.052
4	5.88	241.3	232.5	0.3	1.055	1.040

$$\sigma_{AV} = 1.05$$

Initial residue 0.84 Rev per sec per min

at 227.5 Rev per sec.

TABLE 6-5 (CONT'D)

VALUES OF σ FOR NITROGEN
ON ROUGH SILVER

(b) Ball 4, Electron Bombarded.

Counter Time min	Pressure Torr $\times 10^3$	f_1 Rev per sec	f_2 Rev per sec	f_R Rev per sec	σ	σ Corrected
4	4.40	464.5	451.1	0.8	1.080	1.065
3	5.20	434.5	423.7	0.6	1.052	1.038
4	6.30	411.7	395.4	0.8	1.052	1.038
3	7.40	383.9	370.6	0.6	1.047	1.033

$$\sigma_{AV} = 1.04$$

Initial residue 0.20 Rev per sec per min
at 475.0 Rev per sec

Final residue 0.20 Rev per sec per min
at 366.0 Rev per sec.

TABLE 6-5 (CONT'D)

VALUES OF σ FOR NITROGEN
ON ROUGH SILVER

(c) Ball 4, Sintered.

Counter Time min	Pressure Torr $\times 10^3$	f_1 Rev per sec	f_2 Rev per sec	f_R Rev per sec	σ	σ Corrected
4	3.2*	322.5	315.4	0.6	1.075	1.060
3	4.68	304.7	297.7	0.4	1.079	1.063
3	6.60	290.8	281.6	0.4	1.072	1.057

* Values obtained using Simpson's rule of integration

$$\sigma_{AV} = 1.06$$

Initial residue 0.14 Rev per sec per min

at 330.0 Rev per sec

Final residue 0.13 Rev per sec per min

at 260.5 Rev per sec.

TABLE 6-5 (CONT'D)

VALUES OF σ FOR NITROGEN
ON ROUGH SILVER

(d) Ball 4.

Counter Time min	Pressure Torr $\times 10^3$	f_1 Rev per sec	f_2 Rev per sec	f_R Rev per sec	σ	σ Corrected
4	6.23	377.2	362.3	0.9	1.050	1.035
5	6.08	362.3	344.7	1.1	1.060	1.045
3	5.98	344.7	334.9	0.7	1.031	1.016
3	5.93	334.9	325.3	0.7	1.047	1.032

$$\sigma_{AV} = 1.03$$

Initial residue 0.22 Rev per sec per min
at 405.0 Rev per sec

Final residue 0.22 Rev per sec per min
at 317.0 Rev per sec.

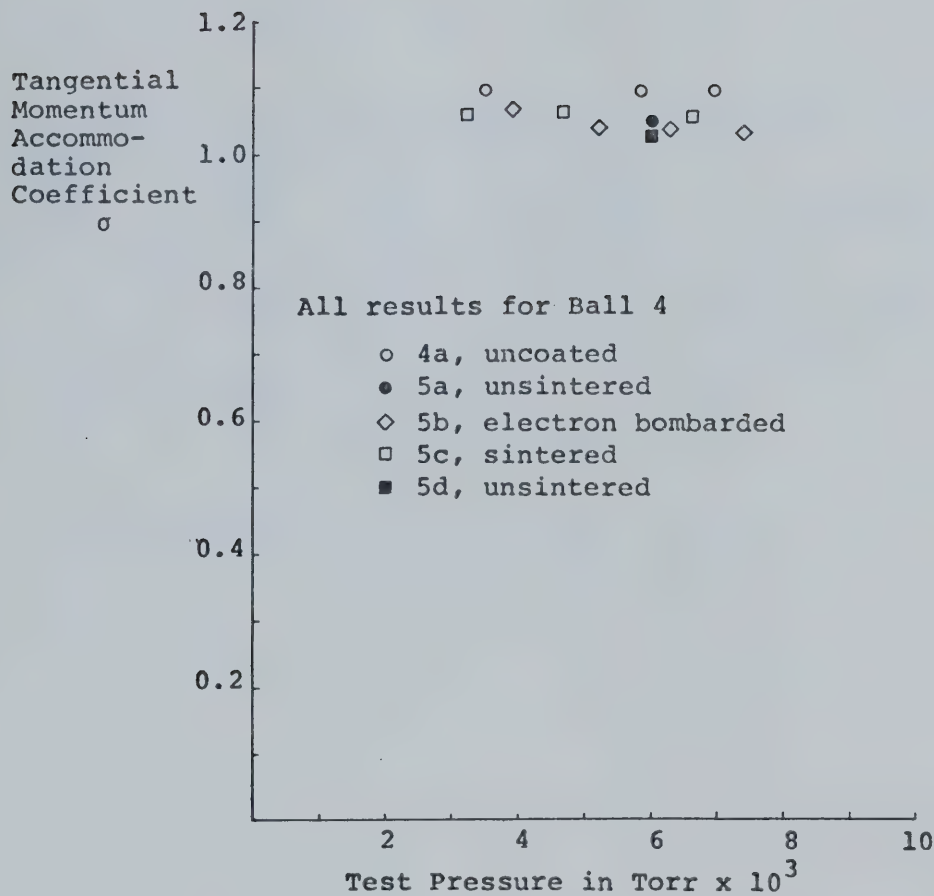


FIGURE 6-4 TANGENTIAL MOMENTUM ACCOMMODATION COEFFICIENTS FOR NITROGEN ON A ROUGH SURFACE

TABLE 6-6

 VALUES OF σ FOR HELIUM
 ON ROUGH SILVER

(a) Ball 4.

Counter Time min	Pressure Torr $\times 10^3$	f_1 Rev per sec	f_2 Rev per sec	f_R Rev per sec	σ	σ Corrected
6	6.60	359.5	349.4	1.0	1.162	1.145

Initial residue 0.20 Rev per sec per min
 at 386.0 Rev per sec

Final residue 0.17 Rev per sec per min
 at 322.0 Rev per sec.

TABLE 6-6 (CONT'D)

VALUES OF σ FOR HELIUM
ON ROUGH SILVER

(b) Ball 4, Sintered

Counter Time min	Pressure Torr $\times 10^3$	f_1 Rev per sec	f_2 Rev per sec	f_R Rev per sec	σ	σ Corrected
6	2.88	413.9	408.7	0.8	1.112	1.096
4	9.40	381.9	372.4	0.6	1.125	1.109
8*	9.30	367.6	349.7	1.2	1.211	1.105

* Resublimation at test pressure

$$\sigma_{AV} = 1.10$$

Initial residue 0.14 Rev per sec per min

at 418.0 Rev per sec

No final residue.

TABLE 6-6 (CONT'D)

 VALUES OF σ FOR HELIUM
 ON ROUGH SILVER

(c) Ball 2, Old Test.

Counter Time min	Pressure Torr $\times 10^3$	f_1 Rev per sec	f_2 Rev per sec	f_R Rev per sec	σ	σ Corrected
3	2.70	961.5	955.4	0.9	1.201	1.184
4	5.20	941.2	927.5	1.2	1.153	1.136
4	5.20	927.5	914.2	1.2	1.133	1.117
6	7.20	899.7	873.5	1.7	1.147	1.130
2.5	9.20	853.8	840.5	0.7	1.159	1.142

$$\sigma_{AV} = 1.14$$

Initial residue 0.30 Rev per sec per min
 at 967.5 Rev per sec

Final residue 0.29 Rev per sec per min
 at 832.5 Rev per sec.

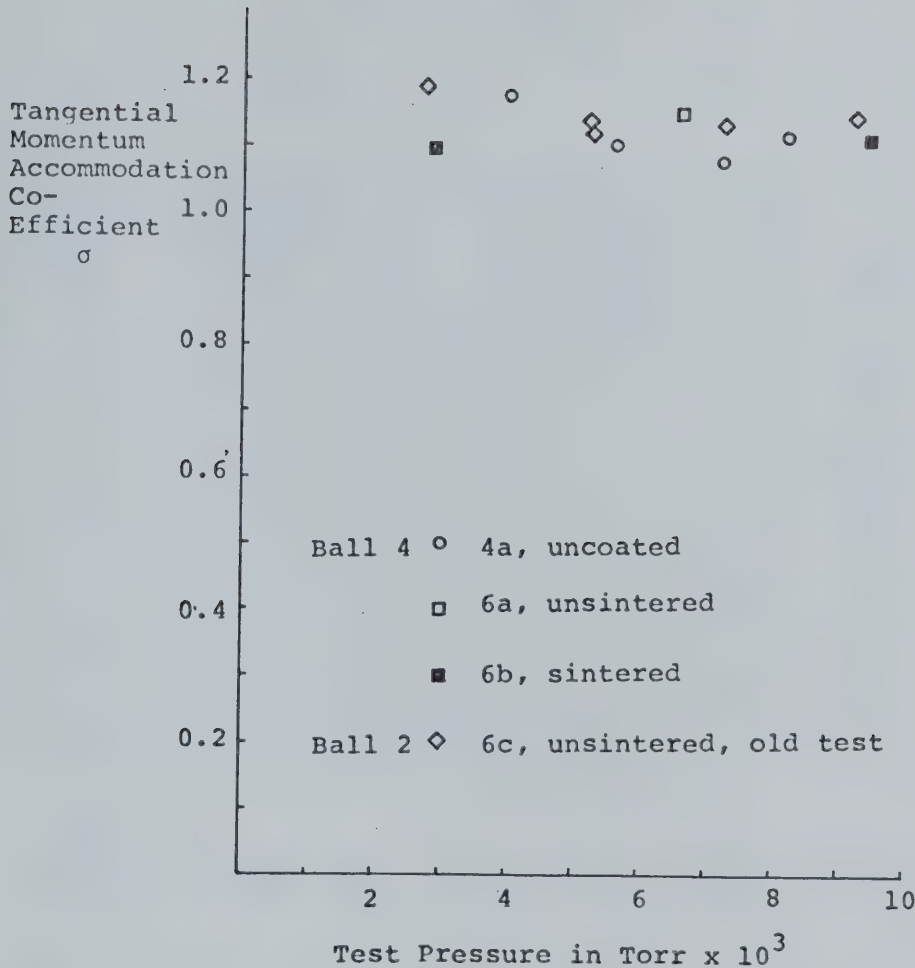


FIGURE 6-5 TANGENTIAL MOMENTUM ACCOMMODATION COEFFICIENTS FOR HELIUM ON ROUGH SILVER

TABLE 6-7

VALUES OF σ FOR ARGON
ON ROUGH SILVER

(a) Ball 4.

Counter Time min	Pressure Torr $\times 10^3$	f_1 Rev per sec	f_2 Rev per sec	f_R Rev per sec	σ	σ Corrected
5	3.30	466.4	450.8	1.0	1.095	1.079
3	4.80	439.0	426.6	0.6	1.074	1.059
4	5.80	414.8	396.6	0.7	1.055	1.040
3	6.60	375.9	361.7	0.5	1.065	1.050
4	7.10	347.6	329.0	0.6	1.063	1.048
4*	7.10	311.6	295.0	0.5	1.061	1.046

* Resublimation at system pressure

 $\sigma_{AV} = 1.06$

Initial residue 0.21 Rev per sec per min

at 475.0 Rev per sec

Final residue 0.13 Rev per sec per min

at 273.5 Rev per sec.

TABLE 6-7 (CONT'D)

VALUES OF σ FOR ARGON
ON ROUGH SILVER

(b) Ball 4, Sintered.

Counter Time min	Pressure Torr $\times 10^3$	f_1 Rev per sec	f_2 Rev per sec	f_R Rev per sec	σ	σ Corrected
3	3.35	425.7	416.9	0.7	1.086	1.070
3	4.40	407.8	397.1	0.7	1.068	1.052
3	5.20	387.1	375.3	0.7	1.059	1.044
3	7.10	362.8	348.2	0.7	1.042	1.027

$$\sigma_{AV} = 1.05$$

Initial residue 0.24 Rev per sec per min
at 430.0 Rev per sec.

No final residue.

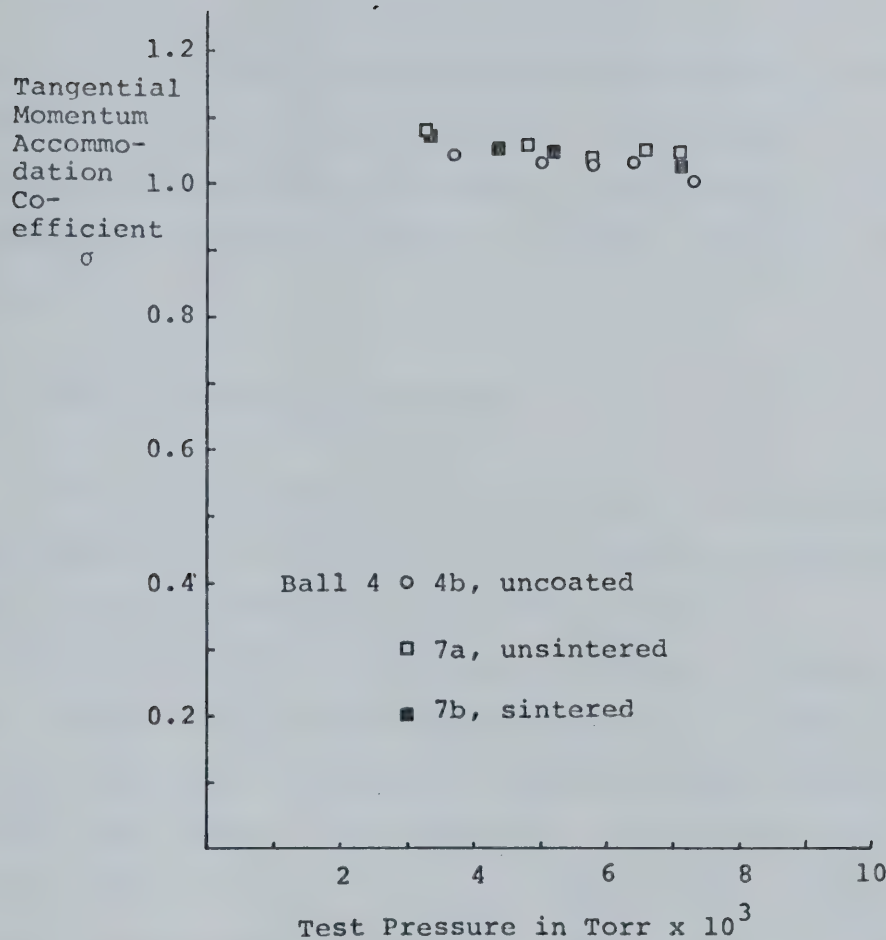


FIGURE 6-6 TANGENTIAL MOMENTUM ACCOMMODATION COEFFICIENTS FOR ARGON ON ROUGH SILVER

Nitrogen and helium accommodations on bare stainless steel are very close in value, however the helium results for each run of that test (4c) are scattered and perhaps unreliable.

Comparison of tests 6a and 6b for helium on fresh and oven sintered silver respectively are interesting because sintering appears to lower σ values. This may be an indication of some surface smoothing. Resublimation in the sintered case failed to produce the higher values of σ found in test 6a.

6-5 Smooth Ball Results for Gold.

Table 6-8 and figure 6-7 present data for nitrogen on gold and table 6-9 and figure 6-8 give data for helium on gold. Table 6c presents σ_{AV} for these tests.

Results for gold are similar in character to those of thick silver films in that large differences in values of σ occur, with some values being relatively small compared to thin film results. The values of σ in tests 8a and 9b are the lowest obtained in any experiments of the thesis. Test 9a is particularly interesting since σ went from 1.428 to 0.94 over the period of the test, smoothly and independently of pressure. The second, third and fourth entries in table 9a are a three part analysis of entry one broken into shorter time periods. These part analyses are less accurate due to low total speed change, but indicate a dramatic change in σ over a short time period.

TABLE 6c

 AVERAGE TANGENTIAL MOMENTUM ACCOMMODATION
 COEFFICIENTS FOR GOLD ON SMOOTH BALLS

	Ball 5 Thick Gold	Ball 6 Thick Gold
σ_{AV} for Nitrogen		8a 0.80 8b 0.89* 8c 0.90+
σ_{AV} for Helium	9a 1.43 to 0.94	9b 0.82

* Oven sintered

+ Allowed to contaminate.

A possible cause of this lowering of σ is spontaneous sintering at room temperature into a smooth surface.

Tests 8a and 8b provide interesting comparison in that 8b, a sintered test, gave higher values of σ than 8a, an unsintered test. The expected higher contamination of the sintered test may account for this difference. Test 8c was done after allowing the gold film of 8b to contaminate at about 5×10^{-9} torr for about 24 hours, and did not change σ_{AV} appreciably.

TABLE 6-8

 VALUES OF σ FOR NITROGEN
 ON SMOOTH GOLD

(a) Ball 6, Thick Film.

Counter Time min	Pressure Torr $\times 10^3$	f_1 Rev per sec	f_2 Rev per sec	f_R Rev per sec	σ	σ Corrected
6	5.15	356.2	341.3	2.2	0.812	0.800
6	6.10	336.7	320.6	1.6	0.831	0.819
6	7.05	315.7	298.7	1.7	0.812	0.800
4	7.45	278.3	267.9	0.9	0.805	0.794

$$\sigma_{AV} = 0.80$$

Initial residue 0.29 Rev per sec per min
 at 365.0 Rev per sec

Final residue 0.21 Rev per sec per min
 at 263.0 Rev per sec.

TABLE 6-8 (CONT'D)

VALUES OF σ FOR NITROGEN
ON SMOOTH GOLD

(b) Ball 6, Thick Film, Sintered.

Counter Time min	Pressure Torr $\times 10^3$	f_1 Rev per sec	f_2 Rev per sec	f_R Rev per sec	σ	σ Corrected
6	5.58	344.8	328.1	2.0	0.900	0.887
6	6.25	323.1	305.7	1.9	0.906	0.893
5	6.85	296.8	282.3	1.5	0.904	0.891

$$\sigma_{AV} = 0.89$$

Initial residue 0.33 Rev per sec per min

at 354.0 Rev per sec

Final residue 0.28 Rev per sec per min

at 277.5 Rev per sec.

TABLE 6-8 (CONT'D)

VALUES OF σ FOR NITROGEN
ON SMOOTH GOLD

(c) Ball 6, Aged in Vacuum.

Counter Time min	Pressure Torr $\times 10^3$	f_1 Rev per sec	f_2 Rev per sec	f_R Rev per sec	σ	σ Corrected
4	3.98	337.9	329.6	1.5	0.884	0.870
4	4.95	325.0	315.2	1.5	0.903	0.889
4	6.30	308.8	297.0	1.3	0.949	0.934

$$\sigma_{AV} = 0.90$$

Initial residue 0.38 Rev per sec per min
at 346.0 Rev per sec

Final residue 0.32 Rev per sec per min
at 290.0 Rev per sec.

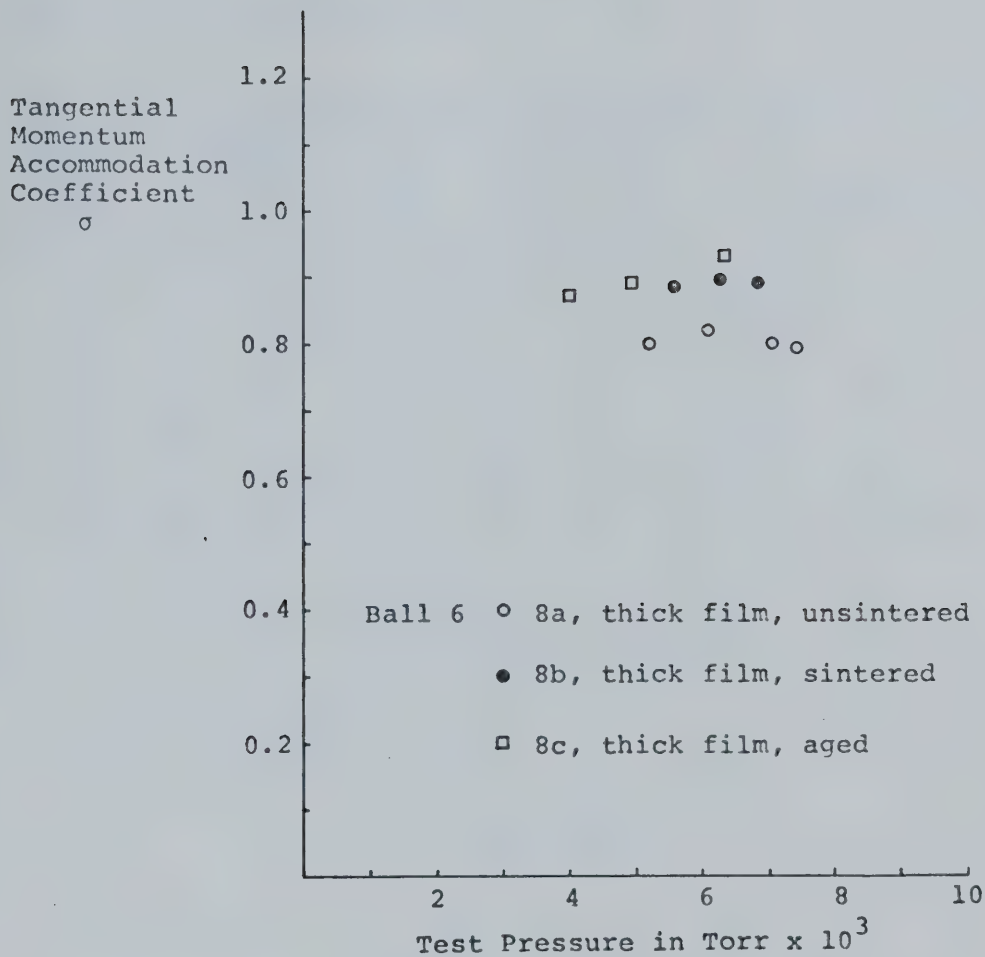


FIGURE 6-7 TANGENTIAL MOMENTUM
ACCOMMODATION COEFFICIENTS
FOR NITROGEN ON SMOOTH GOLD

TABLE 6-9

VALUES OF σ FOR HELIUM

ON SMOOTH GOLD

(a) Ball 5, Very Thick Film.

Counter Time min	Pressure Torr $\times 10^3$	f_1 Rev per sec	f_2 Rev per sec	f_R Rev per sec	σ	σ Corrected
6	4.60	295.8	289.8	0.7	1.399	1.379
2*	4.60	297.2	294.8	0.2	1.449	1.428
2*	4.60	294.8	292.8	0.2	1.194	1.177
2*	4.60	292.8	290.7	0.2	1.269	1.251
9	5.60	281.3	271.5	1.1	1.118	1.102
7	6.95	261.4	253.2	0.9	1.044	1.029
5	8.95	239.2	232.9	0.7	0.950	0.936

* Short time duration runs

Initial residue 0.12 Rev per sec per min
at 305.0 Rev per sec

Final residue 0.13 Rev per sec per min
at 227.5 Rev per sec.

TABLE 6-9 (CONT'D)

VALUES OF σ FOR HELIUM
ON SMOOTH GOLD

(b) Ball 6, Thick Film.

Counter Time min	Pressure Torr $\times 10^3$	f_1 Rev per sec	f_2 Rev per sec	f_R Rev per sec	σ	σ Corrected
4	5.80	335.5	331.1	0.9	0.811	
4	5.80	331.1	326.6	0.9	0.845	
4	5.80	326.6	322.2	0.9	0.833	
12*	5.80	335.5	322.2	0.9	0.835	0.823

* Sum of first three runs

Initial residue 0.23 Rev per sec per min
at 355.0 Rev per sec

Final residue 0.21 Rev per sec per min
at 315.0 Rev per sec.

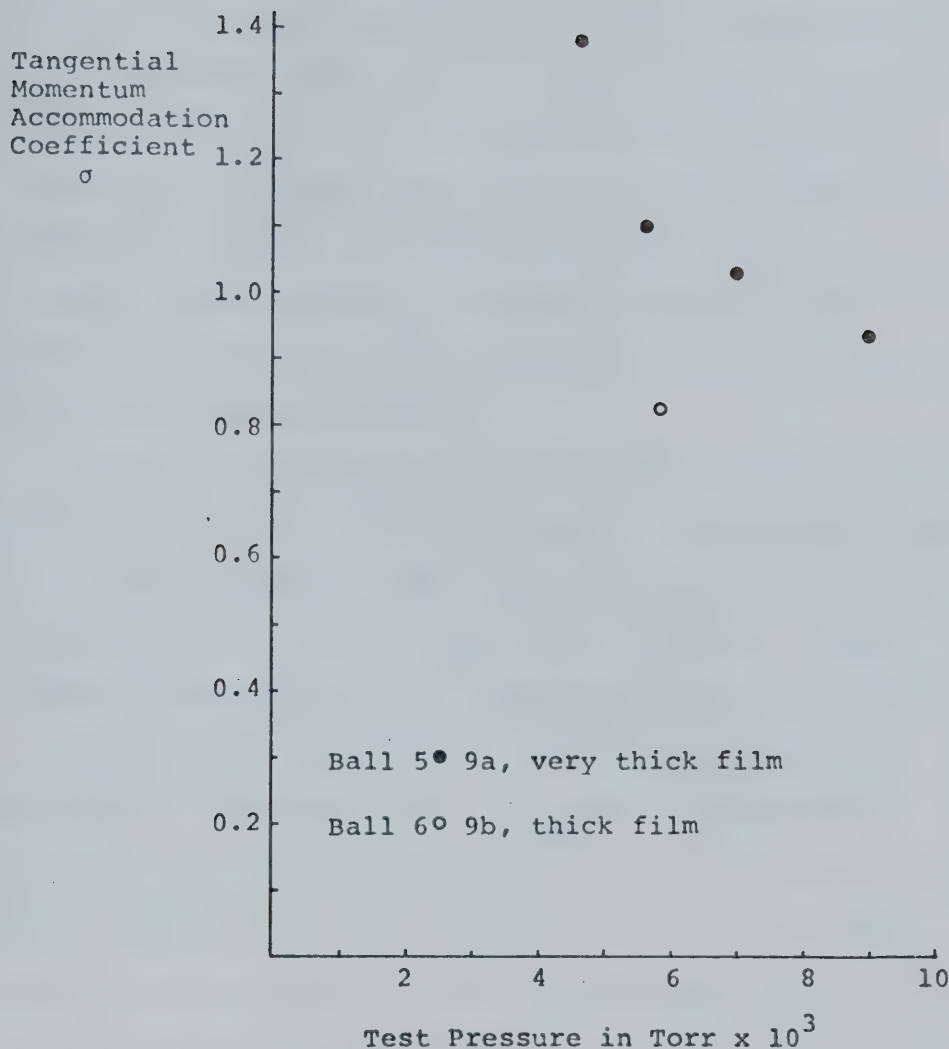


FIGURE 6-8 TANGENTIAL MOMENTUM
ACCOMMODATION COEFFICIENTS
FOR HELIUM ON SMOOTH GOLD

6-6 Energy Accommodation Coefficients

Table 6-10 gives results for energy accommodation coefficient measurements for nitrogen, helium and argon on silver covered tungsten. In all but one case, α determinations were done simultaneously with σ determination, the σ tests being annotated in the appropriate table. An approximate value of α is obtained from calculations assuming the filament to be entirely at the average temperature, with radiation and end conduction losses at that average temperature being subtracted from total power input to determine molecular conduction losses. Table 6-10 illustrates this procedure.

The DC voltage drop ΔV_{FIL} across the filament and ΔV_R across a precision 20.05 ohm resistor in series were measured at the same pressure. From ΔV_{FIL} and ΔV_R , filament resistance R_{FIL} and DC current I_{DC} were calculated. Average filament temperature θ_{AV} was determined from R_{FIL} from a resistance versus temperature calibration presented in Appendix IV. Heating current I_{HEAT} was determined by adding the small AC sensing current to the DC current, and then $I_{HEAT}^2 R_{FIL}$ the total power input was determined.

Several runs were done at very low pressure where molecular conduction is negligible. These runs are noted as at zero pressure, and are used to determine radiation and end conduction losses. For each test, these zero values are plotted as filament power versus resistance. The power for

TABLE 6-10

 VALUES OF α FOR NITROGEN, ARGON AND
 HELIUM ON SILVER ON TUNGSTEN

	P Torr $\times 10^3$	ΔV_{FIL} mV	ΔV_R mV	I_{HEAT} mA	R_{FIL} ohm	Power in Watt $\times 10^4$	ω_{PAD} Watt $\times 10^4$	α_{AV}	θ_{AV} °C	ϵ	α Corr
(a)	Nitrogen	6.75	68.5	96.9	4.871	14.17	3.362	1.925	1.013	15.1	.116 .83
	on Silver	6.50	68.8	97.2	4.886	14.19	3.387	1.970	1.015	15.5	.116 .88
	Test 1b	6.30	68.8	97.2	4.847	14.19	3.387	1.970	1.047	15.5	.116 .91
	$T_w = 25.5^\circ C$	0	54.8	77.0	3.879	14.27	2.147				
		0	52.4	74.0	3.730	14.20	1.976				
		0	48.6	69.2	3.490	14.08	1.715				
(b)	Nitrogen	5.65	81.3	112.2	5.635	14.53	4.614	2.965	.750	24.1	.134 .65
	on Aged	5.30	81.6	112.4	5.645	14.56	4.640	3.300	.887	23.5	.116 .77
	Silver	0	63.2	87.7	4.413	14.45	2.814				
	(No σ test)	0	66.9	91.8	4.618	14.61	3.116				
		0	65.4	90.1	4.533	14.55	2.990				
	$T_w = 24.3^\circ C$	0	64.8	89.3	4.493	14.54	2.935				
		0	63.5	87.8	4.418	14.50	2.830				

TABLE 6-10 (CONT'D)
 VALUES OF α FOR NITROGEN, ARGON AND
 HELIUM ON SILVER ON TUNGSTEN

	P Torr $\times 10^3$	ΔV_{FIL} mV	ΔV_R mV	I_{HEAT} mA	R_{FIL} ohm	Power in Watt	ω_{RAD} Watt $\times 10^4$	α_{AV}	θ_{AV} °C	ϵ	α Corr
(c) Helium on Silver	7.1	63.8	89.5	4.503	14.29	2.898	2.190	.225	17.8	.110	.19
Test 2a	7.1	63.7	89.4	4.498	14.29	2.891	2.190	.223	17.8	.110	.19
$T_w = 24.6^\circ C$	0	59.7	80.6	4.059	14.40	2.372					
	0	48.3	68.8	3.470	14.08	1.695					
	0	49.2	69.9	3.525	14.11	1.753					
	0	51.1	72.4	3.650	14.15	1.835					
(d) Helium on Silver	5.0	63.4	88.4	4.448	14.38	2.845	2.330	.209	20.0	.100	.180
Test 2b	7.1	64.4	90.1	4.433	14.33	2.894	2.240	.212	19.0	.102	.163
$T_w = 24.8$	0	64.6	90.4	4.548	14.33	2.964	2.240	.218	19.0	.102	.188
Sintered	0	59.6	82.6	4.159	14.47	2.503					
	0	56.4	78.8	3.960	14.35	2.261					
	0	53.6	75.5	3.805	14.23	2.060					

VALUES OF α FOR NITROGEN, ARGON AND

HELIUM ON SILVER ON TUNGSTEN

	P Torr x10 ³	ΔV_{FIL} mV	ΔV_R mV	I _{HEAT} mA	P _{FIL} Ohm	Power in Watt $\times 10^4$	ω_{RAD} Watt $\times 10^4$	α_{AV}	θ_{AV} °C	ϵ	α Corr
(e) Argon on	4.8	87.5	116.5	5.849	15.06	5.152	3.940	.96	33.6	.103	.84
Silver	5.8	88.3	118.3	5.559	14.97	5.280	3.720	1.09	31.8	.102	.94
Test 7a	6.6	89.2	119.7	6.009	14.94	5.395	3.660	1.08	31.2	.102	.94
$T_w = 24.8$	7.15	89.8	120.5	6.049	14.94	5.467	3.660	1.04	31.2	.102	.90
	0	81.6	107.2	5.386	15.26	4.427					
	0	72.7	97.7	4.912	14.92	3.600					
	0	69.9	94.6	4.757	14.81	3.351					
	0	71.8	96.7	4.862	14.89	3.520					
	0	72.6	97.8	4.907	14.88	3.583					
(f) Argon on	5.35	74.6	103.3	5.191	14.48	3.902	2.878	1.06	23.0	.115	.92
Silver	7.0	76.9	105.7	5.361	14.45	4.153	2.800	1.10	22.4	.115	.96
(No σ)	0	59.3	83.0	4.179	14.32	2.501					
Test.)		60.8	84.9	4.273	14.36	2.622					
$T_w = 23.8$		62.6	86.9	4.373	14.44	2.751					
		64.0	88.6	4.458	14.48	2.878					

TABLE 6-10 (CONT'D)

 VALUES OF α FOR NITROGEN, ARGON AND
 HELIUM ON SILVER ON TUNGSTEN

(g)	P Torr $\times 10^3$	ΔV_{FIL} mV	ΔV_R mV	I _{HEAT} mA	R _{FIL} ohm	Power in Watt $\times 10^4$	ω_{PAD} Watt Watt	α_{AV}	θ_{AV} °C	ϵ	α Corr
Nitrogen	5.3	68.3	95.1	4.782	14.40	3.293	2.090	.800	20.4	.077	.69
on Silver	4.8	66.6	93.0	4.677	14.36	3.141	2.000	.867	19.6	.076	.75
(No σ	4.6	66.5	92.7	4.662	14.38	3.125	2.050	.836	20.0	.077	.72
(Test)	0	51.4	72.0	3.630	14.31	1.886					
$T_w = 24.8^\circ C$	0	52.6	73.4	3.700	14.37	1.967					
Sintered	0	53.3	74.3	3.745	14.38	2.017					
	0	55.1	76.6	3.895	14.42	2.147					

a given resistance for a high pressure test was read off this plot and subtracted from total power. Figure 6-9 is a sample plot for tests 1b.

As noted before, this procedure of subtracting radiation and end conduction losses gives only an approximation for α , since the real temperature distribution changes with addition of the gas. A better approximation is found using the method explained in Appendix I. From the analysis of Appendix I, emissivity ϵ and energy accommodation coefficient α corrected were determined and noted in each table.

Tests e and f for argon on fresh silver produce large values of α which change slightly with time perhaps indicating contamination effects. Test a for nitrogen had similarly large values of α which appear to change slightly with time.

Test g for nitrogen was made after the film on the wire was sintered to approximately the same temperature as the ball, for about 15 minutes by passing a relatively large current through the wire. Values of α are lower than those found in test a, a similar test with no sintering. Test b was also found to give low values of α in comparison to a, and was obtained after the UHV system was opened to atmosphere and baked twice. The run at 5.65×10^{-3} torr which gave $\alpha = 0.65$ must be considered inaccurate due to the high value of ϵ found. The high ϵ value probably indicates poor accuracy of the radiation and end conduction loss curve. Test b was sintered due to the 300°C baking but certainly the surface was contaminated. This low α found in spite of

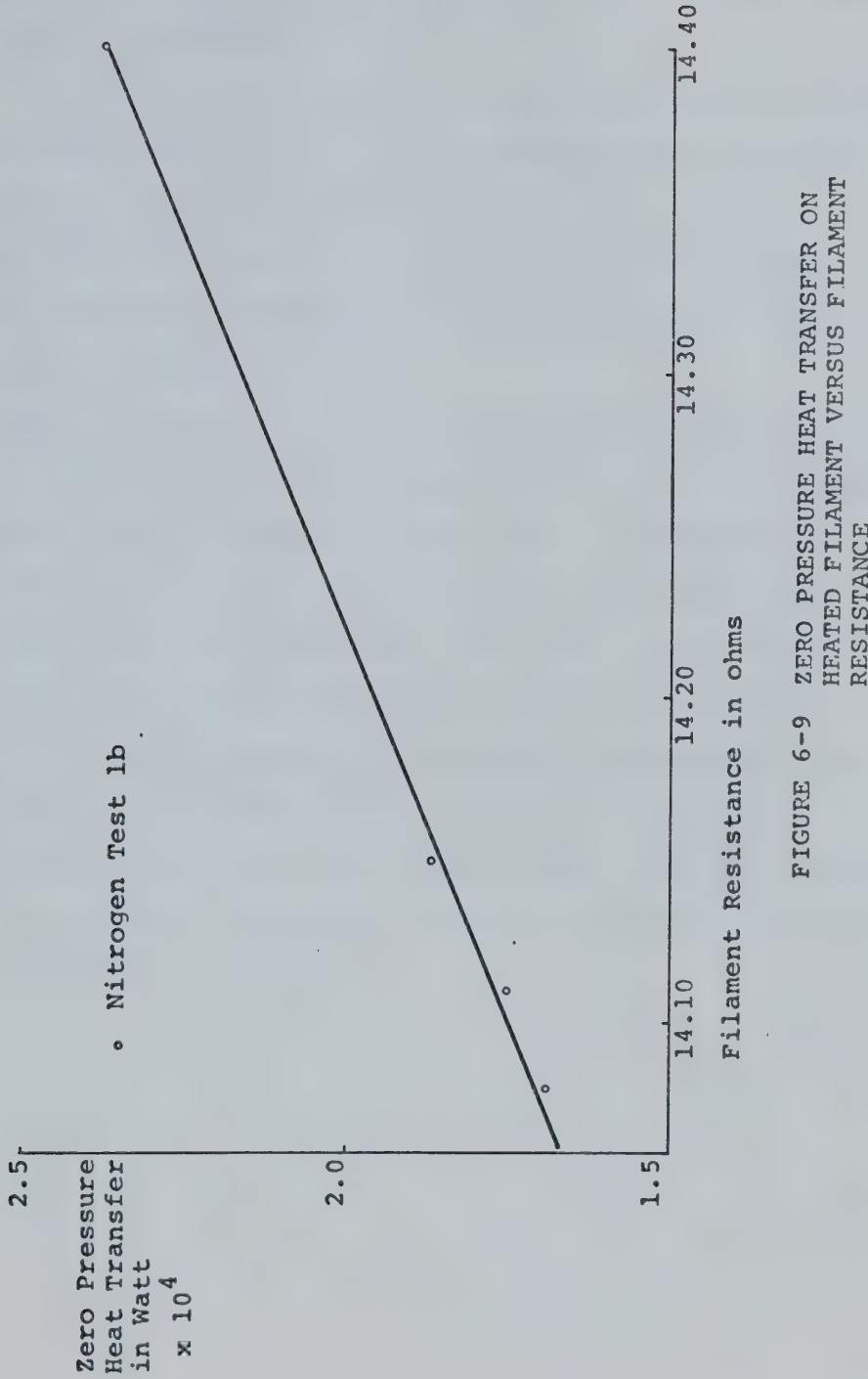


FIGURE 6-9 ZERO PRESSURE HEAT TRANSFER ON HEATED FILAMENT VERSUS FILAMENT RESISTANCE

contamination indicates the great importance of roughness in energy accommodation.

No noticeable change in α occurred for tests c and b for helium, even though c was performed by gas admission through the leak valve and therefore likely to have a higher impurity content. Values of α for c and d were almost the same, though contamination rates would have been quite different.

Some variation in values of ϵ was found throughout tests. Most values were between 0.100 and 0.116 with little variation being found within each test. Values of ϵ of 0.077 for test g were rather lower than for other tests but relatively constant within that test. Since test g was one of the first performed on the wire, it might be assumed that the surface was relatively smoother and could be expected to produce lower ϵ . All data presented at zero pressure was done after pumping away test gas, however data taken before admission of gas after sublimation agreed well with that presented.

CHAPTER VII

DISCUSSION

7-1 Pressure Gauge Drift

In some cases, σ decreases with increasing pressure. Where no final residual drag was obtained, the residual error should be considered to be at least partly responsible. Several argon tests and test 2e for helium showed this effect when no final residual drag was measured. In most cases, the most likely explanation for the effect is pressure gauge drifting, which may be more severe for the initial gas admission. The pressure gauge was observed to drift slightly if any mechanical disturbance occurred in the adjacent areas of the vacuum system. Closing the valve to isolate the reference side of the Baratron was observed to alter the zeroing for a period of time after which it corrected itself.

7-2 Smooth Ball Results

Results for thin layers on smooth balls indicates very little difference in σ for any test gas on silver for a particular ball. Further, all situations produced almost complete accommodation of the tangential momentum of the molecules. This high accommodation might result from small scale roughness or absorbed gas layers.

Contamination of the surface is expected at the impurity levels involved and may be seen in σ measurements as a

secondary effect to roughness from porosity. Measurements of α indicate a lesser interaction between helium and silver than nitrogen or argon and silver, however, no such effect is noticed in σ measurements for smooth films. Even though the silver surfaces on ball and wire are placed on different substrates, it seems reasonable that similar interaction effects would occur in each case. Although the contamination levels on each surface are not precisely known, they should be similar. Therefore it seems reasonable that surface roughness is the main reason why σ values are high and do not change with gas. Only extremely smooth surfaces such as single crystals can be considered smooth to the dimensions of incident gas molecules.

Two forms of roughness are present, substrate topography and overlying film porosity. For thin films, substrate roughness appears to dominate as indicated by the following observed results.

- 1) Sintering had little or no effect on σ
- 2) σ varied from ball to ball, but only slightly for similar tests on one ball, indicating some slight change in substrate from ball to ball
- 3) Thicker layers produced changes in σ while thin layers had little effect.

The change produced by the thicker layers is probably due to the smoothing of substrate contours, since in general σ was lower for thick films. The uncertainty of thick layer results is probably due to uncertainty of crystal structure,

with changes in σ found in some gold tests being due to spontaneous sintering.

7-3 Sandblasted Ball Results

The phenomena observed on the sandblasted ball are discussed with reference to surface roughness obtained from the stereographic scanning electron micrographs.

The simple model presented in section 2-5 which considers a surface made up of furrows shows that for large values of σ , one might indeed expect back reflection. Experimental results of rough balls show that helium on fresh silver gives higher σ than nitrogen or argon. These results are consistent with the lower α values found for helium since more memory of the incident velocity remains for windward slope and therefore back reflected momentum is higher. This fact is demonstrated by the comparison of σ for specular and diffuse reflections where specular reflection represents the lower α value case.

It can be seen from table 6a that for smooth silver covered surfaces that the larger are σ values, the greater the difference between nitrogen and helium values. Results for ball 1 represent these higher values when compared to ball 3 possibly indicating that ball 1 was slightly rougher and therefore provided more back reflection. The differences in σ values for helium and nitrogen is not outside the stated limit of error measurement for a particular reading,

but since quantities in table 6a are averages of several readings, the conclusion may be genuine.

The essential difference between rough and smooth balls cannot be any characteristic size of the simple furrow model assumed, since reducing the width of a furrow and replacing it with several smaller ones, results in the same inclined surface area for a given ϕ . Rather to produce less back reflection and therefore smaller σ , the angle ϕ must be smaller. Therefore, the smooth balls as well as having smaller height of roughness than the rough ball, must have gentler sloping contours. The high σ values obtained for test 9a for gold on smooth surface can be explained as resulting from a severe topography which is modified due to spontaneous sintering as σ values reduce.

7-4 Comparison with Other Work

The experiments by Blankenstein (4) using rotating cylinders which yielded $\sigma = 0.96$ to 1.00 for hydrogen, helium, air and oxygen of polished silver oxide are in general agreement with smooth ball results found in this thesis. The work by Hurlbut (6) which gave $\sigma = 0.90$ to 1.00 for argon, oxygen, air and nitrogen also seems to agree. The soaking discussed by Hurlbut which was thought to allow oil films to settle on the surface produced values of σ down to 0.60. This oil film probably had a smoothing effect similar to that of the thicker metal films of this work, which reduced σ values.

The rough ball work presented in this thesis confirms the $\sigma > 1.0$ data obtained by Thomas and Lord (7). For rough surfaces, helium through neon, argon and xenon gave slightly increasing σ values from 1.040 to 1.075 and increasing α values from 0.553 to 1.395. This is the reverse of increasing σ with decreasing α in this thesis. Possibly the surfaces of Thomas and Lord were less rough than those here, since the roughening was accomplished by rolling in carborundum. Figure 2-12 shows simultaneously increasing σ and α would occur for low ϕ values.

Saltzburg and Smith (28) noted in a publication on molecular beam scattering from silver films that the specular component of their reflection patterns for helium was maintained after several hours exposure to oxygen, water vapour and carbon monoxide in high concentration. The authors attributed this effect to tightly bound layers of gas, which did not affect scattering. In a later paper, Saltzburg, Smith and Palmer (29) after using finer angular resolution of reflection patterns, reported some decrease in their specular peaks; however over short time periods, no change was noticed. In a paper dealing with similar gold results, Saltzburg and Smith (30) found that gold films contaminated much more readily than silver. This work on silver provides evidence that supports the result that little change occurred for a measurement for helium on silver due to expected contamination.

Values of α measured in this thesis are higher than those measured by Thomas and co-workers. In a paper which reviews much of his work (31), Thomas gives $\alpha = 0.0166$ for helium on tungsten and $\alpha = 0.271$ for argon on tungsten, both at about room temperature. Work done by deposition of aluminum or beryllium on tungsten or platinum filaments was stated by Thomas to have problems of inconsistent α values associated with sintering and smoothing of deposits. Aluminum sintered to 1000°K produced $\alpha = 0.087$ for helium, while $\alpha = 0.14$ to 0.15 was found for beryllium and helium, which dropped to 0.045 after heat treatment to 1120°K . Probably much of the reason for the high values of α found in the present experiments was the roughness of the surface layer. The lower values of α obtained for two sintered nitrogen tests bears out this contention. It should be noted that no serious attempt was made to produce very low α values in this work, rather duplication of the surface conditions of the wire and ball was considered important. Temperatures which would allow wire film sintering would probably change the mechanics of surface adsorption. This effect is dealt with by Hayward and Trapnell (24) for gold and silver.

CHAPTER VIII

CONCLUSIONS

The work presented in this thesis indicates that values of momentum accommodation coefficients on metal covered smooth machined surfaces are close to unity and are insensitive to changes in interaction energies of gas and surface molecules, particularly for coatings thin enough not to change the overall roughness. Experimental results for different gases and varying contamination yielded almost the same σ values. Substrate roughness seems to be responsible for the high σ values. The effect of molecular interaction potential, which is important for thermal accommodation, could only be assessed if the substrate roughness was much less than was attained in these experiments. Such substrates could be achieved at a crystal cleavage plane for example.

Some surface smoothing can be achieved by sublimating thick layers onto the machined substrate. Although layer thickness was not measured, it was thought to be of the order of the roughness depth of the substrate. Values of σ for thick films vary from test to test much more than those for thin films, probably because of variations in surface film porosity. In one case of a very thick gold film, the value of σ changed slowly with time possibly due to spontaneous sintering. The lowest σ values for thick gold films were slightly lower than those for thick

silver films.

Values of σ greater than unity can be achieved for very rough sandblasted surfaces where there is a net reflected tangential momentum back against the stream. This occurs only when appreciable areas normal to the surface are present. The values of σ greater than unity produced on rough surfaces are found to be more sensitive to interaction energies than the lower values of σ produced on smoother surfaces. Helium with its lower interaction energy gives higher σ values than argon or nitrogen. A simple approximate model showed how σ greater than unity occurs because the "windward" slope of a roughness hill receives more momentum than a "leeward" slope. For severe enough topography, the specular reflection gives a higher net σ value than the diffuse reflection. Stereo scanning electron micrographs demonstrated that roughness of the actual surface was severe enough to produce the high values of σ found for helium on a sandblasted surface.

In all cases of any but an ideally smooth surface, the tangential accommodation coefficient actually measures a combination of tangential and normal momentum exchange. Difficulties in precise topographical measurements at the microscopic and sub-microscopic levels do not permit separation of these two effects. Therefore, the macroscopic σ value is useful for characterizing a particular real situation.

The free molecular nature of the gas surrounding the rotating ball can be reliably analyzed by considering its momentum characteristics at one mean free path from the ball. This calculation showed the interaction could be considered in the free molecular regime if Knudsen number based on ball diameter is 14 or greater, and this agrees well with experiments made to determine the limit of free molecular flow (9).

BIBLIOGRAPHY

1. L. Trilling, "Theory of Gas-Surface Collisions, Fundamentals of Gas-Surface Interactions, Editors, H. Saltzburg, J.N. Smith and M. Rogers, 1967, p. 372.
2. R.G. Lord and P.J. Harbour, "Aerodynamic Drag Torque on a Rotating Sphere", Rarefied Gas Dynamics, (Fourth Symposium, Toronto, 1964), Volume 2, p. 611, Editor, J.H. de Leeuw.
3. R.A. Millikan, "Coefficient of Slip in Gases and the Law of Reflection of Molecules from the Surface of Solids and Liquids", Physical Review, Volume 21, 1923, p. 217.
4. E. Blankenstein, "Coefficient of Slip and Momentum Transfer in Hydrogen, Helium, Air and Oxygen", Physical Review, Volume 22, 1923, p. 582.
5. L.J. Stacy, "A Determination by the Constant Deflection Method of the Value of the Coefficient of Slip for Rough and for Smooth Surfaces in Air", Physical Review, Volume 21, 1923, p. 239.
6. F.C. Hurlbut, "Influence of Pressure History on Momentum Transfer in Rarefied Gas Flows", The Physics of Fluids, Volume 3, 1960, p. 541.
7. L.B. Thomas and R.G. Lord, "Comparative Measurements of Tangential Momentum and Thermal Accommodations on Polished and on Roughened Steel Spheres", Rarefied Gas Dynamics, (Eighth Symposium, 1972) p. 405.
8. J.W. Beams, J.C. Young and J.W. Moore, "The Production of High Centrifugal Fields", Journal of Applied Physics, Volume 17, 1946, p. 886.
9. G. Benson, "Measurements of Tangential Momentum Exchange Between a Rarefied Gas and a Solid Surface", M. Sc. Thesis, University of Alberta, 1968.
10. W.H. Weinberg and R.P. Merrill, "Atomic and Molecular Diffraction from a Tungsten Carbide Surface Characterized by LEED", Journal of Chemical Physics, Volume 56, 1972, p. 2893.

11. L.B. Thomas and E.B. Schofield, "Thermal Accommodation Coefficient of Helium on a Bare Tungsten Surface", Journal of Chemical Physics, Volume 23, 1955, p. 861.
12. H.Y. Wachman, "The Thermal Accommodation Coefficient and Adsorption on Tungsten", Ph. D. Thesis, University of Missouri, 1957.
13. R.E. Sonntag and G.J. van Wylen, Fundamentals of Statistical Thermodynamics, John Wiley and Sons, 1966.
14. J.F. Lee, F.W. Sears and D.L. Turcotte, Statistical Thermodynamics, Addison - Wesley, 1963.
15. H.Y. Wachman, "The Thermal Accommodation: A Critical Survey", American Rocket Society Journal, Volume 32, 1962, p. 1.
16. G.N. Patterson, Introduction to the Kinetic Theory of Gas Flows, University of Toronto Press, 1971.
17. A.J. Jerofeev, "The Influence of Roughness on Mutual Effects of a Gas Stream and the Surface of a Solid", Journal of Fluid and Gas Mechanics (USSR), Volume 6, 1967, p. 82.
18. K. Diels and R. Jaeckel, Leybold Vacuum Handbook, Pergamon, 1966.
19. H. Ishii and K. Nakayama, "A Serious Error Caused by Mercury Vapour Stream in the Measurement with a McLeod Gauge in the Cold Trap System", 1961 Vacuum Symposium Transactions, 1962, p. 519.
20. C. Meinke and G. Reich, "Influence of Diffusion on the Measurement of Low Pressure with the McLeod Vacuum Gauge", Vacuum, Volume 13, p. 579.
21. The Chemical Rubber Company Handbook of Chemistry and Physics, Editor, R.C. Weast, 54th Edition, 1973.
22. J.R. Young and N.R. Whetten, "Purity of Helium Permeated through Quartz into a Vacuum System", Review of Scientific Instruments, Volume 32, 1961, p. 453.
23. R.L. Wells and T. Fort, "Adsorption of Water on Clean Gold by Measurement of Work Function Changes", Surface Science, Volume 32, 1972, p. 554.

24. D.O. Hayward and B.M.W. Trapnell, Chemisorption, Butterworth, 1964.
25. G. Lewin, Fundamentals of Vacuum Science and Technology, McGraw-Hill, 1965.
26. J. Bagg and L. Bruce, "Sorption of Oxygen and Krypton by Evaporated Silver Films", Journal of Catalysis, Volume 2, 1963, p. 93.
27. S. Tolansky, Multiple Beam Interference Microscopy of Metals, Academic Press, 1970.
28. H. Saltzburg and J.N. Smith, "Molecular-Beam Scattering for the (111) Plane of Silver", Journal of Chemical Physics, Volume 45, 1966.
29. H. Saltzburg, N.N. Smith and R.L. Palmer, "Scattering of Molecular Beams of He, D₂ and H₂ from the (111) Plane of Ag", Rarefied Gas Dynamics (Fifth Symposium), Oxford, 1966, Volume 1, p. 223, Editor, C.L. Brundin, Academic Press.
30. J.N. Smith and H. Saltzburg, "Atomic-Beam Scattering from Epitaxially Grown Gold Films", Journal of Chemical Physics, Volume 40, 1964, p. 3585.
31. L.B. Thomas, "A Collection of Some Controlled Surface Thermal Accommodation Coefficient Measurements", Rarefied Gas Dynamics (Fifth Symposium) Oxford, 1966, Volume 1, p. 155, Editor, C.L. Brundin, Academic Press.

APPENDIX I
APPROXIMATE SOLUTION FOR
ENERGY ACCOMMODATION COEFFICIENT

The differential equation for the heated wire immersed in a free molecular gas is derived in section 2-3, and can be written as

$$\pi a^2 K_o \frac{d^2 T_f}{dx^2} = -\frac{I^2 R_o}{L} \left(1 - \beta (T_f - T_o)\right) + 2\pi a \alpha \left(\frac{g+1}{2}\right) \sqrt{\frac{k}{2\pi m T_w}} P (T_f - T_w) + 2\pi a S_o \epsilon (T_f^4 - T_w^4). \quad (I-1)$$

Defining $\theta = T_f - T_w$, the expression $T_f^4 - T_w^4$ can be expressed as

$$(T_w + \theta)^4 - T_w^4 = 4T_w^3 \theta + 6T_w^2 \theta^2 + 4T_w \theta^3 + \theta^4.$$

Normalizing equation I-1 for θ and L using the substitutions $\bar{x} = \frac{x}{L}$ and $\bar{\theta} = \frac{\theta}{\theta_{AV}}$ we get

$$\begin{aligned} \frac{\pi a^2}{L^2} \frac{K_o \theta_{AV}}{d\bar{x}^2} \frac{d^2 \bar{\theta}}{d\bar{x}^2} &= -\frac{I^2 R_o}{L} \left(1 - \beta \bar{\theta} \theta_{AV}\right) \\ &+ 2\pi a \alpha \left(\frac{g+1}{2}\right) \sqrt{\frac{k}{2\pi m T_w}} P \theta_{AV} \bar{\theta} \\ &+ 2\pi a S_o \epsilon \left(4T_w^3 \theta_{AV} \bar{\theta} + 6T_w^2 \theta_{AV}^2 \bar{\theta}^2 + 4T_w \theta_{AV}^3 \bar{\theta}^3 + \theta_{AV}^4 \bar{\theta}^4\right) \end{aligned} \quad (I-2)$$

if T_o is arbitrarily set equal to T_w .

For test d for helium in table 6-10 numerical values of terms of equation I-2 are calculated for the run at 5.0×10^{-3} torr and $\alpha_{AV} = 0.209$. These values are

$$\frac{d^2\bar{\theta}}{dx^2} = -2.36 - 1.76 \times 10^{-1}\bar{\theta} + \epsilon \left(1.16\bar{\theta} + 1.17 \times 10^{-1}\bar{\theta}^2 + 5.26 \times 10^{-3}\bar{\theta}^3 + 9.46 \times 10^{-7}\bar{\theta}^4 \right)$$

for the 5.0×10^{-3} torr measurement, and

$$\frac{d^2\bar{\theta}}{dx^2} = -2.87 - 2.14 \times 10^{-1}\bar{\theta} + \alpha(2.67)\bar{\theta} + \epsilon \left(1.16\bar{\theta} + 1.17 \times 10^{-1}\bar{\theta}^2 + 5.26 \times 10^{-3}\bar{\theta}^3 + 9.46 \times 10^{-7}\bar{\theta}^4 \right).$$

Since T_w is an order of magnitude greater than θ_{AV} , the second radiation term can be seen to be about 10% of the first term, and the third term is less than 10% of the second term. Also, values of ϵ are about 0.1, making these second, third and fourth terms the smallest in the equation. Therefore, as an approximation, these two terms can be neglected, which makes the equation linear and less difficult to solve.

The non-dimensionalized equation written in terms of θ and neglecting the two smaller radiation terms becomes

$$\pi a^2 K_o \frac{d^2\theta}{dx^2} = \frac{-I^2 R_o}{L} (1 + \beta\theta) + 2\pi a\alpha \left(\frac{g+1}{2} \right) \sqrt{\frac{k}{2\pi m T_w}} p\theta + 8\pi a S_o \epsilon T_w^3 \theta \quad (I-3)$$

if $T_o = T_w$.

Equation I-3 a linear equation of the general form

$$\frac{d^2\theta}{dx^2} - A\theta + B = 0. \quad (I-4)$$

The complementary solution to equation I-4 is the solution to the equation $\frac{d^2\theta}{dx^2} - A\theta = 0$, which by substituting $\theta = e^{mx}$, is found to be

$$\theta = c_1 \cosh(\sqrt{A}x) + c_2 \sinh(\sqrt{A}x).$$

When a particular solution is found to equation I-4, the general solution is

$$\theta = c_1 \cosh(\sqrt{A}x) + c_2 \sinh(\sqrt{A}x) + B/A. \quad (I-5)$$

Constants c_1 and c_2 can be evaluated from the boundary conditions which are

$$\text{at } x = 0, \theta = 0$$

$$\text{at } x = L/2, \frac{d\theta}{dx} = 0 \text{ from symmetry.}$$

Solving for c_1 and c_2 , the solution becomes

$$\theta = \frac{B}{A} [1 - \cosh(\sqrt{A}x)] + \frac{B}{A} \tanh(\sqrt{A}L/2) \sinh(\sqrt{A}x). \quad (I-6)$$

$$\text{where } A = \left(\frac{-I^2 R_o}{L} \beta + 2\pi a \alpha \left(\frac{g+1}{2} \right) \sqrt{\frac{k}{2\pi m T_w}} p + 8\pi a S_o \varepsilon T_w^3 \right) / \pi a^2 k$$

$$\text{and } B = \frac{I^2 R_o}{L} / \pi a^2 k.$$

As the purpose of this analysis is to obtain values of α , equation I-6 is not a useful form because α , ε and $\theta(x)$ are all unknown. From experiments, values of θ_{AV} as well as values of I for the zero pressure and higher pressure are measured. Average temperature difference

$$\theta_{AV} = \frac{L}{2} \overbrace{\int_0^{L/2} \theta(x) dx}^{L/2},$$

which can be evaluated using equation I-6. Performing the integration,

$$\theta_{AV} = 2/L \frac{B}{A} \left[L/2 - \frac{1}{\sqrt{A}} \tanh(\sqrt{A}L/2) \right].$$

For a given measurement of θ_{AV} and B the value of A can then be found, in this case using a simple computer program which estimated A through successive approximation. First, taking an initial run at θ_{AV} for zero pressure, a value of A was obtained which allowed calculation of ϵ . Having obtained ϵ , a corresponding A for a higher pressure run at the θ_{AV} was found. Knowing this A and ϵ , an α value was determined.

The computer program was also used to find a temperature distribution by a direct calculation from equation I-5. This temperature distribution $\theta(x)$ is presented in figure I-1 for the helium test 1d table 6-10. $\theta(x)$ is presented for $p = 0$ and $p = 5.0 \times 10^{-3}$ torr. The distribution shown in figure I-1 indicates that the $p = 0$ case gives a higher maximum temperature, but the higher pressure case gives slightly higher temperatures nearer the end supports. Plots for the other measurements would be similar in character.

$$\theta = T_f T_w$$

in $^{\circ}\text{C}$

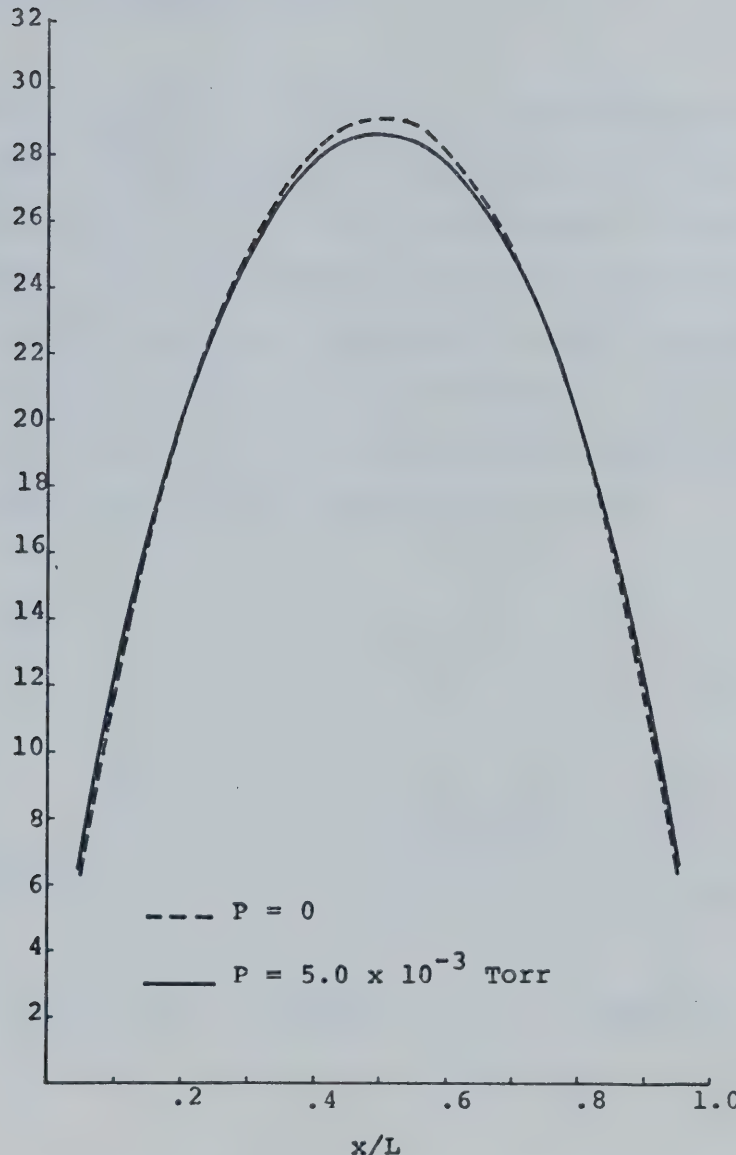


FIGURE I-1 TEMPERATURE DISTRIBUTION
ON HEATED FILAMENT $\theta(x)$
VS x/L HELIUM TEST d

APPENDIX II
ELECTRONIC CIRCUITS

II-1 Magnetic Suspension System.

Figure II-1 shows a schematic of the suspension system electronics. As previously explained, the photodiode monitored the light from a bulb and therefore the position of the ball. The light induced photodiode signal was amplified in a high current gain amplifier A_1 which contained networks to prevent oscillation of the ball. This signal was used to correct the current produced by the high power driving stage which excites the suspension coil.

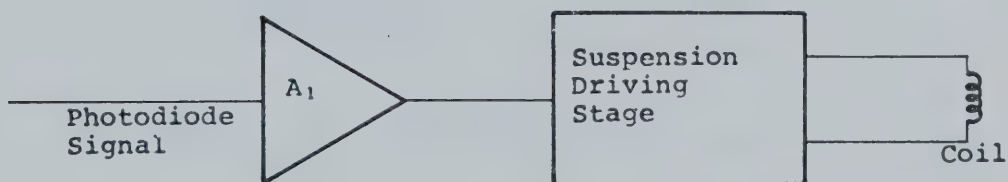


FIGURE II-1 SUSPENSION CIRCUIT SCHEMATIC

The suspension coil consisted of 1325 turns of #24 magnet wire and passed a normal equilibrium current of about 0.6 amps. While the coil current is ideally

constant, oscilloscope examination indicated some small periodic and random fluctuations of a few milliamps. This oscilloscope trace provided an accurate judgement of circuit performance and was used for fine tuning of the circuit.

II-2 Counting Circuit.

Figure II-2 shows a schematic of the circuits for the counting system. This system had the function of taking the pulsed signal caused by the scratch on the ball and amplifying, shaping and stabilizing it to a form such that the counter gave an accurate count.

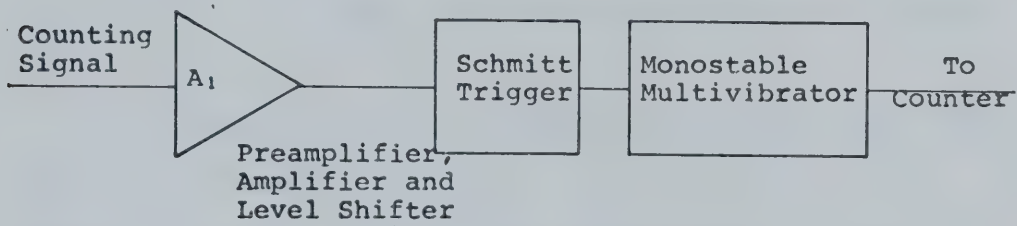


FIGURE II-2 COUNTING CIRCUIT SCHEMATIC

The counting photodiode had to be first preamplified and amplified. Due to the high sensitivity of this circuit, the preamplifier was situated very close to the photodiode and all signals were transmitted using grounded shielded cable. The amplifier output went to two signal conditioning switching circuits, a Schmitt trigger and then a monostable multivibrator.

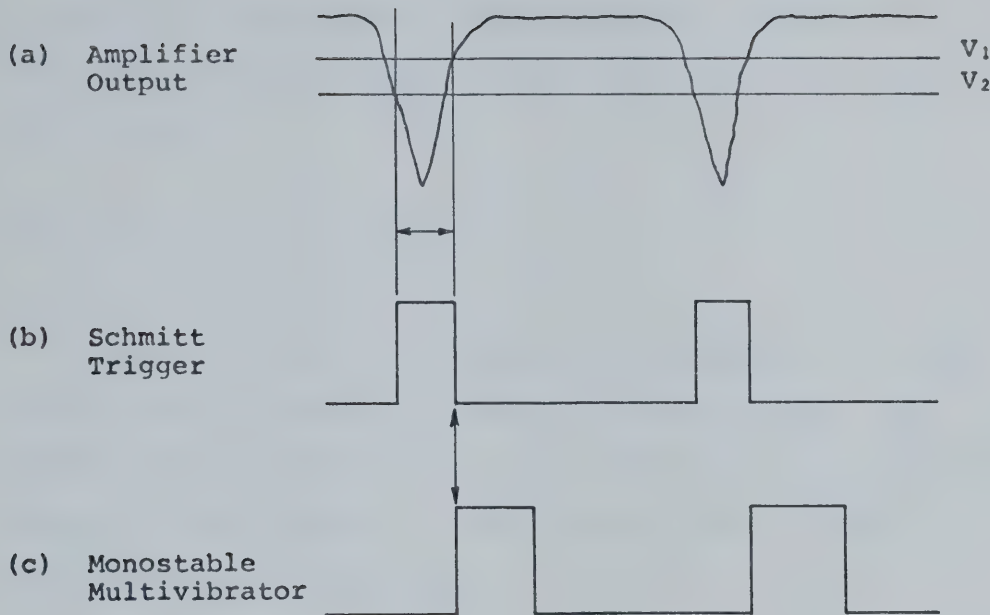


FIGURE II-3 COUNTING OSCILLOGRAPH TRACE

The function of these switching circuits is illustrated in figure II-3 which represents an oscillograph of the counting signal in various conditioning stages. Signal (a) represents the amplified pickup from the rotating ball and shows a pulse due to the scratch on the ball. The Schmitt trigger, signal (b), outputs at two distinct levels, the transition of which depends upon voltages v_1 and v_2 shown on signal (a). When the amplified signal is reduced to v_2 , a voltage is produced by the trigger, and when the signal goes back above v_1 , a lower voltage is produced. The monostable multivibrator took the pulse from the Schmitt

trigger and provided another similar pulse which is variable in length. This variable length was found to be useful in eliminating multiple counting which can occur for a noisy input signal.

II-3 Rotational Drive System.

Figure II-4 shows a schematic of the field coil system used to turn the ball. An 8250 Hz sine wave signal was generated by an oscillator and split into two equal amplitude signals 90° out of phase. These signals were then fed to the field coils wound as shown.

II-4 Energy Accommodation Measurement Circuits.

Feedback circuits were required to maintain the tungsten filaments at constant temperature during energy accommodation measurements. Difficulties exist when using the DC heating signal for resistance and temperature control if power requirements vary. Electrical resistance is not directly measurable, but rather a ratio of voltage drop to current must be found. Given a particular initial heat transfer rate from the wire and a corresponding input power, any changing transfer rate requires changing current. Some signal, either voltage across or current in the wire is required to initiate a feedback to maintain constant resistance. Whichever quantity is chosen, the other does not

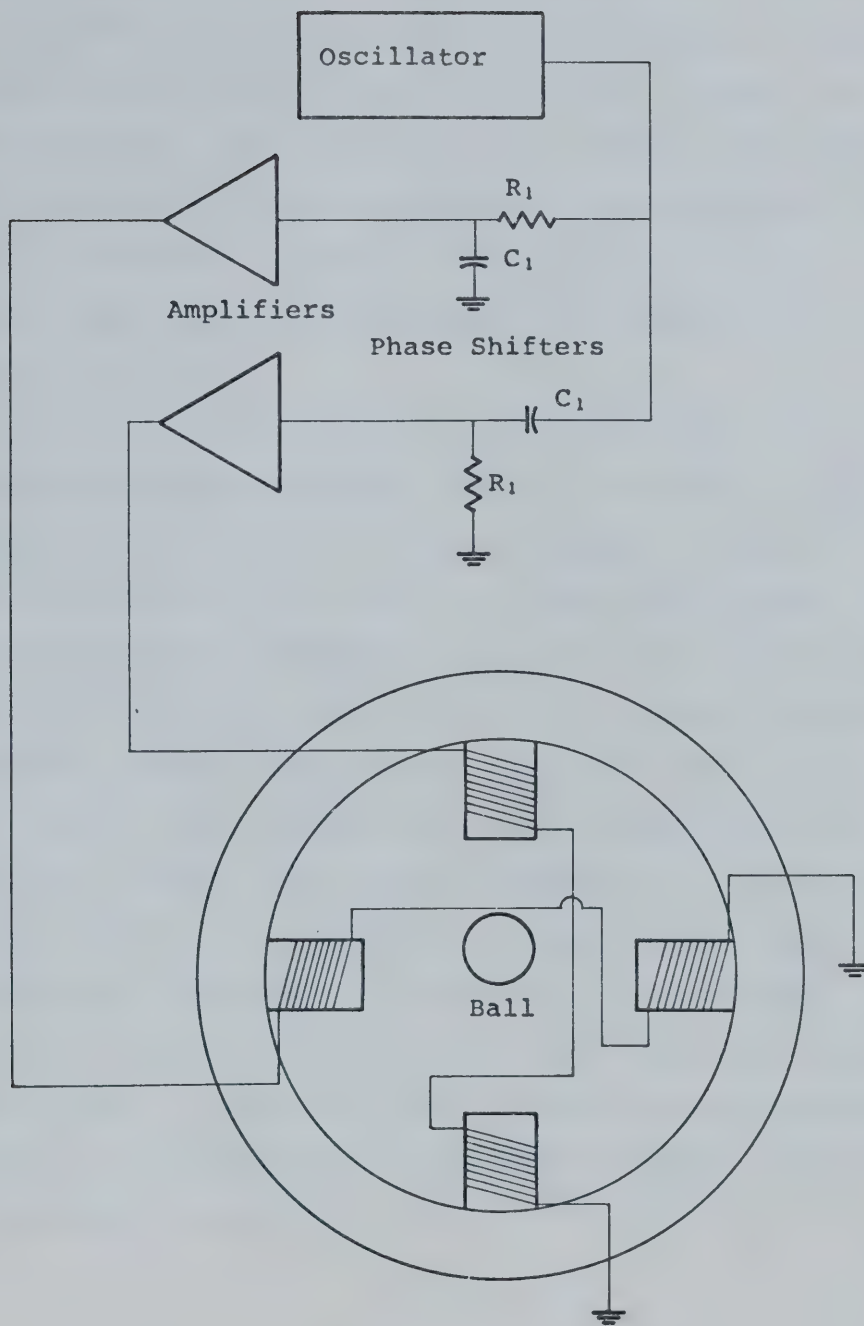


FIGURE II-4 ROTATING DRIVE APPARATUS SCHEMATIC

remain constant making resistance determination difficult.

To overcome resistance measurement problems, a small constant AC current was passed through the filament and the AC voltage drop was measured, this voltage drop being directly proportional to resistance. The voltage drop was used to initiate a feedback to the DC heating current. Circuits used for this purpose are shown schematically in figure II-5.

As can be seen in figure II-5, an oscillator produced a stable AC voltage at 688 Hz which was converted in the sensing current source to a small constant AC current. This sensing current was then fed through the filament and a sensing resistor to ground, and an AC voltage was measured across the filament. Amplifier A_1 , an AC coupled differential amplifier separated this signal from other signals and amplified it. The rectifier and filter system took this signal and further amplified it, removed 60 Hz interference and rectified it, to produce a DC voltage proportional to the filament temperature. Amplifier A_2 , a DC coupled amplifier produced an error signal which controlled the DC heater output. The current sensing resistor was a precision resistor, the voltage drop across which provided a measure of the heating current.

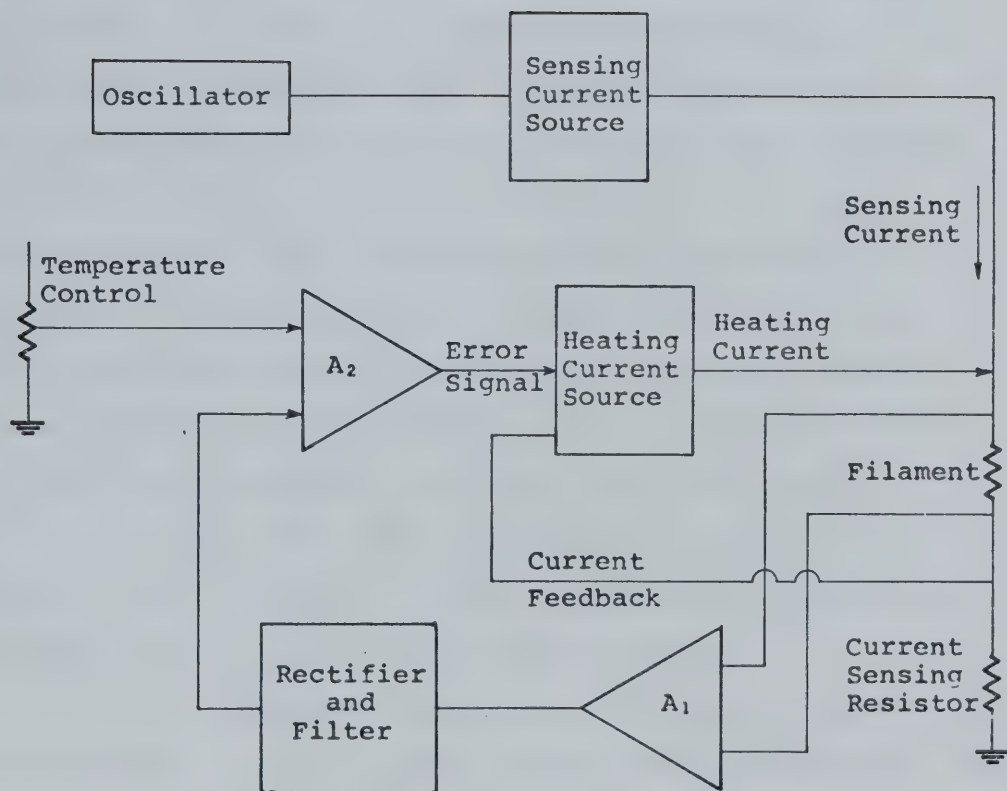


FIGURE II-5 FILAMENT TEMPERATURE CONTROL AND HEATER CIRCUIT

APPENDIX III
CALCULATION OF TEMPERATURE
COEFFICIENT OF TUNGSTEN FILAMENT

The calibration of the tungsten filament resistance was made after the completion of tests for α by immersing the filament in an accurate constant temperature bath filled with ethylene-glycol and water. Temperature was sensed with a quartz thermometer which had been calibrated against an accurate platinum resistance thermometer by the staff member in charge of the Mechanical Engineering standards laboratory. Intermittant heating maintained the bath at a given temperature and a circulating pump kept most of the bath uniformly at that temperature. The resistance of the bath fluid was determined to be large compared to the resistance of the wire. Wire resistance was measured by passing a small measured current of about 20 mA through it and measuring also the voltage across the wire.

Due to the complicated geometry of the energy accommodation tube, it was decided to remove the filament from its nickel supports, and spot-weld it to another set design to fit properly in the bath. This resulted in a loss of about 10% of the filament and meant that resistance for the filament in the bath and during α tests was different; but it is assumed that the temperature coefficient is the same for both situations.

The temperature coefficient of the shortened filament resistance β was found to be 0.00372 at 26°C. At 26°C the filament as in the energy accommodation apparatus was measured to be 13.438 ohms, this measurement being taken with air in the vacuum system by passing a small current of about 3 mA through and measuring voltage drop across the filament. Figure III-1 shows a plot of shortened filament resistance versus temperature as determined in the bath, and figure III-2 a similar plot for the filament as in the energy accommodation tube.

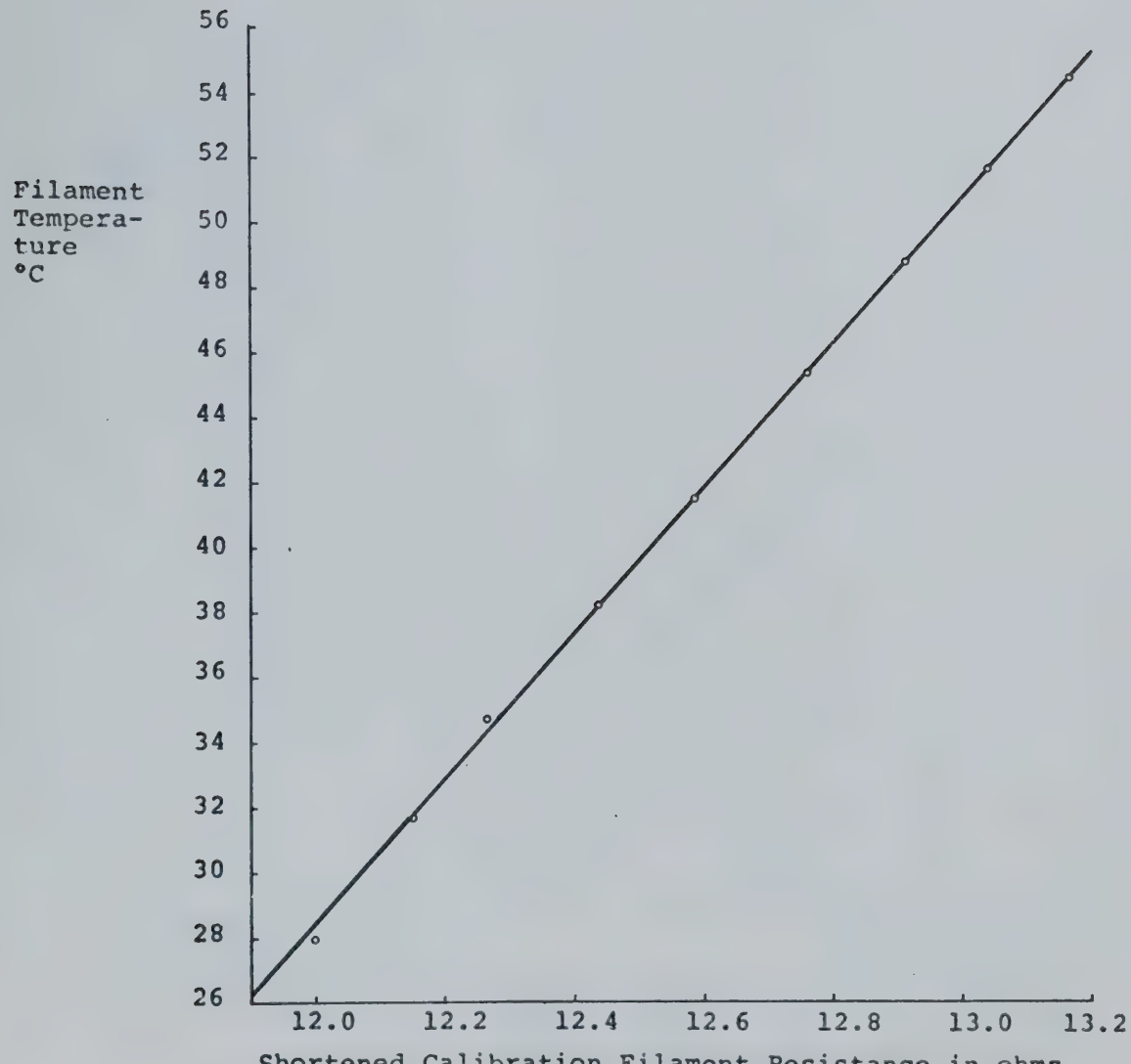


FIGURE III-1 CALIBRATION FILAMENT RESISTANCE VERSUS TEMPERATURE

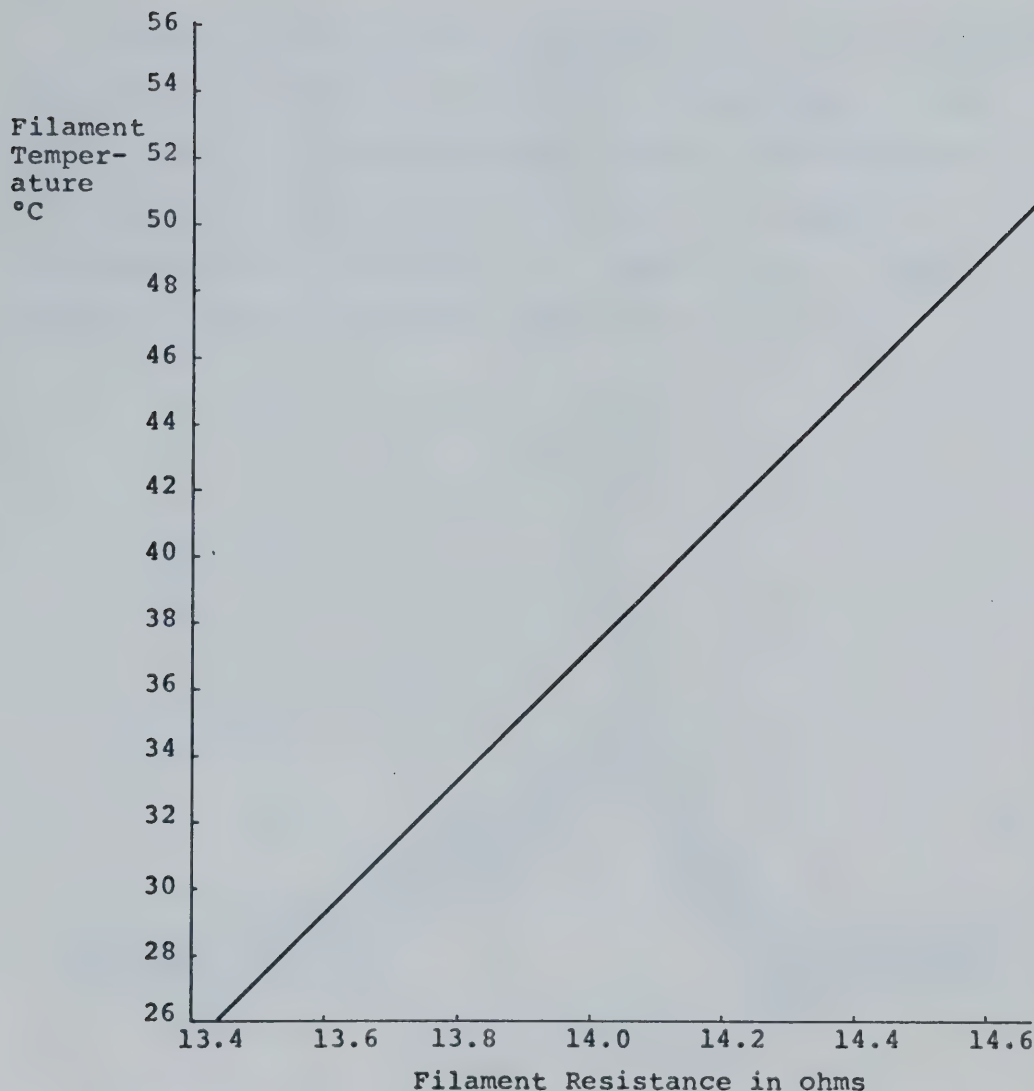


FIGURE III-2 ENERGY ACCOMMODATION FILAMENT
RESISTANCE VERSUS TEMPERATURE

APPENDIX IV
FORMULATIONS FOR STEREOGRAPHIC
HEIGHT DETERMINATION

Given distances between two points x and y on a surface observed at two different angles to the macroscopic normal, it is possible to find the average slope ϕ and difference in elevation d between those two points. The calculation is demonstrated in figure IV-1 for angles 0° and δ where distances a_0 and a_δ have been measured in some manner.

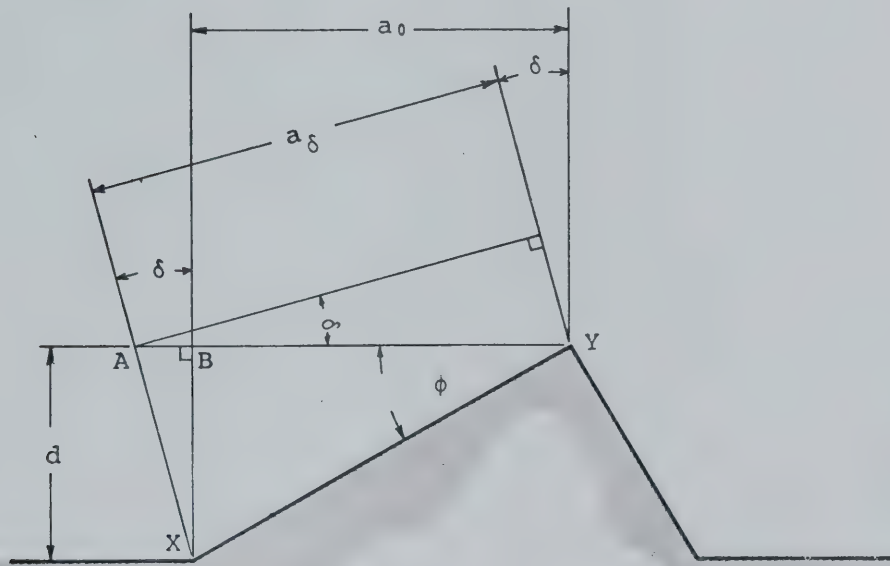


FIGURE IV-1 DIAGRAM FOR STEREOGRAPHIC
HEIGHT DETERMINATION

Examination of figure IV-1 shows that $AB = dtan\delta$.

(IV-1)

Also triangle ACY gives that $a_\delta / (a_0 + AB) = \cos\delta$, (IV-2)

which when combined with equation IV-1, yields the result

$$d = \left(\frac{a_0}{\cos \delta} - a_0 \right) / \tan \delta. \quad (IV-3)$$

B30117